DNA translocases and origin region segregation in *B. subtilis*

INAUGURALDISSERTATION
zur Erlangung der Doktorwürde
der Fakultät für Chemie
an der
Philipps-Universität Marburg

vorgelegt von

Nina El Najjar

Marburg, November 2016

Erklärungen

1. Ich erkläre hiermit, dass ich die vorliegende Arbeit ohne unzulässige Hilfe Dritter und ohne Benutzung anderer als der angegebenen Hilfsmittel angefertigt habe. Die aus anderen Quellen direkt oder indirekt übernommenen Daten und Konzepte sind unter Angabe der Quellen hier weiter unten gekennzeichnet. Insbesondere habe ich hierfür nicht die entgeltliche Hilfe von Vermittlungs- beziehungsweise Beratungsdiensten (Promotionsberater oder anderer Personen) in Anspruch genommen. Niemand hat von mir unmittelbar oder mittelbar geldwerte Leistungen für Arbeiten erhalten, die im Zusammenhang mit dem Inhalt der vorgelegten Dissertation stehen.

a) „Manuscript 4A“, (publiziert im „Journal of Microbiology and Biotechnology“):“ Figure 7“, (Seite 63): Experimente und Abbildungen wurden von Dr. Christine Kaimer (Ruhr-Universität Bochum, Fakultät für Biologie und Biotechnologie) gemacht.

b) „Manuscript 4B“: „Figure 1“, (Seite 84) A, B, C, D, und E: Experimente und Abbildungen wurden von Dr. Christine Kaimer (Ruhr-Universität Bochum, Fakultät für Biologie und Biotechnologie) gemacht. „Figure 2“, (Seite 85), A-F: Vektoren mit den passenden Inserts wurden selbst hergestellt, Transfektionsexperimente und Mikroskopie wurden von Dr. Jihad El Andari (Universität Heidelberg, Center for Quantitative Analysis of Molecular and Cellular Biosystems) gemacht.

   „Figures 3, 4, 5, 6“ (Seiten 86, 87, 88 und 89), und „Table 3“ (Seite 79): Mikroskopie wurde selbst gemacht, Analyse von Daten sowie die Abbildungen wurden von Dr. Thomas Rösch (Philipps Universität Marburg, Synmikro) gemacht.

c) „Manuscript 4C“: „Figure 10“ (Seite 127): Mikroskopie wurde selbst gemacht, Analyse von Daten sowie die Abbildung wurden von Felix Schmidt (Philipps Universität Marburg, Synmikro) gemacht.

2. Die Arbeit wurde bisher weder im In- noch im Ausland in gleicher oder ähnlicher Form einer anderen Prüfungsbehörde vorgelegt.

3. Die Bestimmungen der Promotionsordnung der Fakultät für Biologie der Universität Marburg sind mir bekannt, insbesondere weiß ich, dass ich vor Vollzug der Promotion zur Führung des Doktortitels nicht berechtigt bin.

(Nina El Najjar)

ÜBERSICHT

Die Segregation von Chromosomen wird durch spezielle Mechanismen sicher gestellt, welche die Position des Septums sowie die korrekte Trennung von chromosomalen Dimeren gewährleisten und somit an der Aufrechterhaltung der Integrität der chromosomalen DNA während des gesamten Zellzyklus beteiligt sind.

Anhand des Gram-positiven Modellorganismus *Bacillus subtilis* wurden im ersten Teil dieser Arbeit DNA-Translokasen untersucht, welche über einen direkten Transport die Chromosomen von der zellulären Teilungsebene weg bewegen. Bei SpoIIIE handelt es sich um eine Membran-integrierte Translokase, die während der Sporulation aktiv ist. Es wurde bereits gezeigt, dass SftA hingegen *in vitro* löslich ist und über einen bisher unbekannten Mechanismus mit dem Divisionsseptum assoziiert. Die Löslichkeit von SftA *in vivo* wurde über Zell-Fraktionierungs-Experimente nachgewiesen. Der Teil des Proteins, welcher zur Bindung an das Septum führt, wurde über die Lokalisation von unterschiedlichen, trunkierten und fluoreszenzmarkierten SftA Derivaten identifiziert, wodurch die für die Bindung an das Septum verantwortlichen Aminosäuren eingegrenzt werden konnten (siehe Manuskript, 4A). Über die Expression in einem eukaryotischen, heterologen System konnte eine Interaktion von SftA mit FtsA, jedoch nicht mit FtsZ nachgewiesen werden. Ein weiterer Nachweis hierfür wurde über Experimente durch *single molecule tracking* erbracht, wobei die lösliche Fraktion der SftA-Moleküle bei geringer Expression von FtsA im Vergleich zu dem Wildtyp zunimmt.

Untersuchungen auf Einzelmolekül-Level von SpoIIIE, einer Membran-assoziierten DNA-Translokase in *B. subtilis* und PfkA, einer löslichen Phosphofructokinase, ließen auf ein unterschiedliches Verhalten der beiden Translokasen (SftA und SpoIIIE) schließen: SftA besitzt eine am Septum gebundene Fraktion und eine kleine, sich schnell bewegende, lösliche Fraktion, welche mit der ausschließlich löslichen PfkA-Fraktion vergleichbar ist. SpoIIIE ist im Vergleich weniger dynamisch, wobei sogar die dynamische Fraktion viel langsamer ist als die statische SftA Fraktion. Scheinbar bewegt sich SpoIIIE langsam entlang der Membran, ohne sich am Septum anzureichern; selbst nach der Zugabe von Mitomycin C (MMC, siehe Manuskript 4B).

Der zweite Teil dieser Arbeit befasste sich mit der Anzahl von Nukleoiden, Origin- und Termini unter schnellen und langsamen Wachstumsbedingungen, mit oder ohne Induktion von Doppelstrangbrüchen durch MMC. *B. subtilis* scheint vornehmlich diploid zu sein, mit

polyploiden und monoploiden Zellfraktionen, welche sich abhängig von den gewählten Wachstumsbedinungen verändern. Die Replikation von benachbarten Regionen der Replikationsursprünge nahm nach der Induktion von DNA-Schäden zu, wie schon durch die Zunahme der Anzahl von Origins während der DNA-Reparatur gezeigt wurde, während die Anzahl der Terminatorsequenzen konstant blieb. *Time lapse* Experimente der Segregation von markierten Replikationsursprüngen zeigte, dass sich die Bewegung der Moleküle am besten durch gezielte Diffusion beschreiben lässt, welche sich durch die Zugabe von MMC oder Ciprofloxacin, welches die Topoisomerase IV inhibiert, zwar verlangsamt, sich jedoch als robust und kontinuierlich beschreiben lässt (siehe Manuskript 4C).

SYNOPSIS

Specialized mechanisms involved in chromosome segregation, septum placement, and chromosome dimer resolution contribute to the maintenance of chromosome integrity throughout the cell cycle. The first part of this work focuses on the investigation of DNA translocases in the Gram positive model organism *Bacillus subtilis*, which move the chromosomes away from the division plane by directed DNA transport. SpoIIIE is a membrane-integral translocase that also acts during sporulation, while SftA is associated with the division septum by an unknown mechanism and was reported to be a soluble protein *in vitro*. The solubility of SftA *in vivo* was proven with cell fractionation experiments, and the part of the protein that serves for septal targeting was determined through the localization of different truncations of fluorescently labeled SftA, which helped narrow down the stretch of amino acids responsible for targeting the protein to the septum (see manuscript 4A). Expression in a Eukaryotic heterologous system revealed an interaction between SftA and FtsA, but not FtsZ. Further evidence was provided by single molecule tracking experiments whereby the fraction of soluble SftA molecules increased in an FtsA depletion background as compared to a wild type background. Concomitant investigation on the single molecule level of SpoIIIE, a membrane associated DNA translocase in *B. subtilis*, and PfkA, a soluble phosphofructokinase, revealed a different behavior of the two translocases (SftA and SpoIIIE): SftA has a septal bound fraction, and a small soluble fast moving fraction, comparable in diffusion coefficient to the exclusively soluble PfkA tracked under the same conditions. SpoIIIE is much slower in comparison, and even its "fast" moving fraction is much slower than that of SftA. It seems to move slowly along the membrane with no specific enrichment at the septum, even after Mitomycin C (MMC) treatment (see manuscript 4B). The second part of this work focused on the count of nucleoids, origin, and terminus of replication regions under conditions of fast and slow growth, with or without the induction of double strand breaks with MMC. *B. subtilis* seemed to be predominantly diploid, with a fraction of polyploid and monoploid cells which changed depending on the growth conditions. Replication of the origin proximal regions increased after DNA damage induction, as was shown by the increase in the number of origins during the time of DNA repair, while the number of termini remained constant. Time lapse experiments of the segregation of the tagged origin regions revealed that the movement is best described as directed diffusion, but seems to be quite robust and continues, though slower, after

MMC treatment or treatment with Ciprofloxacin which blocks the topoisomerase IV (See manuscript 4C).

TABLE OF CONTENTS

1. INTRODUCTION

The chromosome is the largest biomolecule in the cell. In *Bacillus subtilis*, the chromosome is about 4.2 Mb, organized in 4100 genes. It is about 2 mm long, and highly compacted to fit within the confines of 3 to 5 µm of cell length. During each cell cycle, the genetic information must be faithfully replicated and segregated to insure that every daughter cell receives a copy of the genome before cell division occurs. A number of processes in the cell are responsible for maintaining the structural integrity of the chromosome to prevent DNA damage. These processes are both spatially and temporally coordinated and involve mechanisms such as DNA compaction and segregation, accurate septal placement, DNA repair, and transformation.

This overview describes the mechanisms that maintain chromosome integrity, and the processes that play a role in chromosome separation. The main focus of this work was to analyze the role and dynamics of DNA translocases in *B. subtilis* during vegetative growth, as well as the real time follow up of origin separation in this organism, and the effect of damage induction on this process.

1.1. *Bacillus subtilis*

B. subtilis is a member of the low-G+C group of Gram-positive bacteria. It is a ubiquitous species broadly adapted to grow in diverse settings in the biosphere (1). It can be isolated from a myriad of environments, both terrestrial and aquatic. *B. subtilis* grows in close association with plant root surfaces. There is evidence that these associations may promote plant growth by out-competing microbes that could adversely affect the plant, by activating the host defense system so that the plant can resist potential pathogens, and by making certain nutrients such as phosphorous and nitrogen more readily available to the plant (2). Previously thought to be a strict aerobe, *B. subtilis* appears to be able to consume its life cycle within the GI tract of plant consuming animals. In fact, growth within the GI tract must be robust enough such that it can out-compete pathogens (3). In response to nutrient deprivation, *B. subtilis* can enter into alternate developmental pathways either to become competent and take up exogenous DNA, enter a motile or biofilm-forming state, or form an environmentally resistant, dormant endospore. *B. subtilis* has been widely used as a model system in microbiology due to the ease of genetic manipulations in this organism. Its spores are

used as a model for studying bacterial development. Studies of *B. subtilis* are also greatly aided by the availability of complete genome sequences for the commonly-used laboratory strains (4, 5).

1.2. The bacterial cell cycle

The mechanisms underlying bacterial cell division have been extensively studied in the model organisms *Escherichia coli*, *Bacillus subtilis*, and *Caulobacter crescentus*. While the details of chromosome segregation and cell division differ between these organisms, the basic processes, many of the central protein complexes involved, and the fundamental regulatory logic appear to be well conserved.

Growth of a bacterial population is divided into characteristic phases: the lag phase during which the cells adapt themselves to the growth conditions, the exponential phase in which cells proliferate, and the stationary phase in which cells stop dividing (Fig. 1.1A). During exponential growth, replication of the chromosomes starts at the origin of replication, and is conducted by a replication machinery located at the center of the cell. DNA binding proteins segregate and reorganize the replicated chromosomes. Finally, cell division is initiated at midcell and accomplished by a multiprotein complex. Chromosome dimers that can arise during replication, and that cannot be segregated, are resolved by translocases before the completion of division. Stationary phase is often accompanied by the production of secondary metabolites that offer an advantage in a competitive environment. *B. subtilis* is able to achieve distinct physiological states in stationary phase which are initiated by different genetic programs. Cells may differentiate into specialized dormant forms that are resistant towards a number of unfavorable conditions like desiccation, heat or radiation (6, 7).

Formation of dormant endospores requires the differentiation into a larger mother cell and a smaller forespore (Fig. 1.1B). Gene expression is subsequently orchestrated through the activity of four compartment-specific sigma factors (σ^F, σ^E, σ^G and σ^K), activated either in the forespore or in the mother cell. Alternatively to endospore formation, stationary phase cells of *B. subtilis* can enter a physiological state called competence (Fig. 1.1C). During competence a special protein complex enables cells to take up DNA from their environment and to either integrate it into their chromosome by homologous recombination, or to maintain it as an autonomously replicating DNA unit. Induction of competence depends on cell density, which is detected by quorum sensing, and is mainly controlled by the global transcription factor ComK (7, 8).

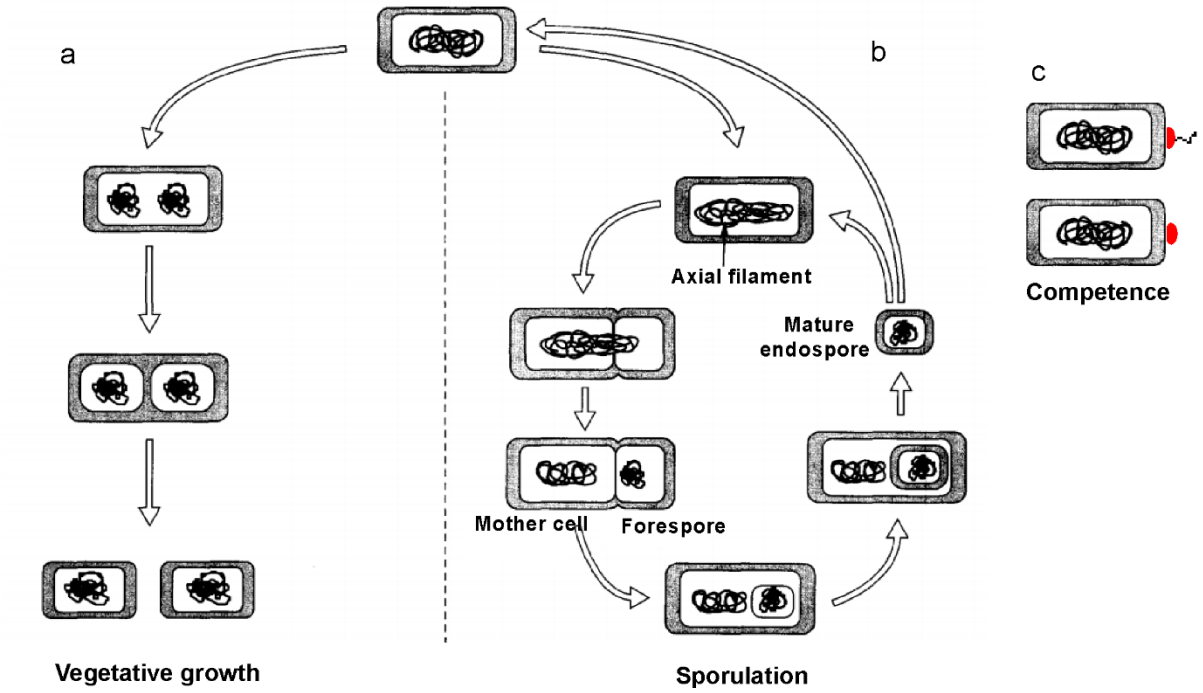

Figure 1.1. Cell cycle and differentiation in *B. subtilis*. **(A)** During exponential growth the chromosomes are replicated and segregated simultaneously. **(B)** Sporulation is accompanied by the formation of an asymmetric septum. **(C)** During competence external DNA (green) is taken up by a protein complex at the cell pole (orange) and can be integrated into the chromosome. Figure adopted and modified from Levin et al., 1998.

1.3. Chromosome replication

Chromosomal replication must be regulated to ensure a constant number of chromosomes in the cell. This means that chromosomal DNA must be replicated only once per cell cycle. To ensure this, bacterial, archaeal and eukaryotic cells have evolved regulatory mechanisms to control the initiation of chromosomal replication (9).

Bacterial chromosomes and plasmids have a single replication origin which exhibits replicon-specific regulation. Initiation of replication requires the formation of organized nucleoprotein complexes on the DNA replication origin. Formation of these multimeric complexes is induced by specific proteins, including DnaA in bacteria and ORC (origin recognition complex) in eukaryotes (10, 11).

In *Escherichia coli*, the origin of replication (*oriC*) region contains 13 residues long AT-rich repeats. DnaA binds either ATP or ADP, but only ATP–DnaA can initiate replication (10, 11). The cellular level of ATP–DnaA fluctuates during the replication cycle, with a peak at the time of initiation (12). ATP–DnaA bind the DnaA boxes consisting of 9 nucleotides sequences with the aid of DnaA initiator-associating protein DiaA, which binds multiple DnaA molecules simultaneously and stimulates their assembly on *OriC* (13), and the integration host factor (IHF). This results in multimerization of ATP–DnaA and local duplex unwinding of the AT-rich region. IHF binds to specific sites in the *oriC* which leads to DNA bending and facilitates binding of DnaA. ATP-DnaA exclusively binds to low affinity DNA boxes which starts the initial unwinding and results in the open complex formation (10, 13). Subsequently, the replicative DNA helicase DnaB, is loaded onto the single stranded region in a manner mediated by the helicase loader DnaC and oriC-bound DnaA. DnaB then migrates along the DNA, expanding the region of single-stranded DNA. DNA primase (DnaG) and the DNA polymerase III holoenzyme (which consists of the Pol III* subassembly and the clamp, (DnaN)) are loaded onto the DNA to form the replisome and mediate the synthesis of primer RNA and complementary DNA, respectively.

DnaA boxes are also found in *oriC* of *Bacillus subtilis* to which the DnaA protein binds (14). In addition to DnaA, four other proteins, DnaB, DnaC, DnaD and DnaI, are engaged in initiation of *B. subtilis* chromosome replication. DnaC is a replicative DNA helicase, a counterpart of *E. coli* DnaB. The remaining three, DnaB, DnaD, and DnaI are part of the primosome and are required for loading of DnaC. (15, 16).

After the initiation reaction, the initiation proteins and the origin DNA are inactivated to prevent re-initiation in the same round of the cell cycle (17-19). In *E. coli* and *B. subtilis*, the main regulatory mechanism of replication initiation is a negative-feedback loop that inhibits the replication reaction, largely by inhibiting the activity of DnaA (9) (Figure 1.2).

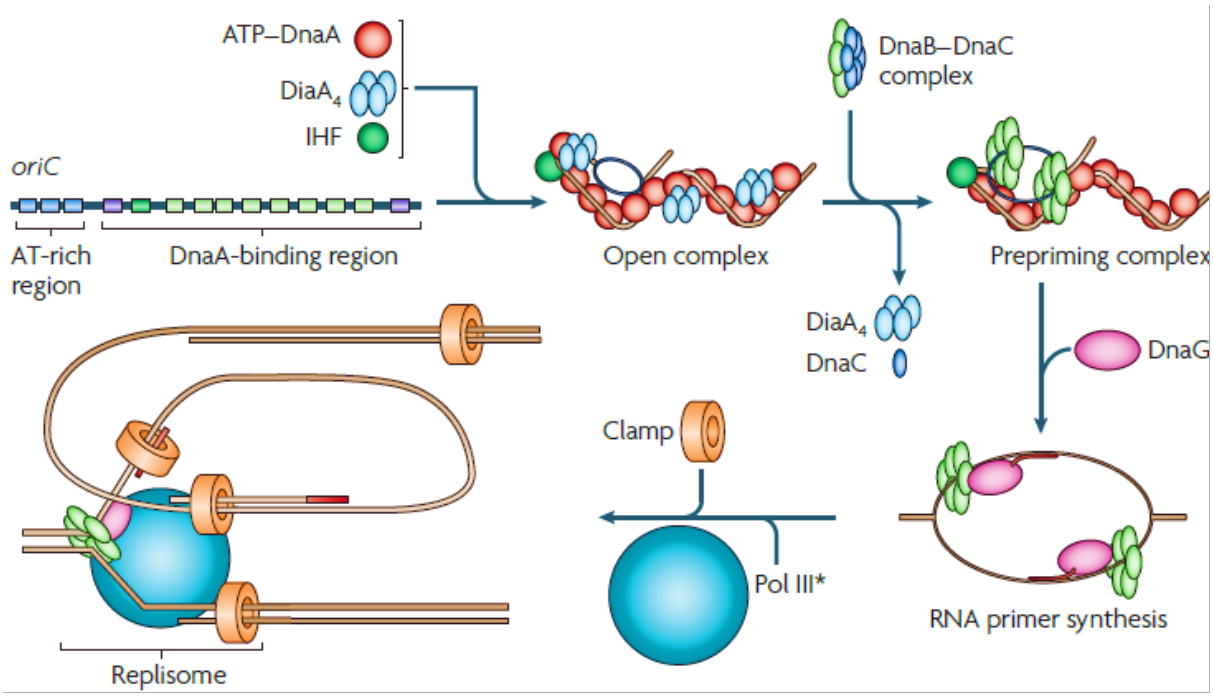

Figure 1.2. Model mechanism of initiation at the origin of replication in *Escherichia coli.* (Figure adopted from Katayama et al., 2010).

1.4. *Bacillus subtilis* DNA Polymerases

1.4.1. PolC

The *B. subtilis* DNA polymerase III encoded by *polC* carries a polymerase active site in its C-terminal part, and a 3'-5' proofreading exonuclease in its N-terminal domain (20, 21). PolC is highly conserved among low G+C gram positive bacteria (22). *polC*, as well as the highly conserved *dnaX, holB, holA* and *dnaN* encode for PolC, τ, δ′and δ subunits of the helicase loader complex, and the β sliding clamp, respectively, and all of them are constituents of the polymerase III holoenzyme. The clamp loader, DnaX complex, uses ATP hydrolysis to open the β ring and load it as a functional sliding clamp along the DNA. In combination, the clamp loader complex and the β clamp provide PolC with a high speed (around 700 nucleotides per minute), comparable to *E. coli* (23).

1.4.2. DnaE

B. subtilis possesses a second polymerase, DnaE, which acts preferentially in lagging strand synthesis (24). DnaE extends RNA primers before handing them off to PolC, in a manner analogous to the eukaryotic pol α, which extends RNA primers at the lagging strand before handing them off to the more processive pol δ (25, 26). DnaE interacts with DnaN, single-stranded DNA binding proteins (SSB), the helicase DnaC, the primase DnaG, the HolA subunit of the DnaX complex and PolC. DnaE is an efficient DNA polymerase, with moderate processivity and no 3′ → 5′-exonuclease activity. Even though the expression of DnaE increases in response the SOS response, it so not likely to function as an error prone polymerase in vivo since its overexpression does not increase the rate of spontaneous mutagenesis (24). This mode of replication in *B. subtilis* is different than in *E. coli* where the same PolIII is assembled asymmetrically to efficiently replicate the two strands.

1.5. Replication progression and termination

1.5.1. Priming reaction

The transition from initiation to elongation is triggered by the recruitment of the DnaG primase through binding to the DnaC replicative helicase, concomitant to the dissociation of the helicase loader DnaB. DnaG promotes the synthesis of RNA primers; this reaction is inhibited in the presence of SSBs (27).

DnaB, DnaD, and DnaI are required to load the helicase at *ori*C and during replication restart. DnaB undergoes proteolysis at its C-terminal in a growth-phase dependent manner, which regulates its interaction with DnaD and its recruitment to *ori*C (28). DnaD has a remodeling activity on supercoiled DNA, creating a protein-DNA scaffold that facilitates docking of DnaA and the initial unwinding (29). The monomeric DnaI ATPase interacts with DnaC and mediates its functional loading on *oriC* by promoting its hexamerization around ssDNA. Both DnaI and DnaB mediate the hexamerization of DnaC (30).

The DnaG primase associates with the helicase to form the primosome that unwinds DNA as it translocates and deposits RNA primers along the ssDNA template. This interaction is mediated by the DnaG C-terminus which activates the ATPase activity of the helicase (31). In *B. stearothermophilis*, the helicase DnaB also modulates the activity of DnaG by reducing the length of the primers. The assembly of the replication machinery is complete when the replicase connects

with the primosome through an interaction between the τ subunits and the helicase. This interaction stimulates helicase activity and is essential for rapid fork progression in *E. coli*. The τ prtein of *B. subtilis* interacts with DnaB of *B. stearothermophilis.* Though the interaction stimulates helicase activity and is essential for for progression in *E. coli*, it fails to stimulate helicase activity but modulates primer synthesis by regulating primase activity through τ-DnaB-DnaG interaction (32).

1.5.2. SSB

During fork pregression, ssDNA corresponding to the template of the lagging strand is generated by the activity of the helicase, and is covered by single stranded DNA binding proteins (SSB). SSBs protect ssDNA from the formation of secondary structures and assist fork progression. Beside their role in DNA binding, SSBs function in fork organization and maintenance.

B. subtilis has two SSB paralogues: SSB and YwpH (SsbB). While *ssb* is transcribed during fast growth and as a response to the SOS response, *ywpH* is induced during competence (33). Like *E. coli* SSB, *Bacillus* SSB binds several helicases known to be involved in re-activation of arrested forks. These are the primary DNA replication restart protein, PriA, and the DNA recombination effectors RecG and RecQ (34). PriA has a helicase activity, can bind to D-loop structures and triggers assembly of the replisome on them (35). DNA also accumulates at active replication forks via interaction with SSB. *B. subtilis* SSB C-terminus interaction network is composed of 12 proteins involved in various DNA metabolism pathways (36).

1.5.3. DNA ligases

In *B. subtilis*, the Okazaki fragments are processed by DNA polymerase I (37, 38), and subsequently joined by a DNA ligase. *B. subtilis* has two ligases: LigA and LigB. While LigA is essential for cell survival and acts on sealing Okazaki fragments processed by PolI, LigB is not essential and participates in DNA non-homologous end joining to repair double strand breaks (39).

1.5.4. Removal of topological constraints

The removal of topological constraints created as the helicase unwinds the double helix is achieved by the action of three DNA topoisomerases: Topoisomerase I (TopA), DNA gyrase (GyrAB), and topoisomerase IV (ParCE), the general DNA binding protein (HBsu), and the SMC-ScpAB complex which is required for DNA condensation and segregation (40-42).

1.5.5. Termination

The two replication forks progress till they reach the terminus region, roughly opposite to the *oriC* on the chromosome map. The terminus region contains multiple Ter sites that act in a polar manner as a "replication fork trap" to prevent the forks from progressing to the opposite arm of the chromosome. In *B. subtilis*, two dimers of the RTP protein bind each Ter site and inhibit the fork helicase, but the mechanism of this interaction is unclear (46, 47) (Figure 1.3). The asymmetry of fork blocking could arise from the different strengths of binding of RTP to the core and auxiliary sites present within Ter sites, of which each can bind an RTP dimer. If the core site is met by the fork first, the fork will be arrested. If the auxiliary site is met first, dimers are displaced and the fork proceeds. Environmental stress induces the accumulation of the guanosinetetraphosphate signaling molecule (ppGpp), which activates a stringent response that shuts down transcription of rRNAs and replication. Replication forks become arrested at around 200 kb from *oriC* at a "replication checkpoint". RTP binding to the checkpoint sites is usually disrupted by transcription through them, which is shut down by ppGpp during the stringent response (48). While the termination system contributes to accurate chromosome partitioning, *rtp* mutants do not exhibit any strong growth phenotypes (46, 47). *E. coli* contains an analogous system of Ter sites even though the RTP homolog in *E. coli*, Tus, shares little homology with RTP (46).

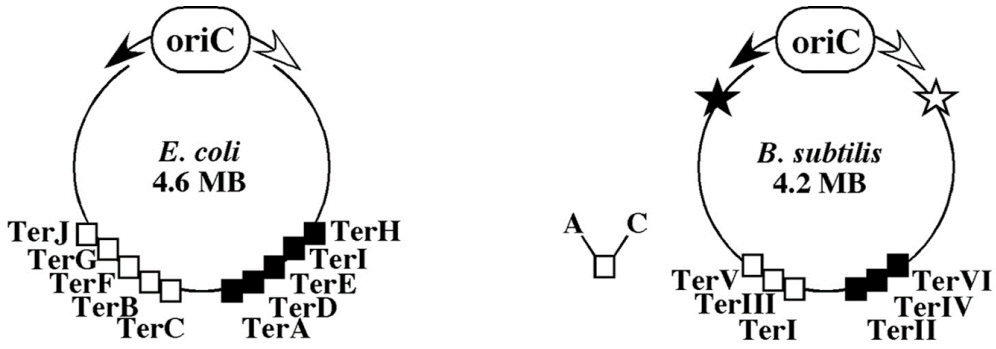

Figure 1.3. Termination of replication. Clockwise (white arrow) and counterclockwise (black arrow) forks start from the bidirectional *oriC*. Ter sites arrest the clockwise (white squares) and the counterclockwise (black squares) forks. Checkpoint replication arrest sites in *B. subtilis* are

indicated by stars: black: arrest of the counterclockwise fork, white: arrest of the clockwise fork. (Figure adopted from Mirkin & Mirkin, 2007).

1.6. Replication restart after accidental arrest

In *B. subtilis* and *E. coli*, each fork must travel more than 2Mbp in a limited time to achieve duplication of the whole chromosome. Any accidental arrest suffered by one of the forks presents a major threat to cell survival. Many pathways evolved to facilitate the restart of arrested forks (49). Assembly of the replisome onto a stalled fork parallels that mediated by DnaA at *oriC*. In both cases, the replicative helicase is the first to be recruited and loaded at the forefront of the replication fork. However, whereas DnaA binds specifically to repeated DNA motifs within the origin, replication restart (RR) proteins recognize specific forked DNA structures. PriA, a helicase, unwinds and remodels forked DNA molecules that present a double-stranded lagging-strand to produce the ssDNA needed for delivery of the replicative helicase. Thus PriA initiates a cascade of events starting with the recognition of arrested forks, followed by the recruitment of DnaD, DnaB, DnaI, and finally the loading of DnaC onto the ssDNA. In combination, DnaB and DnaD can bind SSB coated ssDNA and facilitate the subsequent DnaI-dependent loading of the helicase (50). Three exonucleases RecJ, XseA, and YrrC, also bind to SSB. DnaD, which is the direct partner of PriA, promotes RR in the absence of PriA, suggesting an alternative pathway (51). The helicase loader proteins can also be associated with the highly transcribed rRNA regions. This suggests that DnaD and DnaB act to reload the helicase for replication restart at forks stalled upon encountering RNA polymerases (52). Finally, SSB interacts with DnaE which acts at arrested forks by extending primers laid down by DnaG (53). In *E. coli*, a physical interaction between SSB and RarA and RecO leads to loading of RecA, the central player in homologous recombination. RecA mediates fork rescue after replication arrest (54).

1.7. DNA translesion analysis

Endogenous and exogenous DNA-damaging agents can cause DNA lesions which call for engaging in repair mechanisms. In detrimental conditions, an S.O.S response controlling the expression of repair proteins is activated. Although repair processes can remove most lesions from DNA in an error-free manner, the persistence of non-repaired damages may result in an arrest of the replication fork because the polymerases are unable to incorporate a nucleotide across a non-

instructive damaged base (34). The mutagenesis taking place in both damaged and undamaged sites is increased in cells with an activated SOS response (55). This mutagenesis is due to translesion analysis (TLS), a process mediated by specific polymerases that can synthesize across blocking lesions (56). Lesion bypass is usually highly error prone, producing errors in the newly synthesized DNA opposite to the damage site. The TLS enzymes belong to the Y-family of DNA polymersases. The Y-polymerase displays low fidelity DNA synthesis, low processivity, and low 3'-5' proofreading activity (57). *Bacillus subtilis* has two Y polymerases, PolY1 and PolY2. PolY1 is expressed constitutively at a low level in the normal growth, independently of an SOS response. PolY2, on the other hand, is tightly linked to the SOS response and is responsible for most UV-induced mutagenesis (58). PolY1 also reduces replication stalling in response to transcription of lagging-strand genes. It is responsible for the higher mutation rates of genes on the lagging strand and promotes efficient replisome progression through lagging-strand genes, reducing detrimental breaks and single-stranded DNA at these loci. Without PolY1, transcription is less mutagenic in the head-on orientation of transcription, and consequently, the mutation rate asymmetry of genes in the two orientations of transcription is alleviated. Moreover, association of DnaC, and the recombination protein, RecA, with lagging-strand genes increases in the absence of PolY1 in a transcription-dependent manner. Y-family polymerases can alleviate obstacles to replisome progression by facilitating lesion bypass, extension of D-loops, or excision repair. The nucleotide excision repair (59) proteins UvrA, UvrB, and UvrC, but not RecA, are required for transcription-dependent asymmetry in mutation rates of genes in the two orientations. Furthermore, the transcription-coupling repair factor Mfd functions in the same pathway as PolY1 and is also required for increased mutagenesis of lagging-strand genes (60).

1.8. Chromosome dimer resolution

Faithful segregation of chromosomes prior to cell division is an essential step in the life cycle of all types of cells. While several checkpoints exist in eukaryotes that prevent premature cytokinesis during mitosis (61), in bacteria such *as E. coli* and *B. subtilis*, cell division can occur even when cells fail to achieve the completion of chromosome segregation. For example, in the absence of SMC protein (structural maintenance of chromosomes, or MukB in *E. coli*), the chromosomes are not properly condensed, and are insufficiently separated into daughter cells (62, 63). Cell division

occurs nevertheless, and the chromosomes are trapped within the invaginating septum in a substantial number of cells (64). Chromosome dimers form as a consequence of homologous recombination between sister-chromosomes if an odd number of crossover events occur.

Incompletely segregated chromosomes must be actively transported into the daughter cells to prevent DNA damage. DNA translocases act in a spatially and temporally defined manner and actively move DNA away from the closing septum. The entangled chromosomes must be decatenated, which involves the activity of Topo IV at the division site. Topo IV is the principle enzyme responsible for removing chromosome entanglements and plays a central role in segregation. Chromosome decatenation is the rate-limiting step for segregating the chromosome terminus in *E. coli* (65). Chromosome dimers are resolved by site-specific recombination through the activity of two recombinases at the *dif* sites located near the terminus region: XerC and XerD. In *E. coli*, the DNA translocase FtsK helps complete segregation of the sister chromosomes and brings the newly replicated terminus regions together at the division site. The C-terminal domain of FtsK is an ATP-dependent DNA translocase that moves DNA in a spatially directed manner (66, 67). FtsK arranges the *dif* sites in close proximity at the division septum and directly activates XerD. Directionality of DNA translocation is predetermined by the orientation of short polar sequences on the chromosome (FtsK-orienting polar sequences [KOPS]), which are recognized by the FtsKγ domain and permit the loading of FtsK onto the DNA in one specific orientation (68). KOPS are distributed over the chromosome and oriented toward the terminus region, where they are found at a high frequency (69).

In *B. subtilis*, RipX and CodV are the homologues of XerD and XerC, respectively. They share 35% and 44% sequence identity with their *E. coli* counterparts (70). Both proteins can bind the *dif* site and catalyze strand exchange *in vitro* (71). Two *B. subtilis* DNA translocases are involved in the rescue of DNA trapped by the division septum during vegetative growth: the membrane-associated SpoIIIE and the soluble SftA. Both proteins share substantial sequence identity with the C-terminal domain of FtsK and participate synergistically in dimer resolution through coordinating chromosome segregation and cell division at different stages of the cell cycle (72).

SftA is a component of the divisome. It facilitates dimer resolution by bringing the *dif* sites into close proximity, most likely using a KOPS-like mode for directionality of DNA translocation. SftA translocates DNA during septation, while SpoIIIE is exclusively recruited to rescue septum-entrapped DNA after division is completed (73).

SpoIIIE is a ring-shaped, membrane-anchored, ATP-fuelled motor that segregates DNA across membranes. The process is directional and requires the recognition of highly skewed octameric sequences, SRS, (SpoIIIE recognition sequence) distributed along the chromosome. Pre-assembled SpoIIIE hexamers bind to non-specific DNA, reach SRS/KOPS and activate at SRS. SpoIIIE is essential for sporulation, but not during vegetative growth. However, SpoIIIE becomes indispensable under conditions where chromosome segregation is impaired.

SpoIIIE forms paired DNA conducting channels across fused membranes. DNA translocation occurs through an aqueous DNA-conducting pore that could be structurally maintained by the divisional machinery, with SpoIIIE acting as a checkpoint preventing membrane fusion until completion of chromosome segregation (74). Neither SpoIIIE nor SftA is essential for RipX-dependent recombination at *dif* (47, 71, 75). RipX and CodV form a preassembled complex on the chromosome during the cell cycle, probably to allow an immediate initiation of dimer resolution. The *sftA spoIIIE* double mutant strain has a more severe phenotype than either single mutant, suggesting considerable overlap in their roles (76). Figure 1.4 shows a scheme for the translocases in *B. subtilis.*

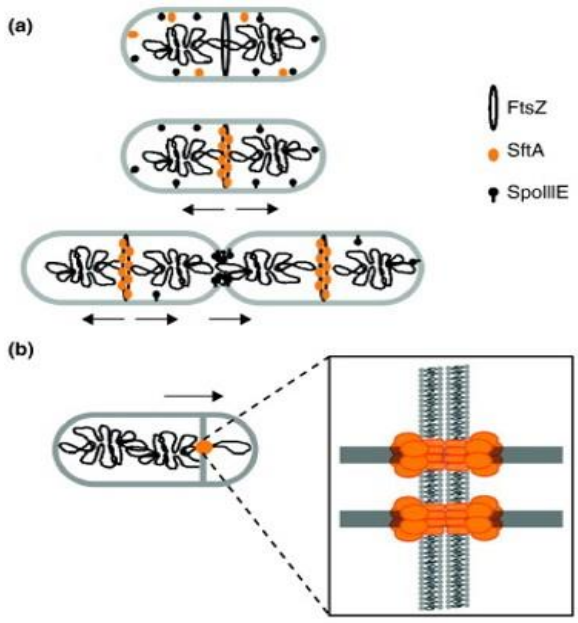

Figure 1.4. A. Function of DNA translocases during the cell cycle. **B.** Model for double hexamers of SpoIIIE translocating DNA into the forspore during sporulation in *B. subtilis*. Arrows indicate

the direction of DNA transport. (Figure adopted from Kaimer & Graumann 2011).

1.9. The divisome

Cell division in bacteria is carried out by about a dozen proteins which assemble at midcell and form a complex known as the divisome. The FtsZ ring assembles early and concomitantly with FtsA, ZapA, and EzrA (77). FtsZ is an essential division protein that forms a contractile ring structure (Z ring) at the future cell division site. The regulation of the ring assembly controls the timing and the location of cell division. FtsZ recruits other cell division proteins to the septum to produce a new cell wall between the dividing cells. It binds GTP and shows GTPase activity (78, 79). FtsA tethers FtsZ to the membrane (79). ZapA is an activator of cell division: it inhibits FtsZ GTPase activity, therefore promoting FtsZ assembly into bundles of protofilaments necessary for the formation of the division Z ring. It is recruited early at mid-cell, but it is not essential for cell division (80). EzrA, on the other hand, is a negative regulator of FtsZ ring formation; it modulates the frequency and position of the FtsZ ring formation, and inhibits FtsZ ring formation at polar sites. It interacts either with FtsZ or with one of its binding partners to promote depolymerization (81). After a time delay of at least 20% of the cell cycle, a second set of division proteins, including GpsB, FtsL, DivIB, FtsW, Pbp2B, and DivIVA, are recruited to midcell (81). Together with EzrA, GpsB plays a role in the elongation–division cycle of *B. subtilis* through controlling the sites of cell wall synthesis. They are involved in the cell cycle dependent localization of the major transglycosylase/transpeptidase, PBP1. EzrA promotes the recruitment of PBP1 to division sites, while GpsB facilitates its removal from the cell pole, after the completion of pole maturation (82). FtsL, DivIB, DivIC, and PBP-2B all have a single transmembrane span and a substantial extracellular domain (83). FtsL acts synergistically with EzrA in the regulation of FtsZ, by promoting FtsZ ring dissociation and constriction (81). DivIB is involved in stabilizing or promoting the assembly of the division complex. It plays an essential role in division at high temperatures, either by protecting FtsL from degradation or by promoting formation of the FtsL-DivIC complex. It is also required for efficient sporulation. It influences the Spo0J/Soj system of chromosome segregation (84-86). FtsW is an essential cell division protein which transports lipid-linked peptidoglycan precursors from the inner to the outer leaflet of the cytoplasmic membrane (87). The essential penicillin-binding protein PBP 2B is required for both the initiation of division and continued septal ingrowth. The recruitment of the protein to the division occurs continually

during septal ingrowth (88). DivIVA directs MinCD to the polar septation sites and inhibits MinCD at the midcell site of division. It ensures correct positioning of the septum and midcell, and is also required for polar localization of the chromosome during sporulation (89). SepF might have a role that overlaps that of FtsA (90). SftA, also part of the divisome, seems to be recruited at an early stage, depending on the initiation of divisome assembly by FtsZ but not on late divisome components like the FtsL/DivIB/DivIC complex (72). Figure 1.5 shows a schematic representation of the *B. subtilis* divisome.

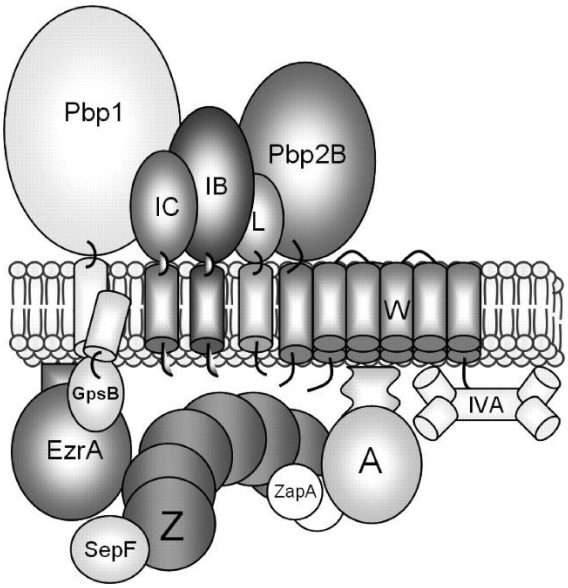

Figure 1.5. *B. subtilis* divisome. Protein names have been abbreviated by excluding Fts and Div. (Figure adopted from Gamba et al., 2009).

1.10. Cellular Organization of the chromosome

The first cytological studies aimed at defining the subcellular localization of chromosomal loci were done in *B. subtilis* (91). Replication initiates at or near mid-cell and newly replicated origins rapidly segregate to the outer edges of the nucleoid. On completion of replication, the nucleoid is organized in a way that the origins are near opposite cell poles, the termini at mid-cell, and the left and right chromosome arms lie between them. How and when the origin moves to mid-cell to initiate a new round of replication is still unknown (92). Thus, chromosomes in *B. subtilis* adopt

an‘ori–ter ter–ori’ layout (93). In *C. crescentus*, the origin and terminus are present at opposite poles, with other loci organized along the axis of the cell in an order correlated with their genomic position. Replication initiates at the pole, and the newly replicated origin rapidly moves to the opposite pole. Replicated loci on the left and right arms follow. Upon completion, the sister chromosomes have an ori–ter, ter–ori organization (94). The right and left arms of the chromosome are symmetric, linearly organized along the ori–ter axis, spatially separated, and twist around each other about one and a half times. Thus, it appears that this bacterium condenses its chromosome along its length (95). In *E. coli*, the origin localizes near mid-cell with the left and right chromosome arms in opposite cell halves. In order to complete the circle, the terminus region spans the length of the cell to bridge the two arms. During and after replication, the sister chromosomes are organized into a left–ori–right, left–ori–right conformation. This organization is consistent with the low frequency of recombination between loci in the left and right macrodomains (Figure 1.6).

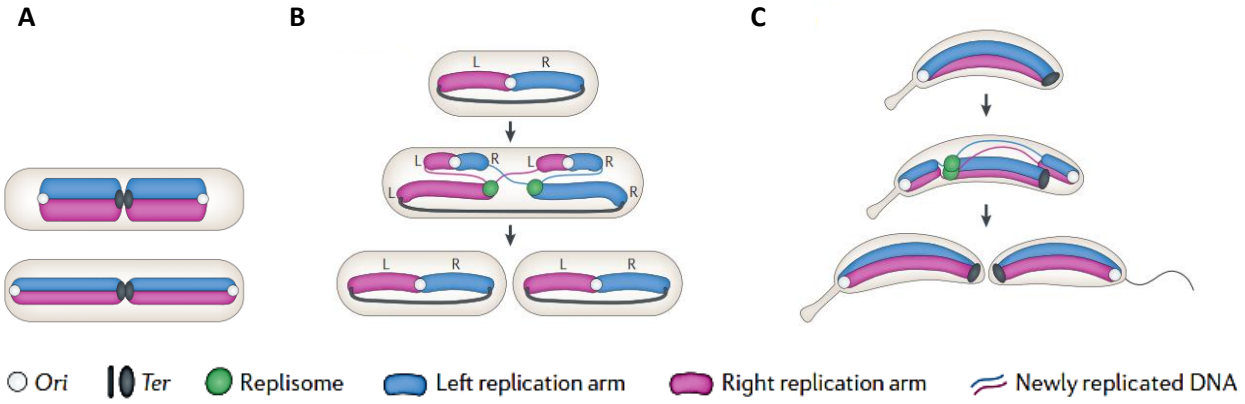

Figure 1.6. Spatial organization of chromosomes in **A**. *B. Subtilis*, **B**. *E. coli*, and **C**. *C. Crescentus.* (Figure adopted from Wu & Errington, 1998).

1.11. Chromosome segregation

The mechanisms that mediate chromosome segregation in bacteria are poorly understood.
The origin attachment model proposed by Jacob, Brenner and Cuzin in 1963 was among the first proposed. It postulates that the two newly replicated origins are tethered to the cell envelope close to mid-cell and separated by cell growth between them. It is now clear that cell elongation in rod-shaped bacteria is not restricted to zonal growth at mid-cell but occurs throughout the cell length. Furthermore, the movement of the origins away from mid-cell is much faster than the rate of cell growth. Thus, this model cannot account for origin segregation.
Despite evidence of dynamic movement of chromosome regions, mitotic-like mechanisms that act on the bacterial chromosome have only been demonstrated in few cases. For instance, the *Vibrio cholerae* ParAI and ParBI proteins are components of an apparatus that pulls the origin region of the large *V. cholerae* chromosome to the cell pole and anchors it there. ParBI interacts with an origin-proximal, centromere-like site (*parSI*) that, following chromosome replication, segregates asymmetrically from one pole to the other. While segregating, *parSI* stretches far away from neighboring chromosomal loci. ParAI forms a dynamic band that extends from the pole to the segregating ParBI/*parSI* complex. Movement of ParBI/*parSI* across the cell occurs in concert with ParAI retraction. Deletion of *parAI* disrupts proper origin localization and segregation dynamics (96) (Figure 5). *Caulobacter crescentus* also segregates its chromosome using a partitioning (Par) apparatus that has surprising similarities to eukaryotic spindles. *C. crescentus* ATPase ParA forms linear polymers *in vitro* and assembles into a narrow linear structure *in vivo*. The centromere-binding protein ParB binds to and destabilizes ParA structures *in vitro*. This ParB-stimulated ParA depolymerization activity moves the centromere to the opposite cell pole through a burnt bridge Brownian ratchet mechanism. In addition, the pole-specific TipN protein is a component of the Par system required to maintain the directionality of DNA transfer towards the new cell pole (97) (Figure 1.7).

1 **2**

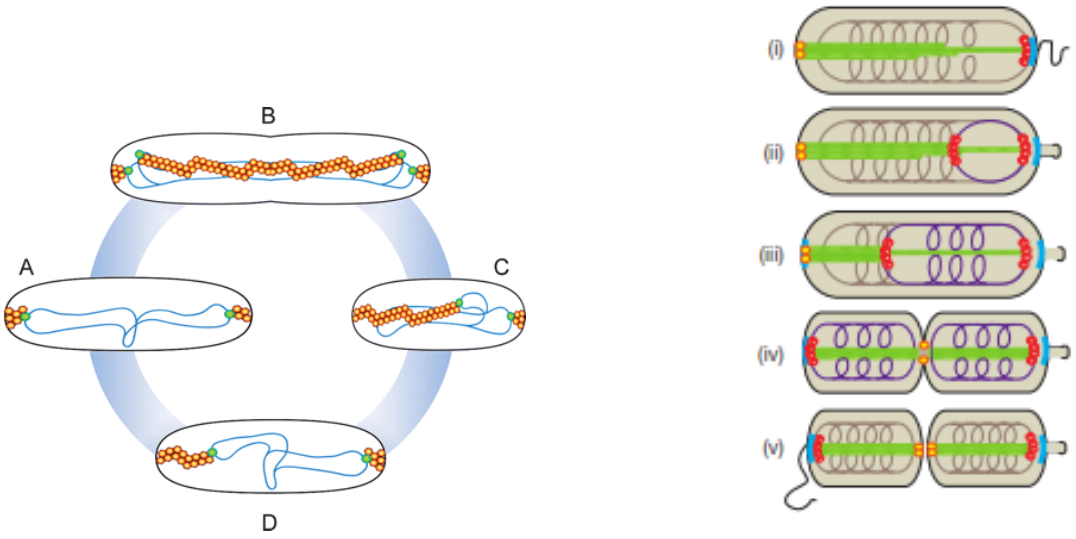

Figure 1.7. Par mediated segregation in **1**. *V. cholera* chrI, *and* **2**. *C. crescentus.*

1. A. The origin region is attached to the pole through an interaction between ParAI and ParBI-*parSI*. **B**. ParAI nucleates at the forming septum and polymerizes toward both poles. One ParB-*parS1* is captured by the ParAI already present at the old pole; the other is captured by the ParAI extending from the closing septum. **C**, **D**. Completion of cytokinesis: ParBI-bound DNA in daughter cells is pulled across the cell by retracting ParAI polymers. (Figure adopted from Fogel et al., 2006).

2. (i) The chromosome associated with ParA is tethered to the old pole via ParB (78) interactions with PopZ (cyan). TipN (yellow) is positioned at the new pole. (ii) The ParB–*parS* complex is released from the pole and duplicated *parS* are bound with ParB. (iii) ParB–*parS* encounters and binds ParA filaments. (24)The ParB–*parS* complex disassembles the ends of some ParA protofilaments, ratcheting along a receding ParA structure, leaving other ParA filaments behind. (v) ParB–*parS* is tethered to the polar PopZ complex. The ParA structure reorganizes, and TipN is recruited to the division site to be positioned for subsequent rounds of segregation (Figure adopted from Ptacin et al., 2010).

1.11.1. Replication factory model

Active DNA replication forks are stationary at midcell while the duplicated chromosome sites are positioned towards opposite cell poles. This supports the factory model in which the replisome pulls the DNA template through itself and releases the duplicated copies outwards (43). The replication factory contains at least two replisomes assembled at two forks, each replicating one half of the chromosome. Time lapse microscopy has showed that the factory is mobile around the cell center, suggesting that it's not rigidly fixed at a specific mid-cell position. A PolC-GPF focus was shown to split into two foci and merge again later, suggesting that the replisomes are able to separate and come back during the round of replication (44). Many regulatory and DNA repair proteins are recruited to the replication factory, supporting the evidence that the chromosome and extra-chromosomal elements replicate at specific intracellular locations in bacteria (45) (Figure 1.8).

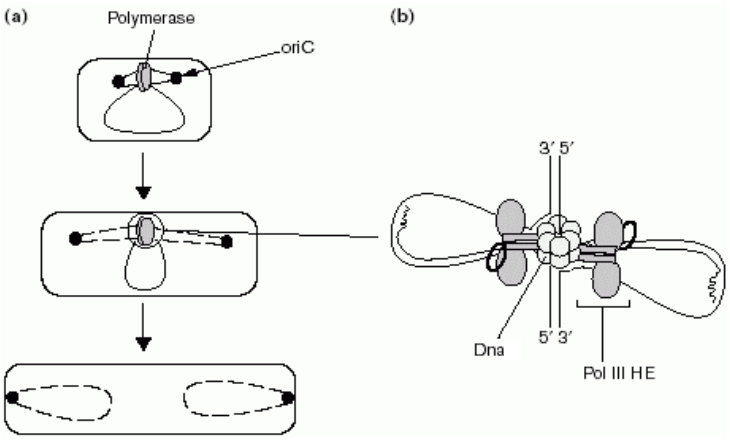

Figure 1.8. The factory model of DNA replication**. A.** DNA pol (grey) does not move, while DNA threads through it, as seen by the migration of the origin (black circles) towards the pole. **B.** Schematic of a replisome, with a double hexameric helicase. For simplicity, the replisomes are drawn before the initiation of lagging strand synthesis. (Figure adopted from Davey & O'Donell, 2000).

1.11.2. The extrusion capture model

It has been proposed that *B. subtilis* harnesses the energy released during replication to power, at least partly, partitioning of newly duplicated chromosomal regions (43). In this model, the replisome pulls the DNA template into the cell center, duplicates it, and then releases the products into opposite cell halves. Movement away from the center is kept orderly by proteins involved in chromosome organization, compaction, and supercoiling. A transient association of newly duplicated DNA with the inner face of the membrane, as suggested for *E. coli* (98), might facilitate origin migration. The force generated during transcription by a single stationary RNA polymerase is ~25 picoNewtons (99), more powerful than either a myosin or kinesin motor. The rate of transcription is 10-fold higher than the rate of translation, and together, DNA polymerase and the replicative helicase can contribute to template movement. The extrusion-capture model postulates that once released outward from the replisome, the origins are captured and held on opposite sides of the cell, possibly via a membrane-associated anchor. The bulk of partitioning can be then achieved by a combination of ongoing DNA replication and chromosome recompaction. Finally, specialized mechanisms exist to ensure that sister terminus regions are not caught in the division septum (47).

1.11.3. Entropy can drive segregation

The immense difference in scale between proteins and chromosomes makes it difficult to understand how the local actions of specific proteins can result in global changes during the organization, decatenation and segregation of chromosomes. This is particularly pertinent to proteins like type II topoisomerases or the SMC proteins (100).

Polymers confined in a box can actively segregate, whereas disconnected but otherwise physically identical particles always mix. Using the terminology of polymer physics, the overlapping chains have fewer conformational degrees of freedom, or less conformational entropy, than the ones that are completely separated. Thus, entropic forces can actively segregate mixed polymers from one another.

2. AIMS OF RESEARCH

Chromosome integrity is maintained through the spatially and temporally coordinated progression of the bacterial cell cycle, and is ensured by several dedicated mechanisms. The major aim of this work was to gain detailed insight into the dynamics of the DNA translocases in *B. subtilis* on the single molecule level. Translocases act at the transition of chromosome segregation and cell division by moving DNA away from the division septum into the daughter cells.

The *E. coli* DNA translocase FtsK has been extensively investigated, and a precise view of its function during cell division, chromosome segregation and dimer resolution has been established. The action of DNA translocases at the division site seems to be a common principle. In *B. subtilis*, the FtsK homologue SpoIIIE has been studied in detail for its role during sporulation, as well as during vegetative growth. Recently, advanced microscopy techniques such as PALM imaging have been deployed to unravel the detailed geometry of the translocation pore. *B. subtilis* has another translocase, SftA, which acts synergistically with SpoIIIE during vegetative growth to clear DNA before septum closure. We were particularly interested in comparing the dynamics of the two proteins in vivo via single molecule tracking, and in gaining an insight into the mechanisms of septal targeting of SftA and the interactions that might be involved in the process.

Another major focus of this work was the replication and chromosome seperation in *B. subtilis*. We tried to see the effect of double strand breaks and temperature on the polyploidy of the microorganism. We also followed with time lapse imaging the separation process of the origin of replication under different conditions in an attempt to get an insight into the mode of the movement and governing the process.

3. General Materials and Methods

3.1. Chemicals and Kits

Unless stated otherwise, chemicals were purchased from Sigma (Seelze, Germany), Roth (Karlsruhe, Germany), AppliChem (Darmstadt, Germany), GE Healthcare (Munich, Germany) or Difco (Lawrence, KS, USA). Endonucleases, PCR-reagents, ligases and other enzymes were purchased from New England Biolabs (Frankfurt a. M., Germany). Kits from Qiagen (Hilden, Germany), Zymo research (Freiburg, Germany), E.Z.N.A (Omega Biotek, USA), or Analytic Jena (Jena, Germany), were used for gel extraction of DNA fragments, plasmid purification (Zymo and E.Z.N.A), PCR product, and chromosomal DNA purification.

3.2. Bacterial growth media and supplements

E. coli and *B. subtilis* cultures were grown in Luria Bertani (LB) medium and LB agar, which were purchased from Roth. The cultures were incubated at either 30°C or 37°C in INFORS-HT multitron shakers (Bottmingen, Switzerland) at 200 rounds per minute (rpm). Protein overexpression was performed in 2 YT medium with incubation at 28 °C only for the SftA protein prior to purification experiments. For microscopy $S7_{50}$ minimal medium was used (101). Tables 3.1 and 3.2 specify the detailed composition of the growth media.

Table 3.1. Composition of LB medium, LB agar, DSM agar, and 2 YT medium

	Components	Concentration
LB medium	Tryptone	10 mg/ml
	Yeast extract	5 mg/ml
	NaCl	10 mg/ml
LB agar	Tryptone	10 mg/ml
	Yeast extract	5 mg/ml
	NaCl	10 mg/ml
	Agarose	15 mg/ml
DSM agar[1]	Difco Nutrient Broth	8 mg/ml
	$MgSO_4$	0.012% (w/v)
	KCl	0.1% (w/v)
	NaOH	1 mM
	Agarose	16 mg/ml
	$Ca(NO_3)_2$	10 mM
	$MnCl_2$	0.1 mM
	$FeSO_4$	0.01 mM
2 YT medium[2]	Yeast extract	10 mg/ml
	Tryptone	16 mg/ml
	NaCl	5 mg/ml

[1]$Ca(NO3)_2$, MnCl2 and $FeSO_4$ were supplemented after autoclaving.

[2]The pH was adjusted to 7.0 with 5N NaOH.

Table 3.2. $S7_{50}$ minimal medium.

	Components	Amount
$S7_{50}$	$S7_{50}$ Salts (10x)	10 ml
	$S7_{50}$ Metals (100x)	1 ml
	Fructose (50%)	2 ml
	Glutamate (10%)	1 ml
	Casaminoacids (1%)	200 µl
	H_2O	Add till 100 ml
$S7_{50}$ Salts (10x)	MOPS	10.47 g
	$(NH_4)2SO_4$ (100 mM)	1.34 g
	KH_2PO_4 (50 mM)	0.68 g
	H_2O	Add till 100 ml
$S7_{50}$ Metals (100x)	$MgCl_2$ (1 M)	20 ml
	$CaCl_2$ (1 M)	7 ml
	$MnCl_2$ (1 M)	0.5 ml
	$ZnCl_2$ (10 mM)	1 ml
	Thiamin-HCl (2 mg/ml)	5 ml

HCl (1 M)	0.2 ml
$FeCl_3$ (1 M)	1 ml

The $S7_{50}$ medium was sterilized by filtration while the other media were sterilized by autoclaving. Antibiotics, inducers, and other additives were supplemented when necessary as indicated in table 3.3.

Table 3.3. Antibiotics and other additives with final concentration.

Antibiotic/Additive	Final concentration
Ampicillin sodiumsalt	100 µg ml^{-1}
Chloramphenicol	5 µg ml^{-1}
Spectinomycin dihydrochloride	100 µg ml^{-1}
Kanamycin sulphate	10 µg ml^{-1}
Tetracycline hydrochloride	10 µg ml^{-1}
Erythromycin	1 µg ml^{-1}
Lincomycin hydrochloride	25 µg ml^{-1}
Xylose	500 µg ml^{-1}
Isopropyl ß-D-thiogalactopyranosid	0.25 µg ml^{-1}
Mitomycin C (MMC)	25-50 ng ml^{-1}
L-Alanine	10 mM

3.3. Preparation and transformation of chemical competent *E. coli* cells

For preparation of competent *E. coli* cells, 400 ml of LB medium were inoculated to a dilution of 1:100 with an overnight culture and incubated at 37 °C in a 200 rpm Infors-HT shaker till an OD_{600} of 0.6 was reached. Cells were incubated for 15 minutes on ice to halt their growth and centrifuged at 500 rpm in a precooled Avanti j-26 XP (Beckman Coulter®) at 4 °C for 10 minutes. The supernatant was discarded and the pellet was carefully resuspended in 2.7 ml ice-cold 0.1 M $CaCl_2$ and 2.3 ml ice cold 50% (v/v) Glycerol. Aliquots of 250 µl were shock frozen in liquid nitrogen and stored at -80 °C. For transformation cells were thawed on ice and plasmid DNA or ligation was added and kept on ice for 20 minutes. The cells were heat-shocked for 1 minute on a 42 °C heating block (Eppendorf) and immediately incubated for another 10 minutes on ice. After addition of 1 ml pre-warmed LB medium, the cells were incubated for 1 hour, 200 rpm at 37 °C. Cells were pelleted in a tabletop centrifuge (Eppendorf 5424 R) and the pellet was resuspended in 70 µl supernatant and plated on LB plate containing the appropriate antibiotics.

3.4. Preparation and transformation of electrocompetent *E. coli* cells

For preparation of electrocompetent cells, a culture was grown in 400 ml LB medium at 37°C to exponential phase (OD_{600} 0.5-0.8), and then incubated on ice for 30 minutes. All following steps were performed on ice or at 4°C. The cells were harvested by centrifugation (10 min at 5000 rpm; centrifuge Avanti J-26 XP (Beckman Coulter) and rotor JLA 9.1000), and subsequently washed with 1 volume and 1/2 volume ice cold, sterile ddH_2O. Cells were then washed once with 8 ml ice cold 10% (v/v) glycerol and finally resuspended in 0.8 ml 10% (v/v) glycerol. Aliquots of 40 µl were shock frozen in liquid nitrogen and stored at -80°C until use. For transformation, an aliquot was thawed on ice and carefully mixed with 10 µl of a ligation reaction (paragraph 3.7.4), which was desalted by dialysis prior to transformation. Cells were transferred into an electroporation cuvette (2 mm, Eurogentech) and electroporation was performed at 2500 V (Easyject prima, Equibio). Immediately after the pulse, 1 ml pre-warmed LB medium was added, and cells were incubated at 37°C for 1 h to allow the expression of resistance genes. Finally, cells were spread on an LB agar plate containing the appropriate antibiotic(s) for selection, and incubated at 37°C.
For the transformation of plasmid DNA, chemical competent cells of *E. coli* strains XL-1 or BL21 were used.

3.5. Preparation and transformation of competent *B. subtilis* cells

At the beginning of the stationary phase of growth, *B. subtilis* develops natural competence (102) and is therefore capable of taking up exogenous DNA. If the DNA contains homologous regions to the genome the DNA is incorporated into the genome. *B. subtilis* can also take us plasmid DNA (103).
For preparation of competent *B. subtilis* cells, 20 ml of SpC-medium (Table 3.4) containing the appropriate antibiotics was inoculated with a *B. subtilis* strain to an OD_{600} of 0.3. The cells were incubated at 30 °C in an Infors-HT shaker with 200 rpm for a minimum of 4 hours till stationary phase was reached. The cells were then diluted 1:5 in spII medium (Table 3.6) supplemented with the appropriate antibiotics and incubated for 90 minutes at 30°C (Infors-HT, 200 rpm). The culture was subsequently centrifuged in an Allegra® X-15R centrifuge (Beckman Coulter) at 4000 rpm and room temperature (20 °C) for 15 minutes. The

pellet was resuspended in 9 ml supernatant and 1 ml glycerol [50% (v/v) in dH_2O], aliquoted and stored at -80°C (102).

Table 3.4. Media used for preparation of competent *B. subtilis* cells.

	Components	Concentration
T-Base (10x)	Ammonium sulfate	0.13 M
	di-Potassium-hydrogen-phosphate	0.8 M
	Potassium-di-hydrogen-phosphate tri-Sodium-citrate	0.5 M
SpC-Medium	T-Base (10x)	1x
	Magnesium sulfate	0.02% (w/v)
	Casaminoacids	0.03% (w/v)
	Yeast-extract	0.2 % (w/v)
	Xylose (strain with P_{Xyl} construct)	0.5% (w/v)
	Fructose (strain with P_{Xyl} construct)	0.5% (w/v)
	Glucose (strain without P_{Xyl} construct)	0.5% (w/v)
SpII medium	T-Base (10x)	1x
	Magnesium sulfate	0.1% (w/v)
	Casaminoacids	0.01% (w/v)
	Xylose (strain with P_{Xyl} construct)	0.5% (w/v)
	Fructose (strain with P_{Xyl} construct)	0.5% (w/v)
	Glucose (strain without P_{Xyl} construct)	0.5% (w/v)
	Calcium chloride	0.5 mM
	Yeast-extract	0.1%

3.6. Isolation of chromosomal DNA from *B. subtilis*

Extraction of *B. subtilis* chromosomal DNA was done with the innuPREP Bacteria DNA Kit from Analytic Jena according to the manufacturer's instructions.

3.7. Construction of vectors

3.7.1 Polymerase Chain Reaction (PCR)

Polymerase chain reaction (PCR) was used to amplify specific DNA fragments. A standard PCR reaction mix contained 33.5 µl water, 10 µl 5xHF Phusion reaction buffer, 1 µl template DNA with a concentration in a range between 10 ng and 100 ng per reaction, 1 µl dNTPs (10 mM), 2 µl

of each primer (12 mM), and 0.5 µl Phusion DNA polymerase (NEB; Frankfurt, Germany). The cycling reaction was performed in a thermocycler (Mastercycler Personal, Eppendorf) using a standard program shown in table 3.5.

Table 3.5. Standard PCR program

Number of cycles	Temperature	Time
10	95°C 95°C X°C (between 50°C and 65°C) 72°C 95°C	2 minutes 30 seconds 30 seconds Z seconds 2 minutes
25	Y °C (between 50°C and 65°C) 72 °C 72 °C 16 °C	30 seconds Z seconds 2 minutes ∞

* The annealing temperatures of the primers (X and Y) depend on the melting temperature which can be calculated depending on the base composition of the oligonucleotides depending on the following formula: 2*n (A/T) + 4*n (G/C). The processivity of the Phusion DNA polymerase is 15-30 s/kb and the extension time Z in the PCR reaction was hence calculated based on the desired length of amplification.

3.7.2. Digestion of DNA by restriction enzymes

Restriction enzymes were purchased from New England Biolabs (NEB; Frankfurt, Germany) and used as indicated in the instructions manual. An enzymatic restriction reaction mix consisted of the following: 30 µl DNA containing the corresponding cutting sites of the used enzyme, 4 µl 10x bovine serum albumin (BSA), 4 µl 10x NEB reaction buffer, 1 µl of each restriction enzyme when more than one was used.

3.7.3. DNA purification

Amplified DNA product or digested DNA was purified with the QIAquick PCR Purification Kit (Qiagen; Hilden, Germany) as indicated by the provided manual.

3.7.4. Ligation

For ligating a vector to a PCR product, the mix was prepared so that the ratio of vector to insert was approximately 1:3. The concentration of the DNA was either measured with a Nanophotometer (Implem GmbH; München, Germany), or visually estimated by running on an Agarose gel. A standard ligation mix contained x µl vector, 3 x µl insert, 1 µl T4 Ligase, 1 µl 10 x Ligase buffer, and the adequate volume of ddH_2O to complete the volume to a total of 10 µl. The reaction was incubated between 16 °C and 20 °C overnight. The ligation reaction was subsequently transformed into competent DH5α or XL1 Blue cells.

3.7.5. Agarose gel electrophoresis

Agarose gel electrophoresis is a technique that allows the separation of DNA fragments by size. Gels were prepared by dissolving 1% (w/v) Agarose in TB buffer (Table 3.6) in a microwave oven. The gel was poured in a cast and left to polymerize. The gel was stained prior to pouring with Midori Green Nucleic Acid Staining Solution (Labgene Scientific; Switzerland). As a marker, commercially pre-stained λ-DNA digested with PstI was used. The DNA samples were loaded in the gel wells and run with 120 V for 30 minutes (Pherostab. 500 Electrophesis Power supply, Biotec-Fischer). For visualization of DNA, the gel was illuminated with UV (UV Transilluminator, UVP) and documented digitally.

Table 3.6. TB buffer and DNA loading buffer recipes

TB buffer	
Tris (hydromethyl) amino methane	0.5 M
Boric acid	0.5 M
6x DNA loading buffer	
Glycerin	20% (v/v)
TB buffer (10x)	6x
Bromophenol blue	0.001% (w/v)

3.7.6. Gel extraction of separated DNA samples

For the cases where one specific band or more had to be purified from an agarose gel, the band was cut out under a UV illuminator and the QIAquick® Gel Extraction Kit (Qiagen; Hilden, Germany).

3.8. SDS PAGE

3.8.1. Sample preparation

B. subtilis or *E. coli* cells were pelleted down by centrifugation (8000 rpm, 5 minutes, RT) and then re-suspended in lysis buffer containing 5mg/ml lysozyme. After and incubation for 20 minutes at 37 °C, the lysate was mixed with 4x SDS loading buffer and subsequently denatured by boiling the sample at 95 °C for 10 minutes. The buffers compositions are shown in the below table.

Table 3.7. SDS-PAGE buffers.

Lysis buffer	
NaCl	100 mM
Ethylenediaminetetraacetic acid (EDTA) pH 8.0	50 mM
4x SDS loading buffer	
Tris-HCL (pH 6.3)	100 mM
Glycerol	10% (v/v)
SDS	2 mg/ml
ß-Mercaptoethanol	3% (v/v)
Bromphenol blue	1 mg/ml

3.8.2. SDS-Polyacrylamide-Gel Electrophoresis (SDS-PAGE)

SDS-PAGE allows the separation of proteins according to molecular weight under denaturating conditions. It is used to visualize and estimate relative amounts and purity of proteins. Gels were prepared following the protocol of Laemmli (104), with a 4% stacking gel acrylamide (v/v) and either 10 % or 12 % running gel. Protein samples were treated with 4 × SDS Loading Buffer and heated at 95°C for 10 min prior to loading. The electrophoresis was carried out in running buffer with an amperage of 20-30 mA (Power source 300V, VWR). The gel composition is shown in table 3.8 below.

Table 3.8. SDS gel composition

	Stacking gel (5%)	Running gel (8%)	Running gel (10%)	Running gel (12%)
Rotiphorese Gel 30 (30% Acrylamid (w/v),0.8% *N-N´*-Methylenbisacrylamid	990 µl	4 ml	5 ml	6 ml
Tris(hydroxymethyl)aminomethane pH 8.8 (1.5 M)	-	3.75 ml	3.75 ml	3.75 ml
Tris(hydroxymethyl)aminomethane pH 6.8 (1 M)	1.875 ml	-	-	-
10% (w/v) Sodiumdodecylsulphate	75 µl	150 µl	150 µl	150 µl
Distilled water	4.5 ml	7 ml	6 ml	5 ml
10% (w/v) Ammonium persulphate	50 µl	75 µl	75 µl	75 µl
N,N,N',N'-Tetramethylethan-1,2-diamin	5 µl	7.5 µl	7.5 µl	7.5 µl

SDS running buffer	
Tris-HCL (pH 8.3)	25 mM
Glycine	250 mM
SDS	1 mg/ml

3.8.3. Staining an SDS gel

For visualization of proteins separated by SDS-PAGE, the gels were incubated with Coomassie staining solution for 1 hour at room temperature on a rotating platform. The gels were subsequently incubated in a destaining solution until excessive dye was removed. For more sensitive staining, the SilverQuest™ silver staining kit from Invitrogen was used instead of the coomassie staining.

Table 3.9. Staining and destaining solutions for SDS gels.

Coomassie staining solution	
Ethanol	25% (v/v)
Acetic acid	20% (v/v)
Coomassie Blue R250	0.25% (v/v)

Destaining solution	
Ethanol	30% (v/v)
Acetic acid	10% (v/v)

3.8.4. Western Blot

Protein immunoblot was used to detect specific proteins. The proteins were first separated by size on an SDS gel, and then transferred on a nitrocellulose membrane using the Bio-Rad Trans-Blot SD semi-dry transfer cell. For this purpose, the gel was placed on three Whatman papers on the cathode of the cell, which had been presoaked in transfer buffer. A water activated nitrocellulose membrane (Immobilon-P, Millipore) was placed on the gel and covered with three additional presoaked Whatman papers. The transfer was carried out with 55 mA for 1.5 h. After transfer, the membrane was incubated overnight in PBST buffer with 3% BSA to block nonspecific sites. Antibodies were added in PBST buffer with 3% BSA to the membrane and incubated for 1 h at room temperature. The membrane was washed three times for 5 min with PBST. When needed, as in the case for the GFP detection, a second antibody (HRP conjugated anti-rabbit antibody) was applied after the series of washing, followed by three washes in PBST. The membranes were then incubated in the dark with the mix of solution A and B for 1-2 min. Finally, the chemiluminescence was detected by imaging with the Bio-Rad Universal Hood III imaging system (Bio-Rad Laboratories, Inc.). Buffers compositions are shown in the below table.

Table 3.10. Western blot and immuno-staining buffer compositions.

Transfer Buffer	
Tris	48 mM
Glycin	38 mM
SDS	0.035%
Methanol	20%

PBST Buffer	
Na_2HPO_4	80 mM
NaH_2PO_4	20 mM
NaCl	100 mM
Tween-20	0.2% (v/v)

Solution A	
Tris	100 mM, pH 8.5
Luminol	2.5 mM
Coumaric Acid	0.4 mM

Solution B	
Tris	100 mM, pH 8.5
H_2O_2	0.02% (v/v)
Coumaric Acid	0.4 mM

3.9. Fluorescence Microscopy

3.9.1 Cell growth and preparation

B. subtilis was cultivated by adding an inoculum from a fresh overnight plate to 5 ml LB and incubating at 30 °C till they reached an OD~ 07-1. The cultures were then diluted 1:20 in $S7_{50}$ minimal medium (101) complemented with 0.002 casamino-acids and incubated at 25°C. For induction of expression of constructs under the xylose promoter, glucose was exchanged for 0.5% fructose, and xylose was added in a range between 0.002% an 0.5%, depending on the experiment. Imaging was always performed on exponentially grown cells with an OD~ 0.5-1.

Observation of living cells requires a supply of nutrients as well as a low background fluorescence. Therefore, 3 µl of cells were mounted on agarose gel pads (1% agarose in $S7_{50}$ minimal medium) that were then placed on top of object slides. The spectral

properties of fluorescent proteins used as markers to image the investigated proteins are specified in table 3.11.

3.9.2. Stains used in fluorescence microscopy

For staining of DNA, 4', 6-diamidino-2-phenylindole (DAPI) was applied to a final concentration of 0.2 ng/ml. DAPI associates with the minor groove of dsDNA, preferentially binding to AT clusters. The advantage of DAPI is in its ability to pass through an intact membrane, making it useful in live cells. Fluorescence was observed by exciting with a UV light (Excitation/Emission 358/461, respectively). Membranes were stained with FM 4-64 (2.5 mg ml^{-1}). FM 4-64 is a non-toxic lipophilic styryl compound. It is excited at 515 nm and detected 640 nm.

Table 3.11 Spectral properties of fluorescent protein markers

Fluorescent protein	Excitation wavelength	Emission wavelength
GFP mut1	488	507
YFP	516	527
CFP	433	475

3.9.3. Image acquisition

Fluorescence microscopy was performed at a Zeiss Axioimager, using 100 × TIRF objectives with a numerical aperture (NA) of 1.45. Images were acquired with a digital EM-CCD camera (Photometrix Cascade). The microscope setup was controlled using Metamorph 6.3 (Molecular devices) software.

4. MANUSCRIPTS

4.1. Manuscript 4A

Accepted

Requirements for septal localization and chromosome segregation activity of the DNA translocase SftA from *Bacillus subtilis*

Nina El Najjar[1], Christine Kaimer[2], Thomas Rösch[1], Peter L. Graumann[1*]

[1]SYNMIKRO, LOEWE Center for Synthetic Microbiology, and Department of Chemistry, Philipps Universität Marburg, [2]Fakultät für Biologie und Biotechnologie, Lehrstuhl Biologie der Mikroorganismen, Ruhr-University Bochum, Germany

*corresponding author, email: peter.graumann@synmikro.uni-marburg.de

49(0)64212822210

Abstract

Bacillus subtilis possesses two DNA translocases that affect late stages of chromosome segregation: SftA separates non-segregated DNA prior to septum closure, while SpoIIIE rescues septum-entrapped DNA. We provide evidence that SftA is associated with the division machinery via a stretch of 47 amino acids within its N-terminus, suggesting that SftA is recruited by protein/protein interactions with a component of the division machinery. SftA was also recruited to mid-cell in the absence of its first 20 amino acids, proposed to contain a membrane-binding motif. Cell fractionation experiments showed that SftA can be found in the cytosolic, and to a minor degree in the membrane fraction, showing that it is a soluble protein *in vivo*. The expression of truncated SftA constructs led to a dominant *sftA* deletion phenotype, even at very low induction rates of the truncated proteins, indicating that the incorporation of non-functional monomers into SftA hexamers abolishes functionality. Mobility shift experiments and surface plasmon binding studies showed that SftA binds to DNA in a cooperative manner, and showed low ATPase activity when binding to short nucleotides rather than to long stretches of DNA.

Introduction

Bacterial cell division occurs with remarkable fidelity across a wide range of environmental conditions. However, certain types of stress can damage DNA and disrupt the normal progression of the replication fork. Therefore, cells have evolved pathways that coordinate the process of cell division with DNA replication. This ensures that cell division occurs reliably even when segregation is perturbed [Crozat et al., 2014; Kaimer and Graumann, 2011a]. DNA translocation is also important for the resolution of chromosome dimers, which occur in 15% of the cells due to uneven recombination events between sister chromosomes [Crozat et al., 2014], and which lead to a block in the cell cycle.

In *E. coli*, the membrane-integral ATP dependent translocase FtsK is recruited as a regular component of the division septum via its N-terminal domain, which is essential for cell division. The protein is anchored in the membrane via its central membrane spans, and its C-terminal domain mediates DNA translocation. FtsK functions in segregating sister chromosomes during the late stages of the cell cycle in a wide range of bacteria [Barre, 2007; Bigot et al., 2007; Stouf et al., 2013] through activating site-specific recombination by XerCD at *dif* [Aussel et al., 2002]. The motor domain, $FtsK_C$, is composed of α-, β-, and γ-subdomains. The α- and β-subdomains form a dsDNA translocase [Massey et al., 2006]. The γ-subdomain plays a role in the recognition of the FtsK orientating polar sequence (KOPS) that guides FtsK toward the *dif* site at *ter* [Sivanathan et al., 2006], as well as in the activation of XerCD-*dif* recombination [Aussel et al., 2002]. KOPS are distributed over the chromosome and oriented toward the terminus region, where they are found at a high frequency [Bigot et al., 2005; Bobay et al., 2012]. FtsK arranges the duplicated *dif* sites in close proximity at the division septum facilitating dimer resolution [Bigot et al., 2005].

Activation of recombination requires direct interaction between the γ-subdomain and XerD [Yates et al., 2006]. XerC and XerD bind the *dif* site located within the terminus region, *ter*, unlink catenated chromosomes, and resolve chromosome dimers formed by homologous recombination [Barre and Sherratt, 2005; Grainge et al., 2007; Hallet and Sherratt, 1997; Sherratt et al., 1995].

Single molecule experiments using DNA curtains revealed that $FtsK_C$ can push, evict, and bypass proteins bound to DNA as it translocates. $FtsK_C$ stops at least transiently and/or dissociates at XerCD bound to *dif* [Collins et al., 2014; Graham et al., 2009; Lee et al., 2014]. FtsK locates KOPS through random collisions, preferentially in the ADP-bound state, and is incapable of

recognizing KOPS while translocating along DNA [Lee et al., 2012]. Reversals in translocation direction were previously reported to occur spontaneously and in response to XerCD bound to *dif* [Lee et al., 2012; Pease et al., 2005]. However, in a recent study employing singly tethered labeled DNA, as well as labeled $FtsK_C$, $FtsK_C$ translocation and its interaction with synaptic complexes of XerCD on the single molecule level was observed. $FtsK_C$ seemed to assemble on DNA as a single hexamer, which then translocated rapidly. Upon reaching XerCD bound *dif*, whether in a synapsed or unsynapsed conformation, it resided briefly and then dissociated without reversal. $FtsK_C$ activated recombination when it met synapsed XerCD-*dif* complexes, and then dissociated before the completion of recombination by XerCD [May et al., 2015].

In *Bacillus subtilis*, RipX and CodV are the homologues of XerD and XerC, respectively, and share 35% and 44% sequence identity with their *E. coli* counterparts [Sciochetti et al., 1999]. Both RipX and CodV were reported to bind to the *B. subtilis dif* site and to catalyze strand exchange *in vitro* [Sciochetti et al., 2001].

Two *B. subtilis* DNA translocases share homology with FtsK and are involved in the rescue of DNA that might become trapped by the division septum during vegetative growth: the membrane-associated SpoIIIE protein and the soluble SftA protein. The two proteins participate synergistically in dimer resolution through coordinating chromosome segregation and cell division at different stages of the cell cycle in *B. subtilis* [Kaimer et al., 2011]. SftA is a component of the divisome. It translocates DNA during septation, while SpoIIIE is exclusively recruited to rescue septum-entrapped DNA after division is completed [Biller and Burkholder, 2009; Kaimer et al., 2009; Sharpe and Errington, 1995].

Localization in different genetic backgrounds indicated that SftA is probably recruited as an early divisome component [Biller and Burkholder, 2009; Kaimer et al., 2009; Sharpe and Errington, 1995]. Biochemical characterization showed that the full-length protein forms hexamers, but the isolated C-terminal translocase domain was monomeric, which means that it is the N-terminus that is capable of favorising hexamerization [Kaimer et al., 2009]. In *E. coli*, it was shown that 50 residues overlapping the N-terminus and the linker region were involved in the stabilization of an active hexameric form of the protein [Aussel et al., 2002]. Though the C-terminal domain of SftA (residues 490-952) shares 50% and 56% identity to DNA translocases FtsK and SpoIIIE respectively, including the ATP and DNA binding motifs, the glutamate and proline rich N-terminus (residues 1-439) shows no homology to any of these translocases [Kaimer

et al., 2009; Kaimer and Graumann, 2011b]. While no transmembrane spanning regions were predicted, a recent review suggested the existence of three putative N-terminal transmembrane helices based on BlastP analysis of 2,385 sequences of FtsK homologues thought to lack a transmembrane domain [Crozat et al., 2014]. SftA localization at midcell depends on the initiation of cell division by FtsZ and is most likely based on direct protein-protein interaction via its N-terminal domain.

In this work, we investigate the specific region of SftA required for septum recruitment, as well as the *in vitro* DNA binding and ATPase activity of the protein. We find that SftA contains a region within its N-terminus that is required for stable anchoring at the septum. We also show that SftA binds cooperatively to DNA, in agreement with its formation of DNA-binding hexamers.

Results and discussion

SftA is a soluble protein

SftA can be produced as a soluble enzyme in vitro. To test if SftA is membrane-attached, or also soluble, *in vivo*, we performed cell fractionation experiments. Fig. 1A shows that SftA is predominantly present in the soluble fraction of *B. subtilis* exponential cells, with a minor fraction of the protein being associated to the membrane. As controls, SpoIIIE, a membrane-integral DNA translocase, and PfkA, a soluble glycolytic enzyme (phosphofructokinase), were used [Burton and Dubnau, 2010; Ludwig et al., 2001]. As expected, SpoIIIE was exclusively found in the membrane fraction, while PfkA was solely in the cytosol (Fig. 1A). The same experiment was done in parallel on *E. coli* BL21 cells harboring a vector containing a His-tagged SftA. The protein was once again detected in the cytosolic fraction, as well as in the membrane fraction but to a much lesser extent (Figure 1B). These experiments show that SftA is largely soluble within the cell.

47 amino acids of the N-terminus of SftA can localize the protein to mid cell in *Bacillus subtilis*

In order to narrow down the region of the N-terminus responsible for septal localization, the domain was truncated into fragments of decreasing length and the localization pattern of each construct was investigated in *Bacillus subtilis*. The fragments were cloned into pSG1164y, were integrated into the *B. subtilis* chromosome and were expressed from the original gene locus. Thereby, truncated SftA variants are expressed under the control of the original promoter, while full length SftA can be expressed by the xylose promoter that is inside pSG1164y. A map depicting the vector construction and integration is displayed in supplementary figure S1. All the truncations were chosen at random. The N-terminus of SftA ($SftA_{(1-439)}$-YFP) showed a normal septal localization pattern in *B. subtilis* when expressed from the *amyE* locus (Fig. 2B). Figure 2A shows a map of the various truncations included in this study, while figure 2B-I shows the localization of these truncations. The first 246 residues ($SftA_{(1-246)}$-YFP) showed a localization pattern similar to that of the wild type protein (Fig. 2D). Fluorescence was detected in all cells, and the truncation localized to the new septum in 50% of the cells, and to the cell middle in 31% of the cells, mostly forming two adjacent dots within the membrane, while 19% of the cells (n=400) showed faint

lateral fluorescence (Fig. 2D). Of note, 4 to 5% of the cells expressing the truncation showed segregation defects, e.g. non segregated nucleoids in cells larger than 3.7 µm, which is never observed in wild type cells, suggesting that the presence of a SftA truncation interferes with the function of wild type SftA (see below).

$SftA_{(1-137)}$-YFP also localized normally (Fig. 2E). The same was observed for a shorter truncation whereby $SftA_{(1-105)}$-YFP also localized to the septum in 48% of the cells, the cell middle in 26%, and the rest showed lateral localization (n=500) (Fig. 2F). $SftA_{(1-67)}$-YFP also localized in around 60% of the cells (n=372), mostly to the new septa and to mid-cell (Fig. 2G).

It is possible that a fragment of the N-terminus of SftA can localize through hexamerization with full length SftA. The original copy of the gene was deleted in two different truncation-variant strains in order to investigate the role of complex formation with full-length protein. The truncations 105 and 67 were cloned each into pSG1193y and were integrated into the *amyE* locus via a double crossover event. The original s*ftA* was deleted by transforming the resulting *B. subtilis* truncation strains with genomic DNA from strain CK 150 (*sftA::tet*) [Kaimer et al., 2009]. The strains were grown to exponential phase in $S7_{50}$ fructose, induced with 0.05% xylose for one hour and then analyzed. The 105 base pairs truncation ($SftA_{(1-105)}$-YFP) localized to the septa and mid-cell both before and after deletion of the original s*ftA* in rates of 79% (n=400) and 85% (n=300), respectively (Fig. 2F and Fig. 2H). Likewise, the 67 residues long fragment ($SftA_{(1-67)}$-YFP) localized normally when expressed from the *amyE* locus in the presence of a full-length original copy of the gene, foci were detected in 88% of the cells (n=318) (Fig. 2G). The deletion of the original *sftA* did not affect this localization pattern (Fig. 2I). This finding suggests that the first 67 residues of the SftA N-terminus are capable by themselves of an interaction with an unidentified partner that integrates the protein into the septum early in cell division. Deleting the foremost 20 residues of the N-terminus of SftA also did not affect the localization (Fig. 4A). A truncation $SftA_{(20-105)}$-YFP was capable of localizing normally, whether in a wild type or an *sftA* deletion background (Fig. 4B and Fig. 4C). $SftA_{(20-67)}$-YFP, localized normally in a wild type background, but showed an aberrant localization in the deletion background, whereby foci were only seen in 50% of the cells (Fig. 4D and Fig. 4E), in contrast to 80% for full length SftA-YFP. This experiment shows that the stretch between 20-67 residues is sufficient for normal septal targeting, and suggests that hexamerization with wild type SftA contributes to mid-cell recruitment. Deleting the first 60 obliterated septal recruitment (Fig. 4G), and the truncations shorter than 67 residues

did not localize, as is seen in figure 4 panels H and I**,** for $SftA_{(1-50)}$-YFP and $SftA_{(1-34)}$-YFP, respectively. It has been shown for FtsK in *E. coli* that the protein lacking all transmembrane segments still allows the efficient resolution of chromosome dimers if it is connected to a septal targeting peptide through a sufficiently long linker. This means that a direct membrane insertion is not needed for functional translocation [Dubarry and Barre, 2010], but an efficient septal targeting is.

Stoichiometry and functionality

For all the truncation strains mentioned so far, the phenotypic outcome of their expression was similar to that of an *sftA* deletion, whether an original copy of the gene existed or not: all of the merodiploid strains had DNA trapped by a septum or showed non-segregated nucleoids in cells larger than 3.7 μm in about 5% of all cells, indicative of a segregation defect, and a subset of elongated cells, all typical for an *sftA* deletion (Fig. 2, table 1). To confirm the idea that the incorporation of a truncated SftA monomer into a hexamer abolishes functionality, the corrected fluorescence of $SftA_{(1-105)}$-YFP foci was calculated in the presence of an intact untagged SftA, expressed from the original locus, and was compared to the fluorescence of the same truncation after deletion of the original locus. Both strains were induced with 0.05% xylose. As can be seen in figure 3, the intensity of the foci, though they showed a lot of fluctuations, was lower in the wild type strain expressing $SftA_{(1-105)}$-YFP (from the *amyE* locus) than in the Δ*sftA* strain expressing the same truncation, suggesting that most of the hexamers present at mid-cell consist of a mixture of the truncated and the intact copies of SftA, which disrupts the function of the hexamer in DNA segregation. To test whether stoichiometry affects the function of the SftA hexamer, different xylose concentrations were used to titrate the truncation in the *amyE*::$sftA_{(1-105)}$-*yfp* strain. Results are summarized in table 1 and figure 5. Western blot analysis was performed with anti-GFP antibodies to detect the expression level of the truncation. In comparison, a strain expressing SftA-YFP from its native promoter was used as a control (Fig. 6). Even at very low induction level (0.02% xylose), the phenotype of the *amyE*::$sftA_{(1-105)}$-*yfp* was still similar to that of a deletion (Fig. 5), though the expression level of the truncation is considerably lower than that of the protein under control of the native promoter (22% as calculated by the band intensity in the western blot and shown in Fig. 6). This could be the outcome of one of two underlying causes: either the slightest disruption of the stoichiometry of the active hexamer leads to a loss of function, or the

short truncations are more favorably incorporated into the hexamer than full length SftA, ultimately disrupting the function; we hold the prior possibility for the more likely one.

Conversely, a study using linked monomers of *E. coli* FtsK showed that two inactive subunits (Walker A or B mutants) within a hexamer did not impair translocation speed, suggesting that several motor subunits must interact with DNA at any time [Crozat et al., 2010]. Another mechanism has been proposed for dsDNA translocases including FtsK and SpoIIIE in which the double-stranded DNA revolves inside a channel formed by the protein, without modifying DNA supercoiling [De-Donatis et al., 2014]. However, the mechanism implies a loss of activity when one subunit is mutated in the ring [Schwarz et al., 2013], which appears in contradiction with the translocation activity retained by a hexamer of FtsK containing two opposed inactive subunits [Crozat et al., 2010].

Interaction of SftA with short double stranded DNA fragments

The capacity of SftA to interact with DNA was tested by gel shift experiments [Kaimer et al., 2009] and surface plasmon resonance. FtsK and SpoIIIE bind to DNA in a non-specific manner, and show high affinity to specific short polar sequences (KOPS) to confer directionality during DNA translocation [Bigot et al., 2005].

Gel shift experiments were performed in order to determine the formation of a stable protein-DNA complex between purified SftA and short DNA fragments. Increasing concentrations of SftA were incubated with 4 pmol of a 60 bp double stranded oligonucleotide, either containing 3 copies of the conserved KOPS sequence (5´-GGGNAGGG-3’), or containing no KOPS. The formation of a slowly migrating protein DNA complex was observed, and was dependent on the concentration of SftA (Fig. 7A). A clear binding preference towards the KOPS-containing fragment could not be detected in this experiment. However, SftA showed cooperativity in DNA binding: a two fold increase in the concentration of SftA, from 12 to 24 pmol, resulted in a drastic increase in SftA/DNA complexes (best seen by the strong reduction in the intensity of the non-bound DNA band), while further increases in protein concentration did not yield a similar enhancement of binding (Fig. 7A).

In vitro studies with FtsK showed that, in isolation, the γ domain preferentially binds to the KOPS over random DNA [Nolivos et al., 2012; Sivanathan et al., 2006]. SpoIIIE was also shown to prefer SRS-containing DNA to random DNA nearly by a factor of 3. This was measured using

30 bp long fragments either containing 2 KOPS sequences, or none [Besprozvannaya et al., 2013]. However, in a conflicting study [Cattoni et al., 2014] that investigated the mechanism of DNA binding by SpoIIIE using a combination of single-molecule, biochemical and structural methods, it was shown that SpoIIIE is able to associate to non-specific DNA with high affinity but no specificity. The DNA binding was unaffected by ATP binding or hydrolysis. Through AFM imaging, SpoIIIE was shown to bind dsDNA as pre-assembled hexamers without requiring a free DNA end. This is more similar to our findings for SftA, and could mean that the translocase is probably loaded onto the chromosome anywhere without sequence specificity, and KOPS or SRS sequences are merely important for loading into the correct orientation.

For further characterization of the SftA-DNA interaction, surface plasmon resonance was performed in order to follow the binding of purified SftA to DNA immobilized on a sensor chip. A 1500 bp PCR fragment biotinylated at the 5´end was coupled to the sensor chip via a biotin-streptavidin interaction. Injection of SftA at different concentrations led to a clear association curve with larger responses at higher protein concentrations (Fig. 7B). Upon washing, dissociation was observed, demonstrating a reversible binding-unbinding equilibrium. Interestingly, the response increased in a non-linear fashion with the concentration of SftA, whereby an increase from 1.5 µM to 2 µM resulted in a much higher response than from 1 µM to 1.5 µM (Fig. 7B). This confirms the results obtained in the gel shift assay that SftA binds DNA in a cooperative manner, either during hexamerization, or due to contact between hexamers. Similarly, SpoIIIE was shown to bind DNA as pre-assembled hexamers [Cattoni et al., 2013].

ATPase activity assay

We have previously shown that SftA can bind to DNA without any sequence specificity, that a hexamer is needed for successful binding since the purified C-terminal failed to achieve detectable binding in gel shift assays, and that binding to circular plasmid DNA induces an ATPase activity that is comparable to SpoIIIE and FtsK [Kaimer et al., 2009].

We next tested if KOPS containing 60 bp-fragments are sufficient to induce ATPase activity in a coupled enzyme assay. A clear increase of the ATP hydrolysis rate was observed in the presence of increasing DNA concentrations (Fig. 7C). However, only a maximal rate of approximately 1.5 ATP/monomer/s was measured (Fig. 7D). Kaimer *et al.* [Kaimer et al., 2009] observed a 6.5 fold

higher ATPase activity when supercoiled plasmid DNA was used, with same molecular amount of base pairs.

This reduced activity is possibly explained by the functional mechanism of DNA translocases: if SftA indeed moves fast along DNA in an ATP dependent manner, as is claimed for FtsK [Bigot et al., 2005] and SpoIIIE [Besprozvannaya et al., 2013], the protein would rapidly reach the end of a short fragment and dissociate. ATP hydrolysis would drop to a very low rate until re-association with DNA, which again induces increased ATPase activity. When short linear DNA fragments are present, the overall ATP hydrolysis rate would therefore be reduced due to permanent dissociation and re-association, which is avoided when longer or circular DNA is available as a substrate. Interestingly, we observed a similar maximal ATP hydrolysis rate of 1.7 ATP/monomer/s for the isolated C-terminal domain SftA-C with circular plasmid DNA as substrate [Kaimer et al., 2009]. It was reasoned that the C-terminal domain, which is not able to oligomerize, cannot establish a stable interaction with DNA and therefore also rapidly dissociates. So in both cases, measurements probably reflect a reduced ATPase activity because the protein-DNA interaction remains transient. However, Besprozvannaya *et al.* [Besprozvannaya et al., 2013] showed that SpoIIIE exhibits length-dependent ATPase activity in which case 61-bp DNA fragments were determined as the minimal dsDNA fragment length that stimulates maximal ATPase activity. This seems not to be the case for SftA where longer fragments are indeed required.

Conclusions

Our data show that the short region from amino acid 20 to 67 is sufficient for targeting SftA to the division site, suggesting that SftA is a bona fide component of the division machinery that is recruited by a protein-protein interaction. The deletion of 20 amino acids from the N-terminus did not abrogate recruitment to mid-cell, indicating that SftA is likely not a membrane-integral protein, but truly cytosolic when not present at the division septum. This was confirmed by cell fractionation experiments, showing that SftA is a largely soluble protein, with a minor fraction being associated with the membrane, most likely through the interaction with a truly membrane-associated protein.

Moreover, we show that SftA binds cooperatively to DNA, which is reflected by a non-linear increase in DNA binding with increasing protein concentrations. This is in agreement with the finding that SftA forms stable hexamers, so a certain threshold of its concentration will enable

stable DNA binding within the hexameric assembly. In a previous study we showed that SftA has a high ATPase activity that is comparable to SpoIIIE and FtsK when a circular plasmid was used as a substrate [Kaimer et al., 2009]. However, with short DNA fragments of just 60 bp, ATPase activity is considerably lower, suggesting that SftA performs large processive translocation events and rapidly dissociates from short DNA molecules.

Our experiments show that despite the fact that SftA bears many similarities to SpoIIIE and FtsK in terms of sequence and function, some distinct features may be important for its role as a DNA pump prior to septum closure. Unlike FtsK and SpoIIIE, SftA seems to be soluble, and is recruited to the septum via another component of the divisome. While the N-terminal regions of SpoIIIE and FtsK contain each 4 transmembrane helices that incorporate them into the membrane [Liu et al., 1998; Yu et al., 1998], only a short span within the N-terminus of SftA is required to target it to the division septum. Since the deletion of SftA and that of a Walker A mutant have the same phenotype [Kaimer et al., 2009], we suggest that the N-terminal part of SftA has no intrinsic function other than mid-cell targeting. This is in contrast to *E. coli* FtsK where a mutation within a loop in the N-terminus resulted in uncoupling invagination of the inner and outer membranes [Berezuk et al., 2014].

SftA forms hexamers *in vitro*. Interestingly, our localization experiments show that the function of the protein is lost when the hexamer is disrupted by the incorporation of a truncated version of the protein, suggesting that to transport DNA, the C-terminal domains perform (possibly sequential) power strokes that do not permit the omission of one of the six domains. In contrast to this, SpoIIIE can still pump DNA if the hexamer contains a non-functional subunit [Liu et al., 2015].

SftA assists in the resolution of chromosome dimers, but is not required to activate the recombinases, and deletion leads only to a mild segregation defect [Kaimer et al., 2011]. FtsK, seems to play a broader role where it has been shown to link division to segregation and to contribute actively to segregating the terminus region of chromosomes, irrespective of dimer formation [Stouf et al., 2013].

SftA, like FtsK, is present in most cells in the division septa, and is recruited as an early component of the divisome [Kaimer et al., 2009]. SpoIIIE on the other hand is not generally recruited to the division machinery, but assembles at sites where DNA becomes trapped within the

septal membranes. Additionaly, SpoIIIE plays a major role during sporulation where it promotes chromosome translocation to the forespore in addition to membrane fission [Shin et al., 2015].

Materials and Methods

Growth conditions

Bacterial strains and plasmids used in this study are listed in table 2, oligonucleotides in supplementary table S1. *Escherichia coli* strain XL1-Blue (Stratagene) was used for the construction and propagation of plasmids and *E. coli* strain BL21 Star DE3 (Invitrogen) for heterologous overexpression of proteins. All *B. subtilis* strains were derived from the prototrophic wild type strain PY79. Cells were grown in Luria–Bertani (LB)-rich medium at 37°C or 30°C, or in minimal medium containing $S7_{50}$ salts [Jaacks et al., 1989] at 25°C. Media were supplemented with antibiotics where appropriate (ampicillin 100 mg ml^{-1}, chloramphenicol 5 mg ml^{-1}, spectinomycin 100 mg ml^{-1}, kanamycin 10 mg ml^{-1}, tetracyclin 10 mg ml^{-1}).

Strain construction

Strain *amyE::sftA$_{(1-439)}$-yfp* was obtained by cloning the N-terminal region of SftA into the *Apa*I and *Eco*RI sites of pSG1193y [Lewis and Marston, 1999] which integrates at the amylase locus by a double-crossover event.

Strains bearing fluorescent truncation variants of SftA (*sftA$_{(1-246)}$-yfp*, *sftA$_{(1-137)}$-yfp*, *sftA$_{(1-105)}$-yfp*, *sftA$_{(1-67)}$-yfp*, *sftA$_{(1-34)}$-yfp*, and *sftA$_{(1-50)}$-yfp*) were constructed by cloning for each construct a corresponding 500-bp fragment of the SftA N-terminal, into the *Apa*I and *Eco*RI sites of pSG1164y [Kidane et al., 2004] and by transformation of PY79 with the resulting vector which integrates at the original locus of the gene by a single-crossover event. Each of the created strains expresses a part of the N-terminal region of SftA fused to a yellow fluorescent protein (YFP) from the native promoter. For the truncation copies that are shorter than 500-bp, a region upstream of the coding sequence was included in the construct in a way that the total length of the cloned region was always around 500-bp. A full copy of the gene was still present and expressed from the xylose promoter of the vector.

To obtain an *sftA::tet* deletion in a truncation background (a*myE::sftA$_{(1-105)}$-yfp sftA::tet and amyE::sftA$_{(1-67)}$-yfp sftA::tet*), the SftA fragments were first cloned each into the *Apa*I and *EcoR*I sites of pSG1193y. PY79 was transformed with the vectors. Chromosomal DNA of CK150 [Kaimer et al., 2009] was used for transformation of PY79 competent cells of the generated truncation-containing strains. Deletion was confirmed by test-PCR, and strains were microscoped

at exponential phase after induction with 0.1% xylose. Constructs a*myE::sftAN*$_{(21\text{-}439)}$*-yfp* and a*myE::sftAN*$_{(61\text{-}439)}$*-yfp* were created by cloning the N-terminal fragments of SftA which are missing the first 20, and the first 60 amino acids, respectively, between the *Apa*I and the *Eco*RI sites of pSG1193y. The plasmids were transformed into cells of competent *sftA::tet* strain.

Cell fractionation experiments

Cell fractionation experiments were done according to the protocol by Zweers et al., 2009. Briefly, Cells were grown overnight in LB medium, collected by centrifugation, and resuspended in protoplast buffer (100 mM TrisHCl, pH 8.2, 20 mM $MgCl_2$, 20% sucrose, 1 mg/ml lysozyme, 0.01% DNase, and Complete protease inhibitors). After a 30-min incubation at 37°C, the cell wall fraction was separated from the protoplasts by centrifugation (10 min, 4,000 x g, 4°C). Protoplasts were resuspended in disruption buffer (50 mM Tris-HCl, pH 8.2, 2.5 mM EDTA) and disrupted with a French press. Cellular debris were removed by centrifugation (10 min, 4,000 x g, 4°C), and the supernatant was ultracentrifuged (30 min, 200,000 x g, 4°C). Next, the supernatant fraction with the cytosolic proteins was collected. The pellet was resuspended in solubilization buffer (20 mM Tris, pH 8.0, 10% glycerol, 50 mM NaCl, 0.03% DDM [n-dodecyl-β-maltoside]) and incubated overnight at 4°C. Solubilized membrane proteins were collected by centrifugation in the supernatant (15 min, 100,000 x g, 4°C). The fractions thus obtained were analyzed by SDS-PAGE and Western blotting.

Fluorescence microscopy

For fluorescence microscopy, *B. subtilis* cells were grown in $S7_{50}$ minimal medium at 25°C under shaking conditions until exponential growth. 3 µl of cells were transferred on an agarose slide - glass slide (Microscope slides standard, Roth) coated with an agarose layer ($S7_{50}$ minimal medium, 10 mg/ml agarose) - and covered with a cover slip (Cover slips, Roth). Conventional light microscopy was performed using a Zeiss Observer Z1 (Carl Zeiss) with an oil immersion objective (100 × magnification, 1.45 numerical aperture, alpha Plan-FLUAR, Carl Zeiss) and a CCD camera (CoolSNAP EZ, Photometrics), or with a BX51 microscope (Olympus) with a Cool Snap EZ camera (Photometrics) and a xenon light source (Olympus). Cells were treated with red fluorescent membrane stain FM 4-64 (excitation: 515 nm/emission: 640 nm, final concentration 1 nM) and

DNA intercalating blue fluorescent dye DAPI (excitation: 358 nm/emission: 461 nm, final concentration 0.72 nM) and incubated for 2 minutes at room temperature prior to microscopy. Electronic data were processed using Metamorph 7.5.5.0 software (Molecular Devices, Sunnyvale, USA), which also allows the calibration of fluorescence intensity, and of pixel size to determine cell length.

Corrected fluorescence intensity measurement

The strains (*sftA*$_{(1-105)}$*-yfp*, *sftA*$_{(1-67)}$*-yfp*, and *sftA-yfp*) were first grown in parallel in S7$_{50}$ minimal medium at 25°C till an OD_{600} of around 0.7 was reached. 3µl of each culture were then added on an agarose slide and the strains were subsequently microscoped on a Zeiss Observer Z1 with an exposure time of 1 second. Foci fluorescence intensity measurement was done using the Java-based image processing program ImageJ (Wayne Rasband, National Institutes of Health), and the numbers obtained were in arbitrary unit. The mean background fluorescence was determined from a hundred punctae from the wild type strain, and was subtracted from the measured intensity of each focus to correct for the basic fluorescence level of *Bacillus subtilis* under the YFP channel.

Calculation of Western blot band intensity

SftA$_{(1-105)}$-YFP was induced with different levels of xylose to evaluate the effect of the incorporation of truncated copies of the protein on the function of the hexamers. The expression level of the construct was assessed on the western blots. Briefly, the intensities of bands were compared according to their grayscale (http://www.lukemiller.org/journal/ 2007/08/quantifying-western-blots-without.html).

Electrophoretic mobility shift assay

Pairs of complementary oligonucleotides were annealed to form double-stranded fragments. Oligonucleotides were mixed in equal amounts (10 µM) in a buffer containing 10 mM Tris-HCl, pH 8.0, 50 mM NaCl. After complete denaturation at 95°C for 5 min, samples were cooled down to room temperature slowly to promote annealing. The formation of double stranded fragments was confirmed by agarose gel electrophoresis. Annealing of oligonucleotides 1250 and 1251 resulted in the –KOPS fragment, the +KOPS fragment consisted of oligonucleotides 1882 and

1883. The DNA fragments were incubated with increasing amounts of SftA according to the protocol described in Kaimer *et al.,* 2009 and analyzed on a native gradient polyacrylamide gel (5-15%).

Surface plasmon resonance

Measurements were carried out using a Biacore 3000 system (GE Healthcare) and streptavidin coated Biacore SA sensor chips. After conditioning the sensor chip with a washing solution (1 M NaCl, 0.05 M NaOH), biotinylated DNA fragments (1500 bp) generated by PCR with primers 1162 and 1164 (table S1) were immobilized on one channel of the sensor chip according to the manufacturer´s instructions resulting in a response of 1800 resonance units (RU). The signal of a blank channel served as reference and was subtracted in all measurements. Purified SftA was injected at 200 seconds at various concentrations at a continuous flow rate of 20 µl min^{-1} in 0.1 M Tris-HCl, pH 8.0, 0.1 M NaCl. All buffers were filtered and degassed before use. After 1 min perfusion, protein injection was stopped at 260 s and the sensor chip was washed with buffer.

ATPase activity assay

The ATPase activity of purified SftA was determined as prescribed in Bath *et al.,* 2000.
Briefly, the enzyme assay couples two reactions: the conversion of phosphoenolpyruvate to pyruvate, and the conversion of pyruvate to lactate, catalyzed by pyruvate kinase and lactate dehydrogenase, respectively. The latter reaction results in the oxidation of NADH to NAD^+, which can be followed by the decrease in absorbance measured at 366 nm. The phosphate resulting from the pyruvate kinase reaction is used to regenerate ADP, the product of ATP hydrolysis by SftA. In summary, 1 mol of NADH is converted for 1 mol ATP. The 60 bp DNA substrate was obtained by annealing oligonucleotides 1882 and 1883.

Acknowledgments

This work has been supported by the Katholischer Akademischer Ausländer-Dienst (KAAD), by the BMBF funded graduate training group NANOKAT, and by the LOEWE funded Centre for Synthetic Microbiology (SYNMIKRO) at the Philipps-Universität Marburg.

References

Aussel L, Barre F-X, Aroyo M, Stasiak A, Stasiak AZ, Sherratt D: Ftsk is a DNA motor protein that activates chromosome dimer resolution by switching the catalytic state of the xerc and xerd recombinases. Cell 2002;108:195-205.

Barre F, Sherratt D: Chromosome dimer resolution. The bacterial chromosome 2005:513-524.

Barre FX: Ftsk and spoiiie: The tale of the conserved tails. Molecular microbiology 2007;66:1051-1055.

Berezuk AM, Goodyear M, Khursigara CM: Site-directed fluorescence labeling reveals a revised n-terminal membrane topology and functional periplasmic residues in the *escherichia coli* cell division protein ftsk. J Biol Chem 2014;289:23287-23301.

Besprozvannaya M, Pivorunas VL, Feldman Z, Burton BM: Spoiiie protein achieves directional DNA translocation through allosteric regulation of atpase activity by an accessory domain. J Biol Chem 2013;288:28962-28974.

Bigot S, Saleh OA, Lesterlin C, Pages C, El Karoui M, Dennis C, Grigoriev M, Allemand JF, Barre FX, Cornet F: Kops: DNA motifs that control e. Coli chromosome segregation by orienting the ftsk translocase. The EMBO journal 2005;24:3770-3780.

Bigot S, Sivanathan V, Possoz C, Barre FX, Cornet F: Ftsk, a literate chromosome segregation machine. Molecular microbiology 2007;64:1434-1441.

Biller SJ, Burkholder WF: The bacillus subtilis sfta (ytps) and spoiiie DNA translocases play distinct roles in growing cells to ensure faithful chromosome partitioning. Mol Microbiol 2009;74:790-809.

Bobay L-M, Rocha EP, Touchon M: The adaptation of temperate bacteriophages to their host genomes. Molecular biology and evolution 2012:mss279.

Burton B, Dubnau D: Membrane-associated DNA transport machines. Cold spring harb. Perspect. Biol. 2: A000406; in., 2010.

Cattoni DI, Chara O, Godefroy C, Margeat E, Trigueros S, Milhiet PE, Nollmann M: Spoiiie mechanism of directional translocation involves target search coupled to sequence-dependent motor stimulation. EMBO Rep 2013;14:473-479.

Cattoni DI, Thakur S, Godefroy C, Le Gall A, Lai-Kee-Him J, Milhiet PE, Bron P, Nollmann M: Structure and DNA-binding properties of the bacillus subtilis spoiiie DNA translocase revealed by single-molecule and electron microscopies. Nucleic Acids Res 2014;42:2624-2636.

Collins BE, Ling FY, Duzdevich D, Greene EC: DNA curtains: Novel tools for imaging protein–nucleic acid interactions at the single-molecule level. Methods in cell biology 2014;123:217-234.

Crozat E, Meglio A, Allemand JF, Chivers CE, Howarth M, Venien-Bryan C, Grainge I, Sherratt DJ: Separating speed and ability to displace roadblocks during DNA translocation by ftsk. EMBO J 2010;29:1423-1433.

Crozat E, Rousseau P, Fournes F, Cornet F: The ftsk family of DNA translocases finds the ends of circles. J Mol Microbiol Biotechnol 2014;24:396-408.

De-Donatis GM, Zhao Z, Wang S, Huang LP, Schwartz C, Tsodikov OV, Zhang H, Haque F, Guo P: Finding of widespread viral and bacterial revolution dsdna translocation motors distinct from rotation motors by channel chirality and size. Cell Biosci 2014;4:30.

Dubarry N, Barre FX: Fully efficient chromosome dimer resolution in escherichia coli cells lacking the integral membrane domain of ftsk. The EMBO journal 2010;29:597-605.

Graham JE, Sivanathan V, Sherratt DJ, Arciszewska LK: Ftsk translocation on DNA stops at xercd-dif. Nucleic acids research 2009:gkp843.

Grainge I, Bregu M, Vazquez M, Sivanathan V, Ip SC, Sherratt DJ: Unlinking chromosome catenanes in vivo by site-specific recombination. The EMBO journal 2007;26:4228-4238.

Hallet B, Sherratt DJ: Transposition and site-specific recombination: Adapting DNA cut-and-paste mechanisms to a variety of genetic rearrangements. FEMS microbiology reviews 1997;21:157-178.

Jaacks K, Healy J, Losick R, Grossman A: Identification and characterization of genes controlled by the sporulation-regulatory gene spo0h in bacillus subtilis. Journal of bacteriology 1989;171:4121-4129.

Kaimer C, Gonzaler-Pastor E, Graumann PL: Spoiiie and a novel type of DNA translocase, sfta, couple chromosome segregation with cell division in *bacillus subtilis*. Mol Microbiol 2009;74:810-825.

Kaimer C, Graumann PL: Players between the worlds: Multifunctional DNA translocases. Current opinion in microbiology 2011a;14:719-725.

Kaimer C, Graumann PL: Players between the worlds: Multifunctional DNA translocases. Current opinion in microbiology 2011b;14:719-725.

Kaimer C, Schenk K, Graumann PL: Two DNA translocases synergistically affect chromosome dimer resolution in *bacillus subtilis*. Journal of bacteriology 2011;193:1334-1340.

Kidane D, Sanchez H, Alonso JC, Graumann PL: Visualization of DNA double-strand break repair in live bacteria reveals dynamic recruitment of *bacillus subtilis* recf, reco and recn proteins to distinct sites on the nucleoids. Mol Microbiol 2004;52:1627-1639.

Lee JY, Finkelstein IJ, Arciszewska LK, Sherratt DJ, Greene EC: Single-molecule imaging of ftsk translocation reveals mechanistic features of protein-protein collisions on DNA. Molecular cell 2014;54:832-843.

Lee JY, Finkelstein IJ, Crozat E, Sherratt DJ, Greene EC: Single-molecule imaging of DNA curtains reveals mechanisms of kops sequence targeting by the DNA translocase ftsk. Proceedings of the National Academy of Sciences 2012;109:6531-6536.

Lewis PJ, Marston AL: Gfp vectors for controlled expression and dual labelling of protein fusions in bacillus subtilis. Gene 1999;227:101-109.

Liu G, Draper GC, Donachie WD: Ftsk is a bifunctional protein involved in cell division and chromosome localization in *escherichia coli*. Mol Microbiol 1998;29:893-903.

Liu N, Chistol G, Bustamante C: Two-subunit DNA escort mechanism and inactive subunit bypass in an ultra-fast ring atpase. eLife 2015;4.

Ludwig H, Homuth G, Schmalisch M, Dyka FM, Hecker M, Stülke J: Transcription of glycolytic genes and operons in bacillus subtilis: Evidence for the presence of multiple levels of control of the gapa operon. Molecular microbiology 2001;41:409-422.

Massey TH, Mercogliano CP, Yates J, Sherratt DJ, Löwe J: Double-stranded DNA translocation: Structure and mechanism of hexameric ftsk. Molecular cell 2006;23:457-469.

May PF, Zawadzki P, Sherratt DJ, Kapanidis AN, Arciszewska LK: Assembly, translocation, and activation of xercd-dif recombination by ftsk translocase analyzed in real-time by fret and two-color tethered fluorophore motion. Proceedings of the National Academy of Sciences 2015;112:E5133-E5141.

Nolivos S, Touzain F, Pages C, Coddeville M, Rousseau P, El Karoui M, Le Bourgeois P, Cornet F: Co-evolution of segregation guide DNA motifs and the ftsk translocase in bacteria: Identification of the atypical lactococcus lactis kops motif. Nucleic Acids Res 2012;40:5535-5545.

Pease PJ, Levy O, Cost GJ, Gore J, Ptacin JL, Sherratt D, Bustamante C, Cozzarelli NR: Sequence-directed DNA translocation by purified ftsk. Science 2005;307:586-590.

Schwarz FW, Toth J, van Aelst K, Cui G, Clausing S, Szczelkun MD, Seidel R: The helicase-like domains of type iii restriction enzymes trigger long-range diffusion along DNA. Science 2013;340:353-356.

Sciochetti SA, Piggot PJ, Blakely GW: Identification and characterization of the dif site from *bacillus subtilis*. J Bacteriol 2001;183:1058-1068.

Sciochetti SA, Piggot PJ, Sherratt DJ, Blakely G: The *ripx* locus of *bacillus subtilis* encodes a site-specific recombinase involved in proper chromosome partitioning. J Bacteriol 1999;181:6053-6062.

Sharpe ME, Errington J: Postseptational chromosome partitioning in bacteria. Proc Natl Acad Sci U S A 1995;92:8630-8634.

Sherratt DJ, Arciszewska LK, Blakely G, Colloms S, Grant K, Leslie N, McCulloch R: Site-specific recombination and circular chromosome segregation. Philosophical Transactions of the Royal Society of London B: Biological Sciences 1995;347:37-42.

Shin JY, Lopez-Garrido J, Lee S-H, Diaz-Celis C, Fleming T, Bustamante C, Pogliano K: Visualization and functional dissection of coaxial paired spoiiie channels across the sporulation septum. eLife 2015;4:e06474.

Sivanathan V, Allen MD, de Bekker C, Baker R, Arciszewska LK, Freund SM, Bycroft M, Lowe J, Sherratt DJ: The ftsk gamma domain directs oriented DNA translocation by interacting with kops. Nat Struct Mol Biol 2006;13:965-972.

Stouf M, Meile J-C, Cornet F: Ftsk actively segregates sister chromosomes in escherichia coli. Proceedings of the National Academy of Sciences 2013;110:11157-11162.

Studier FW: Protein production by auto-induction in high-density shaking cultures. Protein expression and purification 2005;41:207-234.

Yates J, Zhekov I, Baker R, Eklund B, Sherratt DJ, Arciszewska LK: Dissection of a functional interaction between the DNA translocase, ftsk, and the xerd recombinase. Molecular microbiology 2006;59:1754-1766.

Yu XC, Tran AH, Sun Q, Margolin W: Localization of cell division protein ftsk to the *escherichia coli* septum and identification of a potential n-terminal targeting domain. J Bacteriol 1998;180:1296-1304.

Table 1. Phenotypes of wild-type, truncations, and mutant cells.

Strain		%cut[a]	%long[b]	%anucleate	%mononucleate[c]	%abnormal	Cells
wt		0	0.7	0.1	2	1.1	1025
sftA-yfp		0.3	1.1	0	3	1.85	1000
amyE::sftA$_{(1-67)}$-yfp[d]		1.33	2.1	0.11	29	7.89	900
sftA$_{(1-105)}$-yfp		1.16	1.97	0	27	7.18	860
sftA$_{(1-246)}$-yfp		1.03	1.9	0	25	6.7	1160
amyE::sftA$_{(1-105)}$-yfp[e]	0%	0.73	0.86	0	23	4.89	814
	0.02%	0.97	1.43	0	26.6	6.39	977
	0.05%	1.2	1.8	0	27.1	7.06	1500
	0.5%	1.22	2	0	29	7.57	1800
sfta::tet		1.4	2.13	0	26	7.6	1500

a. DNA bisected by a septum.

b. Cells longer than 5.5 µm.

c. In cells 3.7-5.5 µm (15% of wild-type cells).

d. Cells induced with 0.05% xylose.

e. *amyE::sftA$_{(1-105)}$-yfp* with different xylose induction concentrations.

Table 2. Strains and plasmids used in this study.

***E. coli* Strains**		**Resistance**	**Source/Reference**
XL 1-Blue	endA1 gyrA96(nal^R) thi-1 recA1 relA1 lac glnV44 F'[::Tn10 proAB$^+$ lacI^q Δ(lacZ)M15] hsdR17(r_K^- m_K^+)	Tet	Stratagene
BL21 Star (DE3)	BF$^-$ ompT gal dcm lon hsdS_B($r_B^-m_B^-$) λ(DE3 [lacI lacUV5-T7 gene 1 ind1 sam7 nin5]) [malB$^+$]$_{K-12}$(λ^S)	none	Invitrogen
Plasmids			
pSG1729			Lewis and Marston, 1999
pSG1193y			Feucht and Lewis, 2001
pSG1164y			Kidane *et al*., 2004
pETDUET-1			Novagen
***B. subtilis* strains**	**Relevant genotype**	**Resistance**	**Source/Reference**
PY79	Wild type	none	Youngman *et al*.,1983
NEJ1	*amyE::sftA$_{(1-490)}$-yfp*	Spec	This study
NEJ2	*sftA$_{(1-246)}$-yfp*	Cm	This study
NEJ3	*sftA$_{(1-137)}$-yfp*	Cm	This study
NEJ4	*sftA$_{(1-105)}$-yfp*	Cm	This study
NEJ5	*sftA$_{(1-67)}$-yfp*	Cm	This study
NEJ6	*sftA$_{(1-50)}$-yfp*	Cm	This study
NEJ7	*sftA$_{(1-34)}$-yfp*	Cm	This study
CK150	*sftA::tet*	Tet	Kaimer *et al.,* 2009
NEJ8	*amyE::sftA$_{(1-105)}$-yfp sftA::tet*	Spec/Tet	This study
NEJ9	*amyE::sftA$_{(1-67)}$-yfp sftA::tet*	Spec/Tet	This study
NEJ10	*amyE::sftA$_{(21-439)}$-yfp*	Spec	This study
NEJ11	*amyE::sftA$_{(21-100)}$-yfp*	Spec	This study
NEJ12	*amyE::sftA$_{(21-100)}$-yfp sftA::tet*	Spec/Tet	This study
NEJ13	*amyE::sftA$_{(21-67)}$-yfp*	Spec	This study
NEJ14	*amyE::sftA$_{(21-67)}$-yfp sftA::tet*	Spec/Tet	This study
PG2664	*pfkA-yfp*	Cm	Graumann laboratory stock
CK55	*spoIIIE-yfp*	Cm	This study
NEJ15	*amyE::sftA$_{(61-439)}$-yfp*	Spec	This study
CK70	*sftA-yfp*	Cm	Kaimer *et al*., 2009

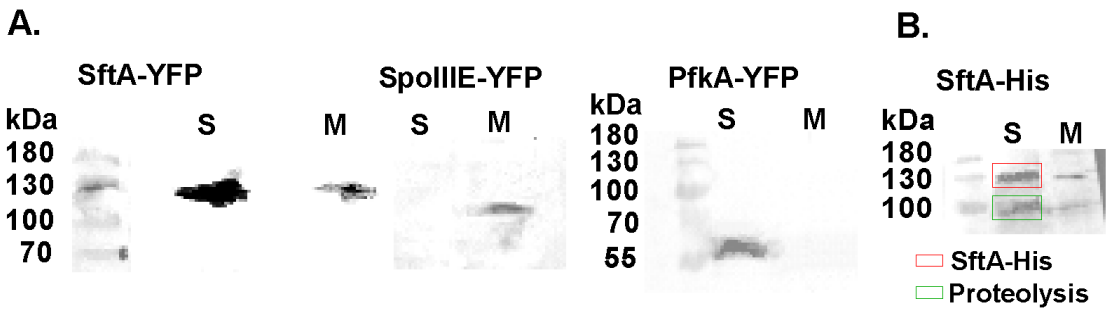

Figure 1. **A**. Western blot with anti- GFP antibodies for the detection of YFP tagged proteins of SftA-YFP, SpoIIIE-YFP, and PfkA-YFP expressed from their original promoters in the soluble (S) and membrane (M) fractions of each corresponding *B. subtilis* culture following cell fractionation experiments. **B.** Western blot with anti-His antibodies for the detection of overexpressed His tagged SftA in the soluble (S) and membrane (M) fractions of an *E. coli* BL21 strain harboring SftA in a pETDUET-1 vector under an IPTG inducible promoter.

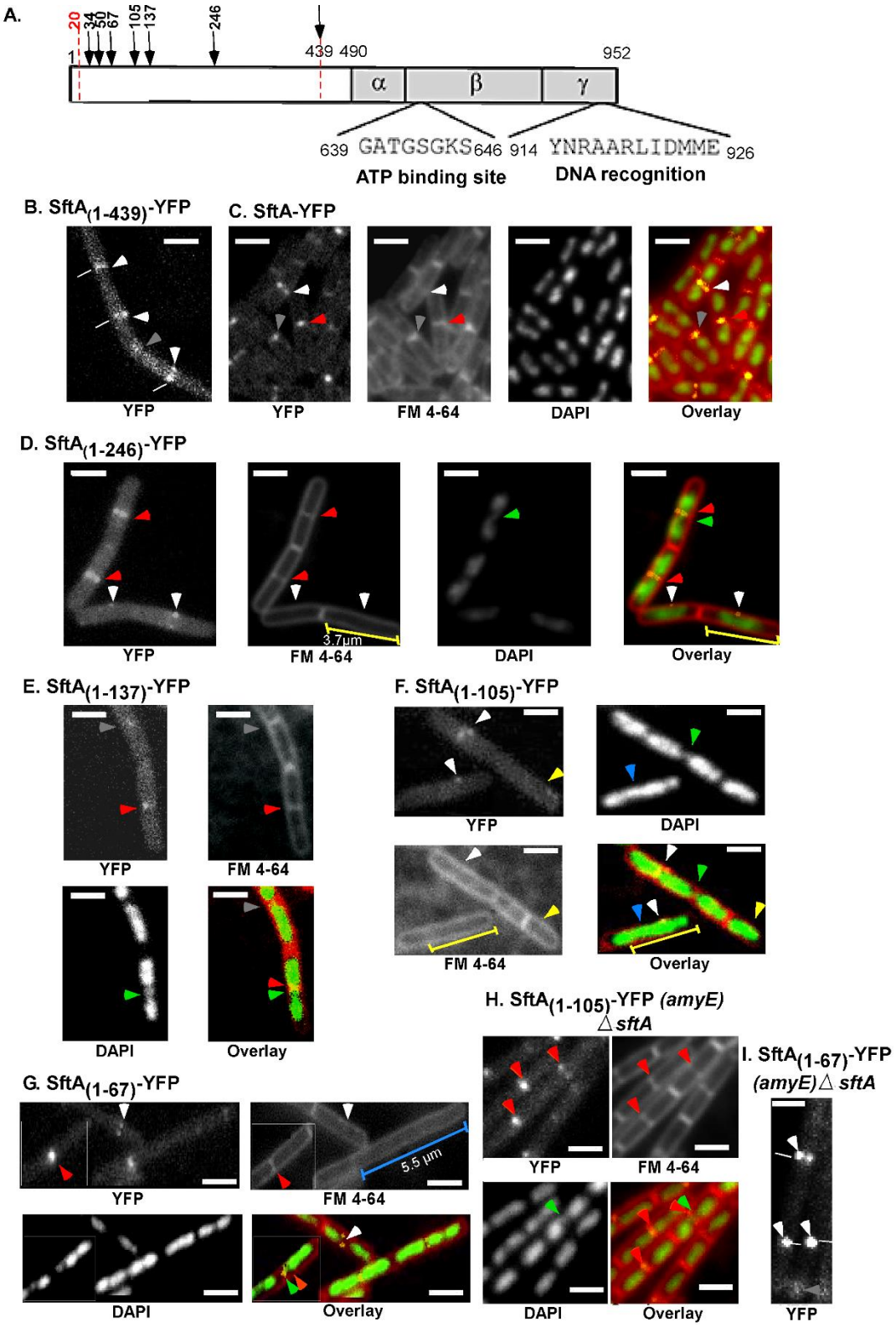
A.
20
34
50
67
105
137
246
1
439 490
952
α
β
γ
639 GATGSGKS 646 914 YNRAARLIDMME 926
ATP binding site
DNA recognition
B. SftA(1-439)-YFP
C. SftA-YFP
YFP
YFP
FM 4-64
DAPI
Overlay
D. SftA(1-246)-YFP
YFP
3.7μm
FM 4-64
DAPI
Overlay
E. SftA(1-137)-YFP
YFP
FM 4-64
DAPI
Overlay
F. SftA(1-105)-YFP
YFP
DAPI
FM 4-64
Overlay
H. SftA(1-105)-YFP (amyE) ΔsftA
YFP
FM 4-64
DAPI
Overlay
I. SftA(1-67)-YFP (amyE)Δ sftA
YFP
G. SftA(1-67)-YFP
YFP
5.5 μm
FM 4-64
DAPI
Overlay

Figure 2. **A**. Map depicting the length of the different truncations. The red dashed lines represent the whole N-terminus of the protein except for the first 20 residues. **B-K**. Localization patterns of the truncations in a wild type background. The yellow ruler represents 3.7 µm, the blue ruler represents 5.5 µm. White arrows point at mid-cell, red arrows at new cell poles, grey arrows at old poles, green arrows point at nucleoids bisected by a septum, and blue arrows point at unsegregated nucleoids in elongated cells. White dashes indicate mid-cell in YFP images for which no FM 4-64 is shown. Scale bars 2 µm.

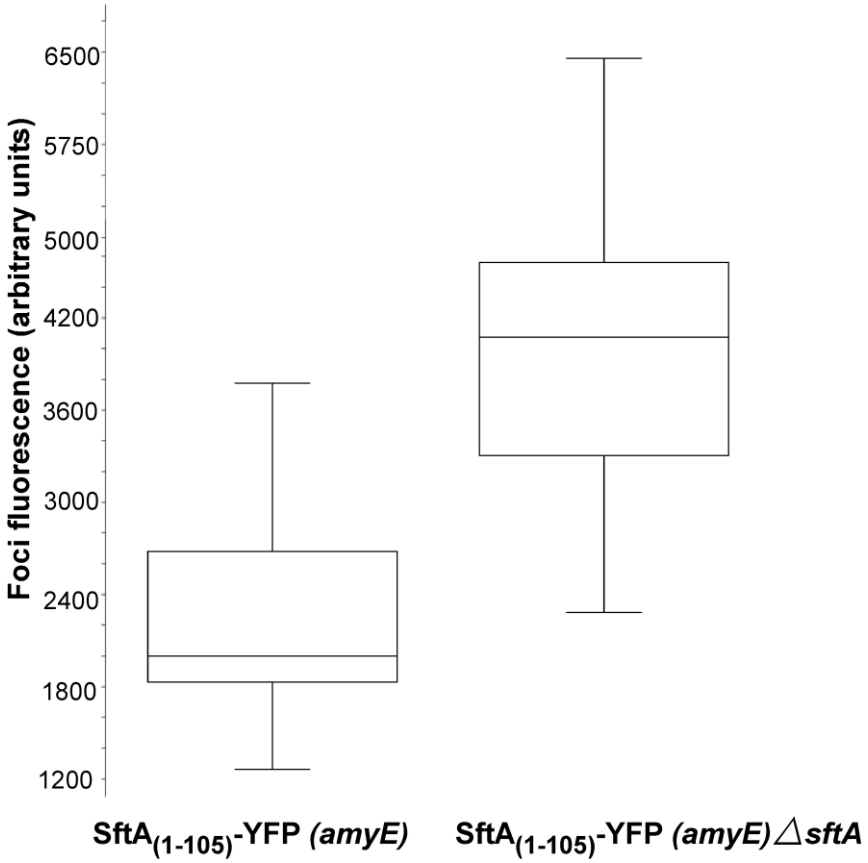

Figure 3. Corrected fluorescence intensity for $SftA_{(1-105)}$-YFP foci in the presence of the *sftA* original locus and after the deletion of the original locus. The intensity is measured in arbitrary units. The boxes represent the values between the first and the third quartiles, the middle line being the median. The whiskers show the lowest and highest values.

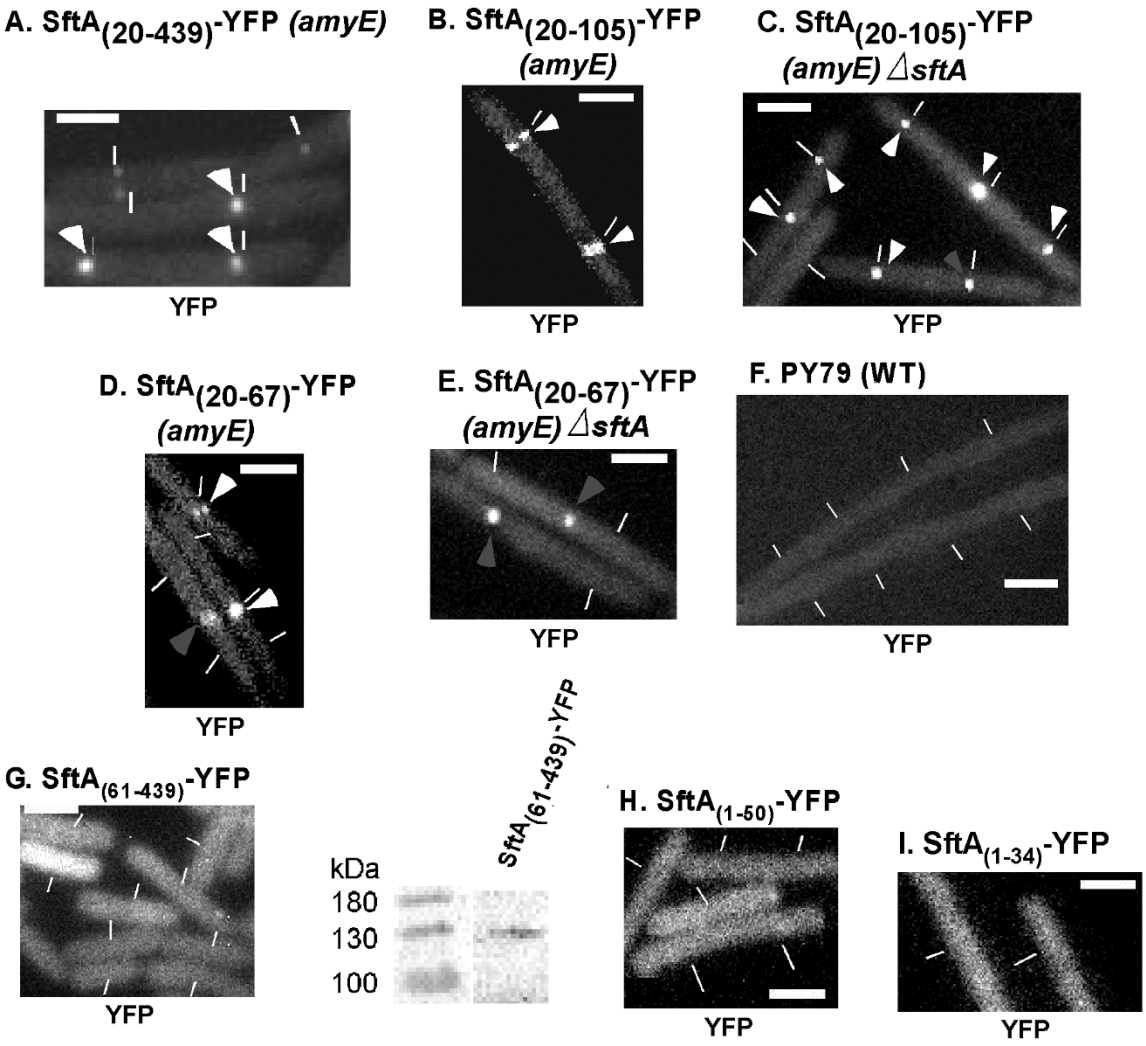

Figure 4. Localization of **A.** $SftA_{(20-439)}$-YFP, **B-E:** $SftA_{(20-105)}$-YFP and $SftA_{(20-67)}$-YFP both in a wild type and an *sftA* deletion background. Panels **G-I** show the non-localizing truncations: **G** shows a fluorescence picture of the $SftA_{(60-439)}$-YFP and a western blot of the construct with anti-GFP antibodies. **H** and **I** show $SftA_{(1-50)}$-YFP and $SftA_{(1-34)}$-YFP respectively. Panel **E** shows as a comparison background fluorescence levels of wild type *B. subtilis,* which appear to be lower than the fluorescence detected in non-localizing truncations. White dashes indicate mid-cell, white arrows indicate mid-cell localization, while grey arrows point at old cell poles. Scale bars 2 µm.

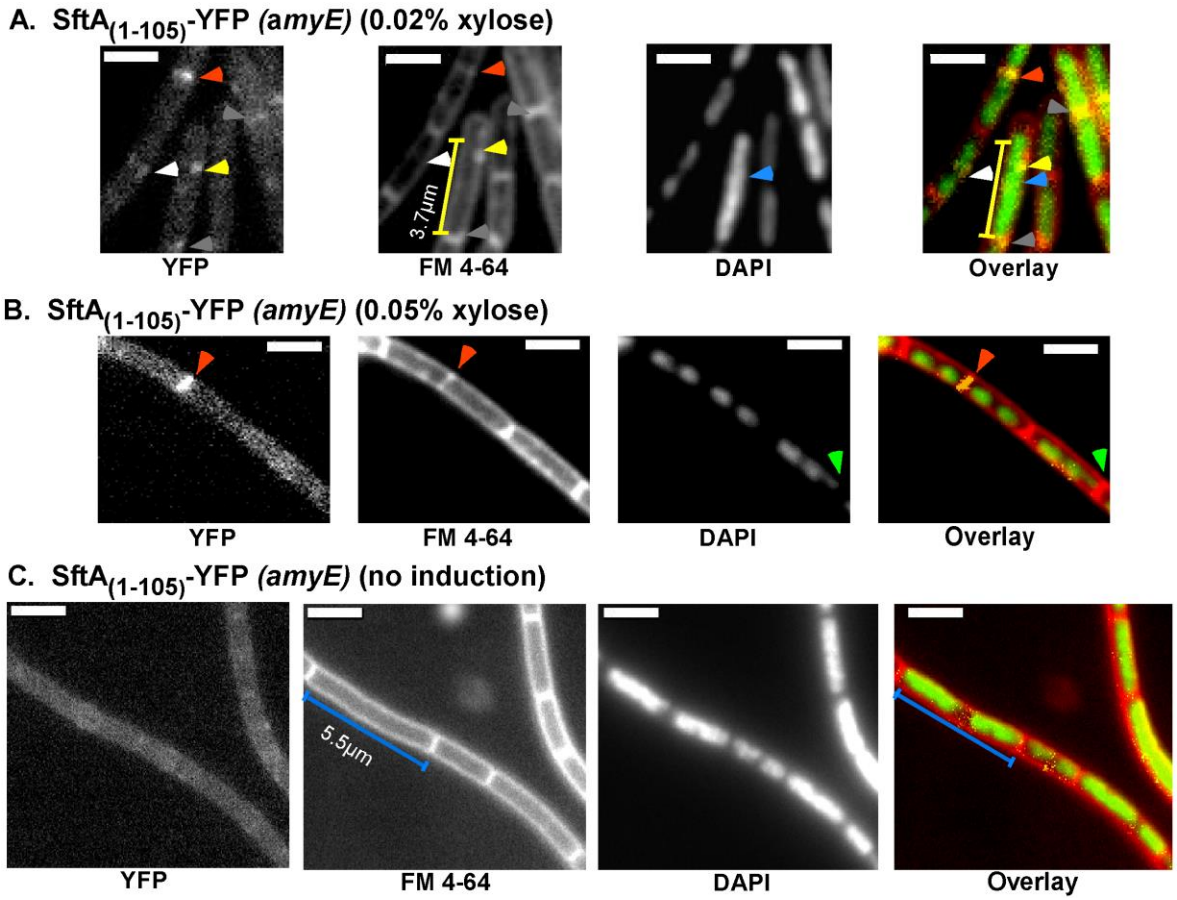

Figure 5. Localization of SftA$_{(1-105)}$-YFP cloned at the *amyE* locus under different induction-levels (xylose). **A.** 0.02% xylose, and **B.** 0.05% xylose. White arrows point at mid-cell, orange arrows at new cell poles, grey arrows at old cell poles, green arrows at a nucleoid bisected by a septum, blue arrows at unsegregated nucleoids, and yellow arrows at SftA localizing at one side of the membrane. The yellow ruler represents 3.7 µm. The elongated cell in **A.** indicated by a ruler has an unsegregated and elongated nucleoid. Scale bars 2 µm.

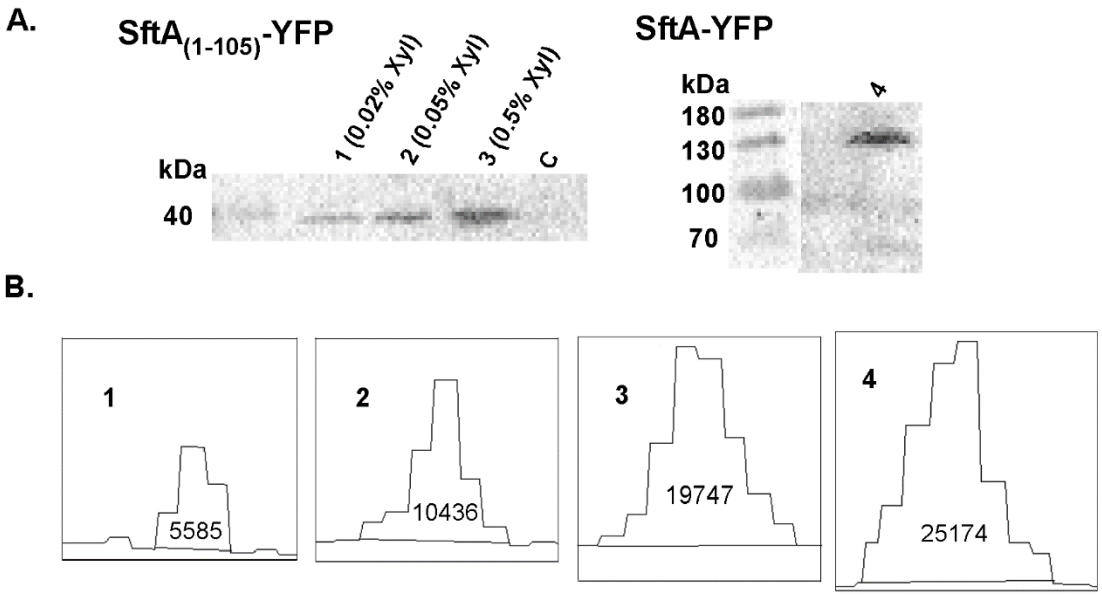

Figure 6. A. Western blot with anti- GFP antibodies for the detection of $SftA_{(1-105)}$-YFP induced with different xylose concentrations from an ectopic locus. SftA-YFP expressed from the original locus was used as a control. **B.** Intensities of the western blot bands in panel **A** in arbitrary units as calculated by ImageJ.

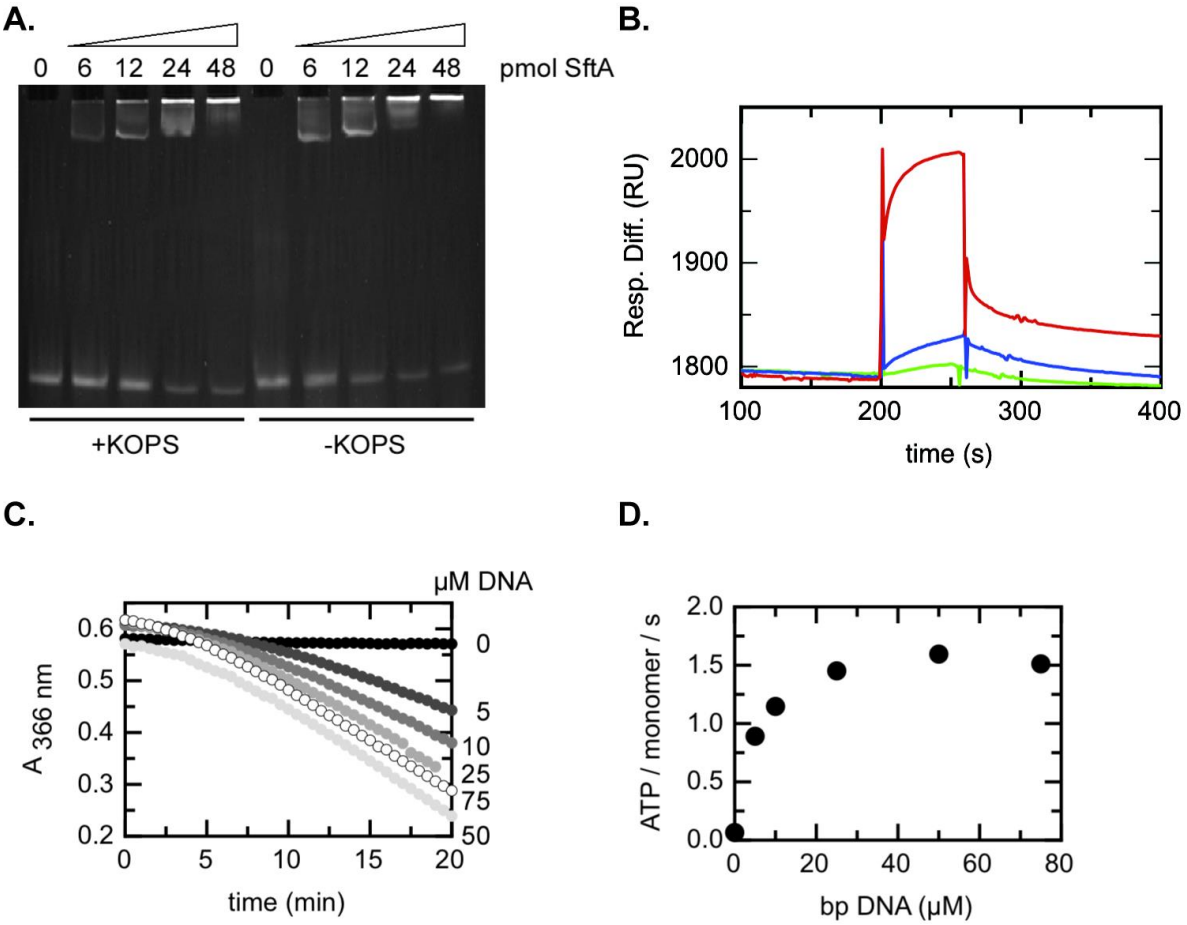

Figure 7. A. Electromobility shift assay. Increasing concentrations of SftA were incubated with a 60 bp dsDNA fragment, either containing KOPS sequences (+KOPS) or not (-KOPS). **B**. Surface plasmon resonance experiments. A sensor chip was coated with a 1500 bp DNA fragment via biotin-streptavidin coupling to a response of 1800 resonance units (RU). Purified SftA was injected at 200 s at a concentration of 1 µM (green), 1.5 µM (blue) or 2 µM (red). After 1 min perfusion, protein injection was stopped and the sensor chip was washed with buffer. The graph shows the response difference (Resp. diff) against time. **C**. Determination of the ATPase activity in a coupled enzyme assay. **1.** 0.06 µM purified SftA were incubated with different concentrations of a 60 bp dsDNA fragment (as indicated) at 25°C. ATP hydrolysis is coupled to the oxidation of NADH, reflected by a decrease in A_{366} nm. **2.** Calculated rate of ATP hydrolysis plotted against the concentration of the DNA substrate.

Table S1. List of oligonucleotides used in this study

Oligonucleotide	Sequence	Construct
2342	5’-CATGGGCCCGACGAACCGAAATCCGCG-3’	1164-sftA$_{(1-246)}$-yfp
2343	5’-CATGAATTCTTGCTCTTCGGCTTGTTCA-3’	
2473	5’-CATGGGCCCTAGCGGCTTGGTTTCTGC-3’	1164-sftA$_{(1-137)}$-yfp
2474	5’-CATGAATTCAACAGATGGTTTTTGATTGAAT-3’	
2410	5’-CATGGGCCCTTAGAAGGAGACTATGAGG-3’	1164-sftA$_{(1-105)}$-yfp
2411	5’-CATGAATTCTGTATGCTGCTC TTCTTCA-3	
2468	5’-CATGGGCCCAAGGATGCAGAGCTTCGTG-3’	1164-sftA$_{(1-67)}$-yfp
2469	5’-CATGAATTCGTATCCGTCAGGCA-3’	
2471	5’-CATGGGCCCGAAACGCTTCAGATCGTCTG-3’	1164-sftA$_{(1-34)}$-yfp
2472	5’-CATGAATTCTACTTCTTGTTGCT-3’	
2527	5’-CATGGGCCCAAGTTGTCGTTGCC-3’	1164-sftA$_{(1-50)}$-yfp
2528	5’-CATGAATTCATATATTTTAGGAT-3’	
2523	5’-CATGGGCCCATGAGTTGGCTTCATAAATTTT-3’	1193-amyE::sftA$_{(1-439)}$-yfp
2526	5’-CATGAATTCCGGAAATACATAGCTGCC-3’	
2579	5’-CATGGGCCCCCGGGAGACAAAACCCGCT-3’	1193-amyE::sftA$_{(21-439)}$-yfp
2619	5’-CATGGGCCCAGTCGTGCCTGA-3’	1193-amyE::sftA$_{(61-439)}$-yfp
1250	5’GCGCTTTCTCATAGCTCACGCTGTAGGTATCTCAG TTCGGTGTAGGTCGTTCGCTCCAAG-3’	60 bp fragment -KOPS
1251	5’CTTGGAGCGAACGACCTACACCGAACTGAGATAC CTACAGCGTGAGCTATGA-3’	
1882	5’TATATTGGGTAGGGAATTATAGGGCAGGGAATAT TGGGAAGGGTATATGGGGAGGGGAATA-3’	60 bp fragment +KOPS
1883	5’TATTCCCTCCCCATATACCCTTCCCAATATTCCCTG C CCTATAATTCCCTACCCAATATA-3’	

Supplementary Materials and Methods

Overexpression and purification of SftA

For purification of SftA, 1 l of autoinduction medium [Studier, 2005] was inoculated with 10 ml overnight culture of *E. coli* BL21 carrying the corresponding expression vector. The 1l culture was then incubated for 12 h at 25°C. Autoinduction is based on the diauxic behavior of *E. coli*. The preferred sugar, in this case glucose, is consumed first, leading to rapid growth, followed by a lag phase. In the lag phase, the cellular machinery used to metabolize the second sugar, lactose, is activated which concomitantly induces overexpression. Cells were then harvested by centrifugation for 10 min at 5000 rpm (Sorvall RC-6+ centrifuge, F94 rotor) and washed two times with Tris buffer (0.1 M Tris-HCl, pH 8.0, 0.1 M NaCl) and stored at -80°C. Prior to use, cell pellets were thawed and resuspended in 10-40 ml of Tris buffer containing a mix of protease inhibitors (complete, Roche). Cells were lysed by two passages through a French press at approximately 20000 psi (Aminco), and lysates were cleared by centrifugation for 30 min at 14000 rpm at 4°C (SS-34 rotor) for two times.

Affinity chromatography was performed using an ÄKTA Prime chromatography equipment (GE Healthcare) and a Ni-chelating column (HisTrap, 1 ml column volume).

Before injection, cell lysates were passed through a filter (Filtropur S, pore size 0.45 µm) to prevent clotting of the column. The sample was loaded in several steps and, after extensive washing to remove contaminants, specifically bound protein was eluted in a gradient (20 ml at 1 ml min^{-1}) of 0-0.5 M imidazol in Tris buffer. Fractions containing SftA were pooled and subjected to gel filtration.

Gel filtration was performed using an ÄKTA FPLC (GE Healthare) and a Superose 6 (10/300 GL) column. Gel filtration columns were equilibrated in Tris buffer, and fractions from affinity chromatography were injected in 100 µl to 2 ml steps and eluted at a constant flow rate of 0.5 ml min^{-1}. Fractions containing SftA were pooled and stored at 4°C until they were used for further experiments. The final concentration of SftA varied from 0.5 to 1.2 g l^{-1}, corresponding to a yield 1 to 2.5 mg per liter of culture.

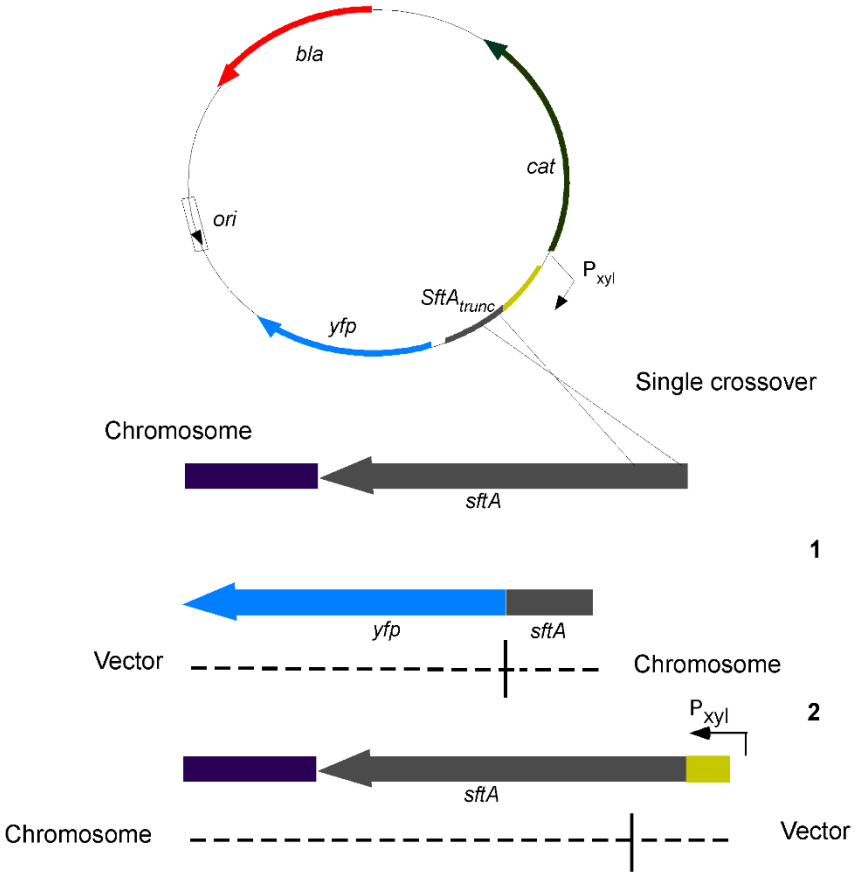

Figure S1. Map for the plasmid integration of pSG1164 [Kidane et al., 2004] truncation containing plasmid. A 500 base pair fragment was cloned between the *Apa*I an *Eco*RI cutting sites. The truncation is shown in the map as a dark grey line. In cases where the truncation was sorter than 500 bp, the rest of the fragment length was cloned from the sequence upstream of the ORF (yellow line). The single crossover resulted in a truncated copy (Part **1**), and in the full length protein being translated downstream of the xylose promoter (Part **2**).

References

Studier FW: Protein production by auto-induction in high-density shaking cultures. Protein expression and purification 2005;41:207-234.

Kidane D, Sanchez H, Alonso JC, Graumann PL: Visualization of DNA double-strand break repair in live bacteria reveals dynamic recruitment of *bacillus subtilis* recf, reco and recn proteins to distinct sites on the nucleoids. Mol Microbiol 2004;52:1627-1639.

4.2. Manuscript 4B

Submitted

FtsA contributes to the recruitment of the soluble DNA translocase SftA to the division machinery in *B. subtilis*

Nina el Najjar[1], Jihad El Andari[1], Christine Kaimer[2], Thomas Rösch[1], Peter L Graumann[1*]

[1]SYNMIKRO, LOEWE Center for Synthetic Microbiology, and Department of Chemistry, Philipps Universität Marburg, [2]Fakultät für Biologie und Biotechnologie, Lehrstuhl Biologie der Mikroorganismen, Ruhr-University Bochum, Germany

*corresponding author, email: peter.graumann@synmikro.uni-marburg.de
49(0)64212822210

Abstract

Like many bacteria, *Bacillus subtilis* possesses two DNA translocases that affect chromosome segregation at different steps. Prior to septum closure, non-segregated DNA is moved into opposite cell halves by SftA, while septum-entrapped DNA is rescued by SpoIIIE. We have used single molecule microscopy and automated tracking (SMT) experiments, which proved to be to be highly efficient in describing the dynamics of the two different DNA translocases in real time. SMT revealed that about 20% of SftA molecules move through the cytosol, while a fraction of 80% of SftA molecules is septum-bound and relatively static. In contrast, SpoIIIE molecules diffuse within the membrane, and do not show any enrichment at the septum. Several lines of evidence suggest that FtsA plays a major role in septal recruitment of SftA: an FtsA depletion affects septal SftA recruitment, and results in an increase in the diffusion rate of the soluble fraction at the single molecule level, and in a decrease in static mid-cell localized molecules. FtsA can recruit SftA to the membrane in a heterologous eukaryotic system, revealing that SftA is at least partially recruited to mid-cell via FtsA. Our experiments show that SftA is a *bona fide* component of the division machinery, and a truly soluble enzyme *in vivo*. *B. subtilis* FtsA plays a dual role in divisome assembly in the recruitment of SftA, besides membrane-attachment of FtsZ. Our data show that SMT is a suitable technique to determine if low-abundant proteins are membrane-bound or cytosolic, to determine ratios of bond and unbound proteins, and in visualizing the subcellular localization of slow and of fast-moving molecules in live cells.

Introduction

Stable transmission of genetic information means that cells must ensure that their DNA is accurately replicated and that each daughter cell receives a completely segregated chromosome. One threat to segregation is the fact that the replication of circular chromosomes can lead to the formation of a chromosome dimer, which results from an odd number of recombination events during replication, and which needs to be properly resolved. Moreover, a delay in segregation can be detrimental if division occurs prior to complete DNA partitioning. Certain types of stress can damage DNA and disrupt the normal progression of the replication fork. Therefore, cells have evolved pathways to ensure that cell division occurs reliably even when segregation is perturbed (1, 2).

In eukaryotic cells, several checkpoints prevent premature cytokinesis during mitosis (3-5). In bacteria however, such checkpoints that separate chromosome segregation and cell division have not been identified. These processes therefore frequently overlap and cell division can occur even when chromosome segregation is not complete. As a consequence, incompletely segregated chromosomes can be trapped by the invaginating division septum and must be actively transported into the daughter cells to prevent a block in the cell cycle. DNA translocases act in a spatially and temporally defined manner to move DNA away from the closing septum.

In *E. coli*, the membrane-integral translocase FtsK is recruited as a regular component of the division septum via its central domain, which anchors the protein in the membrane. The N-terminus plays an essential role in cell division, while the C-terminal domain acts as DNA translocase. FtsK colocalizes with FtsZ to the septum, and its localization is dependent on the early division proteins FtsZ, FtsA and ZipA (6, 7). The C-terminal domain is an ATP-dependent DNA translocase that moves DNA in a spatially directed manner (6). FtsK pumps chromosomes toward the chromosome dimer resolution site (*dif* site) located near the terminus region using polarity of the FtsK-orienting polar sequence (KOPS), which are recognized by the FtsKγ domain and permit the loading of FtsK onto the DNA in one specific orientation (8). KOPS are distributed over the chromosome and oriented toward the terminus region, where they are found at a high frequency (9). Recombination at the *dif* site happens through the action of the site-specific recombinases XerD and XerC (10, 11), which catalyze the formation and resolution of a Holliday junction intermediate at *dif*, where each recombinase mediates a strand exchange reaction (12). FtsK arranges the *dif* sites in close proximity at the division septum and directly activates XerD (13).

In *Bacillus subtilis*, RipX and CodV are the homologues of XerD and XerC, respectively (14, 15). Both RipX and CodV bind to the *B. subtilis dif* sites and catalyze strand exchange *in vitro* (16). Two *B. subtilis* DNA translocases act synergistically in the rescue of DNA that might become trapped by the division septum during vegetative growth: the membrane-associated SpoIIIE and the soluble SftA. Both proteins share sequence identity with the C-terminal domain of FtsK (2). SftA is a component of the divisome. It facilitates dimer resolution by bringing the *dif* sites into close proximity, most likely using a KOPS-like mode for translocation directionality. SftA translocates DNA during septation, while SpoIIIE is only recruited to rescue septum-entrapped DNA after division is completed (1, 2). It recognizes trapped DNA, in a mechanism that is still poorly understood, and pumps one double strand across the septum (17-20). SpoIIIE is essential for sporulation, but not during vegetative growth. However, SpoIIIE becomes indispensable under conditions where chromosome segregation is impaired. *In vivo* studies revealed that neither SpoIIIE nor SftA is essential for RipX-dependent recombination at *dif* (1, 16, 21), but contribute additively to dimer resolution (22). RipX and CodV form a preassembled complex on the chromosome during the cell cycle, probably to allow an immediate initiation of dimer resolution. The *sftA spoIIIE* double mutant strain has a more severe phenotype than either of the single mutants, suggesting considerable overlap in their roles (22).

In this work, we analyze the dynamics of SftA and SpoIIIE at the single molecule level in real time. We find that most SftA molecules are present at the septum, while SpoIIIE molecules are generally mobile within the membrane. We also provide evidence for a potential role of FtsA in the recruitment of SftA to the mid-cell using a heterologous eukaryotic system and an *in vivo* depletion assay.

Materials and Methods

Growth conditions

The bacterial strains and plasmids used in this study are listed in table 1, the nucleotides in table 2. *Escherichia coli* strain XL1-Blue (Stratagene) was used for the construction and propagation of plasmids and *E. coli* strain BL21 Star DE3 (Invitrogen) for the heterologous overexpression of proteins. All *B. subtilis* strains were derived from the prototroph wild type strain PY79. Cells were grown in Luria–Bertani (LB)-rich medium at 37°C or 30°C, or in minimal medium containing $S7_{50}$ salts (23) at 25°C. Media were supplemented with antibiotics where appropriate (ampicillin 100 mg ml^{-1}, chloramphenicol 5 mg ml^{-1}, spectinomycin 100 mg ml^{-1}, kanamycin 10 mg ml^{-1}, tetracycline 10 mg ml^{-1}).

Strain construction

$SftAN_{tap}$ was obtained by using a C-terminal TAP tag in pSG1164 (24) and cloning the last 500 bp of the SftA N-terminus upstream of it between the *Apa*I and *Cla*I sites. An *ftsH::mls sftA-yfp* was generated by transformation of CK70 (2) competent cells with chromosomal DNA from the strain WW01 (25). For the S2 Schneider cells experiment, pFD1 plasmid was used for all clonings (26). To express the N-terminus of SftA, the 5' region of the gene was cloned between *Apa*I and *Cla*I, the full length *sftA* was cloned between *Apa*I and *Eco*RV, *ftsA* was cloned between *Apa*I and *Xho*I whereby the *yfp* was cleaved out, and upstream of the *yfp* between *Apa*I and *Pst*I to create *ftsA-yfp.* FtsZ was cloned between *Apa*I and *Xho*I; in this construct the *yfp* was cleaved out. To create *ftsZ-yfp*, *ftsZ* was cloned between *Apa*I and *Pst*I. $ftsA_{1-425}$ was created by cloning the soluble part of FtsA (residues 1-425) in the expression vector pPR-IBA 101 (IBA lifesciences) between *Eco*RI and *Bam*H1 downstream of the Strep-tag®.

Strains CK100, CK185, CK186 and CK187 were constructed by transformation of CK70 (*sftA-yfp*) competent cells with chromosomal DNA of strains carrying the corresponding mutation of cell division proteins (listed in table S1). For strain CK188, competent cells of an *ftsA* depletion strain were transformed with chromosomal DNA of CK83.

Schneider cell culture and transient transfection

Drosophila melanogaster S2 Schneider cells (26) were grown in Schneider's Drosophila medium (Lonza Group Ltd.) supplemented with 5–10% (v/v) fetal calf serum (FCS) at 25°C. Cells were transferred every 48h and transfected with the corresponding vectors using X-treme GENE HP DNA Transfection Reagent (Roche) as described in detail in El Andari *et al*. (27). Protein expression was induced with a final concentration of 1mM $CuSO_4$ and cells were analyzed after 19 h.

Tandem Affinity Purification

The tandem affinity purification was used to purify proteins expressed at their physiological level under native conditions. The recombinant vector containing the N-terminus of SftA was introduced into *B. subtilis*. Extracts were prepared from 1 liter of culture grown to exponential phase to an OD_{600}nm of ~1. Sequential purification via IgG Sepharose beads (Pharmacia Piscataway, NJ) and calmodulin beads was done as described in Defeu Soufo et al. (28). To identify proteins interacting with the TAP tagged N-terminus SftA, the eluate was run on a SDS– polyacrylamide gel with acrylamide concentration of 10% but not allowed to separate. After silver staining, the band corresponding to the whole eluate was cut out and analyzed by mass spectrometry. The same experimental procedure was done in parallel to a control sample obtained from a 1 l culture of wild type PY79 cells (pSG1729-TAP) expressing the TAP-tag only.

Depletion of FtsA

For single molecule microscopy, strain CK188 was used in order to track SftA-YFP in the absence of FtsA. CK188 was grown to exponential phase in LB medium at 30°C in the presence of 0.2% xylose. The inducer was removed by centrifugation and washing of the cells, and microscopy was performed after 1 h of growth in the absence of inducer.

Fluorescence microscopy

For fluorescence microscopy analysis, *B. subtilis* cells were grown in $S7_{50}$ minimal medium at 25°C under shaking conditions until exponential growth. 3 µl of cells were transferred on a glass

slide (Microscope slides standard, Roth) coated with an agarose layer ($S7_{50}$ minimal medium, 10 mg/ml agarose) - and covered with a cover slip (Cover slips, Roth). Conventional light microscopy was performed using a Zeiss Observer Z1 (Carl Zeiss) with an oil immersion objective (100 × magnification, 1.45 numerical aperture, alpha Plan-FLUAR, Carl Zeiss) and a CCD camera (CoolSNAP EZ, Photometrics), or with a BX51 microscope (Olympus) with a Cool Snap EZ camera (Photometrics) and a xenon light source (Olympus). Cells were treated with red fluorescent membrane stain FM 4-64 (excitation: 515 nm/emission: 640 nm, final concentration 1 nM) and DNA intercalating blue fluorescent dye DAPI (excitation: 358 nm/emission: 461 nm, final concentration 0.72 nM) and incubated for 2 minutes at room temperature prior to microscopy. Data were processed using Metamorph 7.5.5.0 software (Molecular Devices, Sunnyvale, USA), which also allows the calibration of fluorescence intensity, and of pixel size to determine cell length.

Single molecule microscopy and tracking

In contrast to the wide field illumination used in conventional epifluorescence microscopy, the excitation Laser beam used in our setup is directed to under-fill the back-aperture of the objective lens. The effect of this light path is to generate a concentrated parallel illumination profile at the level of the sample, leading to a strong excitation followed by rapid bleaching of the fluorophores. When only a few not bleached molecules are present, their movement can be tracked. In addition, freshly synthesized and folded fluorophores become visible when the sample is excited again. When an observed molecule bleached in a single step during the imaging, it is assumed to be a single molecule (29, 30). Image acquisition was done continuously during laser excitation with the EMCCD camera "iXon Ultra" (Andor Technology, Belfast, UK). A total of 1500 images were taken per field with an exposure time of 0.03 seconds.

The exposed chip size corresponded to 256x256 or 128x128 pixels. The settings of recording conditions were made with the camera's program "AndorSolis 4.2". The microscope used in the process was an "Olympus IX71", with a 100x objective (APON; NA: 1.49, oil immersion). A 514nm laser diode was used as excitation source, and the band corresponding to the fluorophore was filtered out. All imaged proteins are tagged with monomeric YFP, expressed from original gene locus, and the exposure time and laser intensity were the same in all experiments: 30 ms and 10 mW. The acquired movies were first cropped and their format was converted from RAW to TIFF with ImageJ.

Single molecule tracking and analysis of tracks

Single molecules were tracked using MATLAB and U-track-2.3.1. The generated data were analyzed with an MSD-analyzer in MATLAB. Trajectories consisting of a minimum of 5 frames were considered as tracks and included for further analysis. Cells were manually identified using MicrobeTracker. For analyzing the diffusive behavior of single molecules, all tracks are referenced to the corresponding cell such that the long axis of the cell is aligned with the x-axis of a cartesian coordinate system.

Calculation of diffusion constants

A widely accepted method to analyze the diffusive behavior of molecules is by using the mean squared displacement (MSD) versus the time lag curve. This provides an estimate of the diffusion coefficient as well as of the kind of motion. However, the method requires that within a complete trajectory there is only one type of homogeneous motion and that the trajectory is preferably of infinite size. Currently used fluorophores show rather short lifetimes limiting the time of observation to short time intervals, which in turn limits the statistical significance of the results. Additionally, this method does not provide any information if there are different kinds of diffusive molecules within one population. To distinguish immobile and mobile molecules from each other, we compare the frame-to-frame displacement of all molecules in x and the y direction. Using a Gaussian mixture model to fit the probability density distribution function of all frame- to-frame displacements, we are able to finally define the size of small and large molecule movements corresponding to slow and fast diffusion.

Results

The localization pattern of SftA is affected through the depletion of FtsA

Kaimer *et al.* (2009) showed that SftA was recruited as an early component to the cell division machinery before DivIB, DivIC, FtsL or Pbp2B. SftA localized into distinct foci on the membrane in an FtsZ depletion strain, which suggests that SftA has either an intrinsic membrane affinity, or is binding to a membrane-associated protein that is recruited to mid-cell by FtsZ, or is binding to FtsZ directly. To identify alternative recruitment factors, we localized SftA-YFP in mutants lacking early accessory division proteins EzrA, ZapA and SepF (31-33), or in a strain in which FtsA can be depleted. In an *ezrA* deletion background SftA was still recruited to aberrantly formed division septa, and in a *zapA* deletion, SftA-YFP also localized at midcell indistinguishable to wild type cells. The same findings apply to a *ΔsepF* mutant strain, which rules out these latter three proteins as potential interaction partners (Fig. 1). We also tested DivIVA as potential interaction partner for SftA, but did not find a pronounced lack of formation of SftA rings or foci in *divIVA* mutant cells (Fig. 1E).

The depletion of FtsA resulted in the formation of visually elongated cells, but not in a complete block in cell division, showing that we were only able to partially deplete FtsA. In spite of this caveat, mid-cell SftA-YFP assemblies were rarely observed. The assemblies appeared less distinct than in wild type cells, and SftA-YFP spots were often detected only at one side of the cell, indicating that the extension into a ring shaped structure was not accomplished. FtsA therefore appears to have an influence on SftA localization, which could be a direct effect via interaction or an indirect one caused by the aberrant FtsZ localization in absence of FtsA.

We next employed tandem affinity pull-down assays with the SftA N-terminus, which can localize the entire protein (2), and thus likely contains the interaction-surface(s). The eluents for the control and the test fraction were cut out of the gel before a separation into distinct bands. The control in this case was the TAP tag itself cloned into the *amyE* site, while the bait was the N-terminus of SftA cloned upstream of the tag under the original promoter. The bands were analyzed by mass spectrometry and the proteins detected in the test but not in the control were considered as candidates for potential interactions. A number of oxidoreductases, dehydrogenases, transcriptional regulators, the DNA gyrase subunit B, and several transporters and ribosomal subunits were detected, but absent in the control table 2. Of particular interest was a number of

proteins such as FtsH, as well as FtsZ, SepF, FtsE and FtsA that were specifically associated with SftA. SepF was already ruled out in previous experiments as mentioned earlier, and FtsE is needed along with FtsX for recruitment of late division proteins (34), while SftA is recruited at an early time point. In order to assess the role of FtsH on SftA localization, SftA-YFP cloned into a *ΔftsH* strain. The deletion had no effect on the localization of SftA (Fig. 1H), which also excludes FtsH as a recruiting factor for SftA.

Therefore, the two candidates remaining to be investigated were FtsA and FtsZ, since conclusive evidence confirming or denying an interaction between them and SftA were not obtained in previous studies. In spite of our best efforts, we were not able to show a clear interaction between SftA and FtsZ *in vitro* (*data not shown*), and also experiments with purified FtsA lacking the amphipathic helix were not conclusive (*data not shown*). However, FtsA remains the most promising candidate for an SftA recruitment factor. We therefore turned to *in vivo* interaction studies.

Co-expression of SftA and FtsA in S2 Schneider cells

To study the putative interaction of SftA and FtsA, we employed a heterologous expression system. S2 Schneider cells are derived from *Drosophila* flies and are unlikely to contain specific binding partners that interact with bacterial proteins. In order to investigate a possible interaction with FtsA or FtsZ, S2 Schneider cells were co-transfected with SftA-YFP and untagged FtsA or FtsZ. As a control, cells were transfected with either SftA-YFP (full length and N-terminus) alone or FtsA-YFP/FtsZ-YFP alone. Expression of all recombinant YFP-tagged proteins in this experiment was verified by western blot with anti- GFP antibodies (Fig. 2G).

Expression of SftA-YFP, or its N-terminus, in S2 Schneider cells resulted in a diffused fluorescence, which argues against SftA's ability to target the membrane by itself (Fig. 2A and C). (26, 35). In contrast to SftA-YFP, FtsA-YFP formed distinct filaments on the membrane (Fig. 2A & 2D, respectively), in agreement with its possession of an amphipathic helix (36). This is similar to the localization of YFP-MreB or of *B. subtilis* bactofilins, which were shown to be recruited to the membrane by an amphipathic helix and intrinsic membrane affinity, respectively (26, 27). When co-expressed, FtsA caused the recruitment of SftA-YFP to the membrane, where clear assemblies were observed, indicating a direct interaction between the two proteins (Fig. 2E).

FtsZ-YFP expressed in S2 cells forms multiple assemblies across the cell (Fig. 2F). However, when SftA-YFP was co-transfected of with untagged FtsZ, we observed diffuse localization that is reminiscent of SftA localization, but no indication of a specific interaction of SftA and FtsZ. (Fig. 2B).

Single molecule microscopy of SftA, SpoIIIE and PfkA reveals differential localization patterns

SftA can be purified as a soluble enzyme (2). However, inspection of its N-terminal sequence has suggested the presence of a membrane-targeting helix (37). During the depletion of FtsZ, SftA signals can still be observed at the membrane (2). We wished to gain insight into the question whether SftA is a membrane-associated protein, or if it is a truly cytosolic enzyme that becomes recruited to the division site. SftA is not highly abundant, so a possible freely diffusing fraction in the membrane or in the cytosol is not detectable by conventional epifluorescence or by TIRF microscopy. Nevertheless, using highly sensitive single molecule fluorescence microscopy and tracking (SMT), we are able to observe diffusive molecules. By illuminating an area of about 10 μm in diameter by parallel light from the center of a laser beam, which results in an even and intensive illumination, we can follow the real time movement of single molecules, using fast stream acquisitions, once all except for the last molecule have been bleached by the laser. We are using the U-track software (38) for automated spot detection and tracking, which is based on Gaussian fitting of fluorescent spots, resulting in a subpixel resolution, and MicrobeTracker (39) for automated cell detection. Our custom developed single molecule analysis software (Matlab based) integrates the positional coordinates of the molecules into the coordinate system of the cell and quantitatively analyzes its diffusive behavior and localization.

Besides SftA, we imaged and tracked SpoIIIE and PfkA during exponential growth in minimal medium, both expressed from their respective original promoters and each fused to monomeric YFP. Phosphofructokinase (PfkA) is a glycolytic enzyme, which we have used as a control for a freely diffusive enzyme and SpoIIIE served as indicator of a membrane associated DNA translocase. These proteins showed a characteristic localization pattern when we summed up all the pixel intensities from consecutive images of an acquired stream (Fig. 3A). Additionally, we projected the positions of the molecules from all cells and all movies into a normalized bacterial cell (dimensions 3 x 1 μm) and plotted these positions in a density plot (Fig. 3B). The spot

localization for PfkA-YFP shows a clear localization in the cytosol (Fig. 3B). On the other hand, the normalized localization of SftA-YFP showed that there is a higher density of SftA-YFP spots in positions corresponding to mid cell, to the quarter sites and the cell pole. This was not observed for PfkA-YFP where localization was more equally distributed to the center of the cell (Fig. 3B). Contrarily to SftA and PfkA, SpoIIIE preferably localized at the membrane. Note that during stream acquisition, the focal plane is not always exactly at the central plane of the cell; if the focus moves up or down, also molecules that travel along the Y-axis are observed. Therefore, also tracks that appear to be in the cytosol are observed for SpoIIIE.

SftA divides into two fractions, a static (likely septum-bound) and a mobile fraction

As a next step in our evaluation of SMT data, we employed step length analysis, in which the occurrence of individual steps moved between the acquisition times yields information on the diffusion rates, and also on the percentage of steps that resemble the movement of immobile (or very slowly moving proteins) and mobile molecules. Examples of movies for SftA are shown in movies S1 and S2, SpoIIIE in movie S3, and for PfkA in movie S4. Movie S5 shows an overlay of detected SftA-YFP molecule tracks on the stream, which were used to assess the dynamic movement of SftA in living cells (see Table 3 for details).

The probability density function (PDF) of step lengths (the size of the individual steps moved by the molecules between consecutive time intervals) was used to determine the diffusive behavior of molecules. PDF describes the relative likelihood of a random variable to take a given value, based on the measured step lengths. The probability of the variable falling between a particular range of values is given by the integral of the variable's density over time. In the case of SftA, e.g., the probability that a molecule moves a small distance is higher than the probability that a molecule takes larger displacements, meaning that many steps do limited movement resulting in restricted movement of the protein over time (Fig. 4**A**). The probability density curve for SftA can be split into two: one for a mobile and one for an immobile fraction, the majority of steps being in the immobile fraction, which fits well with our experimental data (Fig. 4A and movies S1, 2 and 5), and shows that a majority of SftA molecules are statically bound to the forming or fully assembled division machinery. For PfkA-YFP, the curve representing the mobile fraction is much larger than the one representing the immobile fraction of steps, in agreement with

it being a freely diffusing molecule (Fig. 4**C**). It is possible that the mobile fraction and the diffusion constants for PfkA-mYFP are underestimated because of the long exposure time of about 30 ms. In other words, some very fast PfkA molecules may only be detectable with faster acquisition times. However, given that the same acquisition settings were used, PfkA serves as a good control for the diffusive behavior of SftA, whose pdf curve is much more narrow compared to that of PfkA (Fig. 4A and 3C).

Displacement analysis for SftA-YFP showed that 73% of the steps from the 1063 tracks monitored were static and had a diffusion constant (D) of 0.019 $\mu m^2/s$, which is close to the localization error of our system (20 nm). The remaining 27% were mobile with D = 0.35 $\mu m^2/s$ (Figure 4A). These data suggest that about two thirds of SftA molecules are septum-bound, and one third diffuses through the cytosol. Compared with determined diffusion rates of membrane proteins (40), the mobile fraction of SftA moves much faster, in agreement with SftA being a cytosolic protein.

Table 3: Single molecule data analysis

		movies	Cells	tracks	av. life time [s]	av. cell length [µm]	D* [$\mu m^2\ s^{-1}$]	Fractions [%]	trapping time [ms]
SftA	wt	12	117	1063	0.325	3.84 ± 0.87	0.019[1]/ 0.35[2]	73[1] / 27[2]	106 ± 2.8
	FtsA$^-$	8	200	2452	0.241	3.57 ± 0.99		54[1] / 46[2]	60 ± 1
SpoIIIE	- MMC	30	382	3590	0.349	3.46 ± 0.84	0.021[1] / 0.098[2]	73[1] / 27[2]	166 ± 1.7
	+ MMC	27	230	2278	0.361	4.47 ± 1.33		73[1] / 27[2]	154 ± 2.1
PfkA		8	64	2332	0.246	3.52 ± 0.98	0.023[1] / 0.38[2]	9[1] / 91[2]	-

* A Gaussian mixture model is simultaneously fitted to account for the existence of two fractions (static and dynamic molecules) while the diffusion coefficient does not vary, but the fraction size varies according to the probability distribution of displacements. [1]static fraction, [2]dynamic fraction.

Tracking of SftA-YFP in an FtsA depletion strain

In order to assess the influence of FtsA on the localization of SftA and its behavior at the single molecule level, SftA-YFP was tracked in strain CK188 after 1 hour of FtsA depletion. Mid-cell SftA-YFP assemblies were observed, but much less distinct than in wild type cells. SftA often localizes to only one side of the membrane, as was shown in Fig. 1A. FtsA therefore has an influence on SftA localization. However, the presence of SftA foci could be because the depletion was not complete and FtsA remnants were still present on the membrane.

At the single molecule level, the simultaneous fit of SftA molecules tracked in wild type and FtsA depleted cells showed that in the FtsA depleted strain 54% of the steps were static as opposed to 74% of the steps in wild type cells (Fig 4**A)**. Thus, the percentage of static molecules dropped revealing that SftA becomes more dynamic in the absence of FtsA. The loss of static molecules and the increase in dynamic ones is best seen in Fig. 4**A** by the broader distribution of displacements in the FtsA depletion strain.

We also scored the number of SftA molecules in wild type and FtsA-depleted cells that are immobile for a certain number of consecutive acquisition times. In wild type cells SftA molecules rested in average for about 106 ms in a radius of 120 nm (which is considered as static event), while in FtsA depleted cells, the molecules arrested in average for about 70 ms (Fig. 5A, left panel), which is significantly lower as tested by a two sample Kolmogorov-Smirnov test. Note that due to molecule bleaching, these data are an underestimate of the true dwell times and that for some reason the average bleaching time of the SftA molecules was higher in wild type than in FtsA depleted cells (Table 3). Note that the Y-axis is on a log scale, such that the weight of the short times is much greater than that of the longer dwell times. Even though the molecules showed shorter stop times in cells depleted for FtsA, the effect was lower than we expected if FtsA would be the sole factor recruiting SftA to the septum.

Tracking of SpoIIIE and of SpoIIIE in cells treated with MMC

Since SftA and SpoIIIE act synergistically in *B. subtilis*, we were interested in observing the behavior of SpoIIIE-YFP at the single molecule level. SpoIIIE-YFP was imaged under normal conditions and under conditions where double strand breaks were induced by the use of 50 ng/µl of Mitomycin C (MMC). The microscopy setup used and the exposure time was exactly the same as in the experiments described for SftA.

SpoIIIE assembles at the division septum to rescue septum-entrapped DNA after division is completed and becomes indispensable under conditions where chromosome segregation is impaired (1, 2). Previously, it was thought that during vegetative growth SpoIIIE was monomeric and randomly distributed along the membrane with its assembly being triggered upon DNA binding at the sporulation septum (41). Kaimer *et al*. (2) stated that SpoIIIE forms foci in 1.6% of the cells under wild type conditions, which increases to 5.6% after MMC addition. However, it has been shown through PALM imaging that SpoIIIE was present in division septa in more than 30% of cells, localized to the FtsZ ring during invagination in 55% of cells, and partially assembled into hexameric motors during vegetative cell division (42). Moreover, SpoIIIE either formed dynamic clusters with no defined localization or static clusters that localized to the future septation sites. The dynamic clusters were large, around 100 nm in size, and contained highly dynamic SpoIIIE molecules (42). The latter study only investigated SpoIIIE inside these clusters and not the single SpoIIIE molecules in the membrane. Hence, it did not provide a total description of the dynamics of the protein *in vivo*.

Under our experimental conditions, SpoIIIE was largely static with and without MMC treatment. Under both conditions two populations of steps were detected: a large static/slowly diffusing population and a small slightly more dynamic population (Table 3 and Figure 4**B**). After addition of MMC, our analysis revealed no change in the dynamic behavior of SpoIIIE. Interestingly, although the number of SpoIIIE molecules at the septum increases after the induction of DNA damage (MMC) in a subset of cells, this is also not reflected in longer dwell times of SpoIIIE. A comparison of the cumulative density functions (CDF) shows very little difference between non-treated (Fig. 5B bottom panel, blue curve) and MMC-treated cells (red curve). Therefore, even though SpoIIIE visibly accumulates at the division septum in 5% of the cells upon MMC treatment (Kaimer et al 2009), there is not significant change in the (slow) diffusion rates of the protein.

Visualization of the subcellular position of slow and fast moving molecules

We wished to not only determine the most likely position of the proteins (Fig. 3) or the relative fractions of mobile and immobile molecules (Fig. 4), but to determine the localization of the immobile/slow moving and the mobile fractions. The expectation was to find many immobile proteins at the division septum for SftA, and possibly a mildly increased fraction of SpoIIIE

molecules at the cell centre upon addition of MMC. We defined immobile/slow moving as molecules that do not leave an area of 3 by 3 pixels during their lifetime. Fig. 6 shows slow moving molecules in red, and fast moving molecules in blue. For SftA, mid cell and cell poles represent positions of frequent arrests/slow movement, as expected, and there is a clearly visibly reduction in the number of septum-associated stops during the depletion of FtsA (upper panels, 1000 frames were used for comparison of the two conditions). For SpoIIIE, 5% of cells contain visible fluorescent spots after addition of MMC, due to the assembly of SpoIIIE double hexamers at the division site where DNA is entrapped (2), and this is reflected by a moderate visual increase in static tracks in MMC treated cells (Fig. 6, middle panels). This enrichment is most easily seen when slow and fast tracks are sorted along the long axis (x) of the cells (Fig. S1, middle panels). As described above, SpoIIIE-YFP tracks are detected away from the membrane because the focal plane is not always perfectly in the middle plane of cells, and because due to focal depth molecules are visible that are several hundred microns away from the actual focal plane. As expected for the freely diffusing PfkA enzyme, only few of the 1000 tracks are slow or static (Fig. 6, lower panels). These experiments verify the idea that FtsA contributes to the recruitment of SftA to the division machinery and that only few of the total number of SpoIIIE molecules are recruited to the division site upon induction of DNA damage, while a majority continues to move throughout the cell membrane.

Discussion

Our data strongly argue for the DNA translocase SftA being a soluble component of the division machinery in *Bacillus subtilis*, which is recruited to the cell center via protein/protein interactions. We show that SftA is a cytosolic protein when it is expressed in a eukaryotic cell line, and shows no sign of membrane recruitment, in spite of the fact that it contains a predicted transmembrane helix within its N-terminus (37). We also visualized SftA molecules using single molecule microscopy. A major fraction of the molecules was statically positioned at mid cell, while a minor fraction of molecules moved freely within the cytoplasm, consistent with the idea that non-septum bound SftA molecules are soluble. Compared with the cytosolic enzyme PfkA, mobile SftA molecules moved more slowly, suggesting that SftA migrates as a hexamer within the cell, in agreement with the finding that purified SftA forms stable hexamers *in vitro* (2).

SftA fails to localize to mid-cell in the absence of FtsZ (2). Here, we show that SftA is still recruited to mid-cell in the absence of early division proteins EzrA, ZapA and SepF, but showed reduced recruitment when FtsA was depleted. In single molecule experiments, depletion of FtsA resulted in an increase of the dynamic fraction of SftA. This indicates that FtsA acts as an important element that recruits SftA to the septum. In S2 Schneider cells, SftA interacted with FtsA, but no interaction was detected with FtsZ, while both proteins were enriched in TAP-tag pull down experiments. These findings reinforce the idea that SftA is part of the divisome, and suggest that it may be recruited via interactions with several proteins, including FtsA. The function of FtsA as one of the recruitment factors shows that FtsA plays a dual role in *B. subtilis*, in tethering FtsZ to the membrane (43) and in recruiting the DNA translocase SftA.

In contrast to SftA, SpoIIIE molecules showed movement within the membrane. Under the conditions used, SpoIIIE moved very little or very slowly, and the fraction of mobile molecules remained constant upon the induction of DNA double strand breaks. We did not observe a specific localization pattern of SpoIIIE at the division septum or any other site within the membrane, however, we observed a noticeably increase in the number of static SpoIIIE molecules at mid cell after the induction of DNA damage, reflecting the 5% of cells that show visible assembly of SpoIIIE doble hexamers under this condition (2). SpoIIIE tracks were distributed throughout the cell membrane and did not show a displacement over a large distance. SpoIIIE moved very slowly, suggesting that it also moves as a hexamer. It will be interesting to investigate how a divisome-associated or membrane-diffusing hexamer opens up to bind to DNA.

Our analysis shows that SMT is a powerful method to determine if low-abundance proteins are soluble or membrane-attached and to reveal areas of preferred localization, even for very fast-moving molecules. Further, SMT is able to quantify the number of static (target-bound) and mobile molecules, and to pick up even small changes in the dynamic behavior of proteins. Our analysis is also able to visualize subcellular areas of slow-moving and of fast moving proteins, and should therefore be highly relevant for a plethora of other cell biological experiments.

Acknowledgments

This work has been supported by the deutsche Forschungsgemeinschaft (DFG), by the BMBF funded graduate training group NANOKAT, and by the LOEWE funded Centre for Synthetic Microbiology (SYNMIKRO) at the Philipps-Universität Marburg.

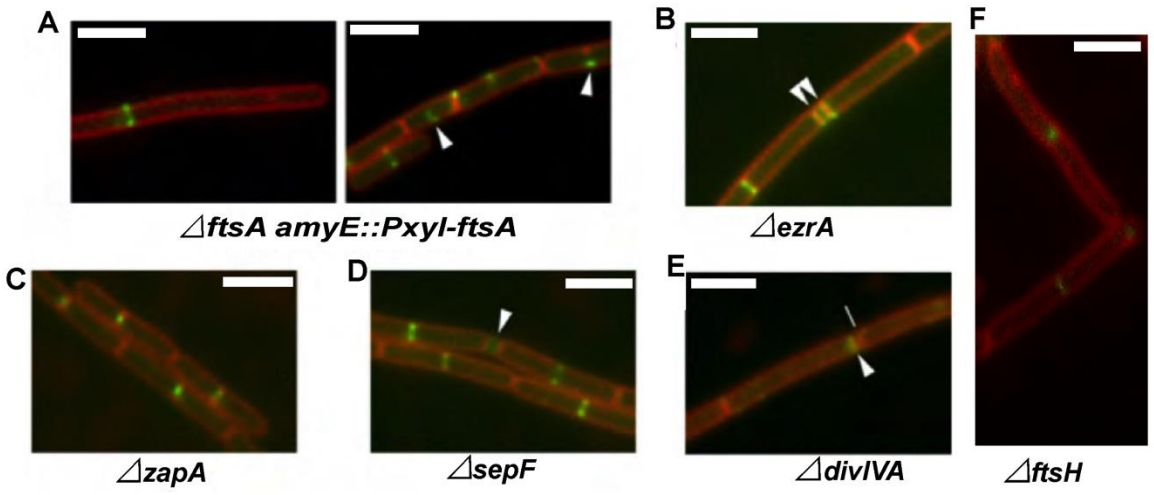

Figure 1. Localization of SftA-YFP in strains that carry mutations of cell division proteins. **A.** After depletion of *ftsA* for 1 h: white arrows: incomplete SftA assemblies; **B.** SftA-YFP in *ΔezrA*; white arrows: double division septa; **C.** SftA-YFP in *ΔzapA*. **D.** SftA-YFP in *ΔsepF*; white arrow: aberrant septum morphology. **E.** SftA-YFP in *ΔdivIVA*; white arrow shows aberrantly formed septum close to the cell pole (white line). **F.** SftA-YFP in *ΔftsH*; Images are overlays of SftA-YFP signals (green) and membranes stained with FM 4-64 (red). White bars 2 µm.

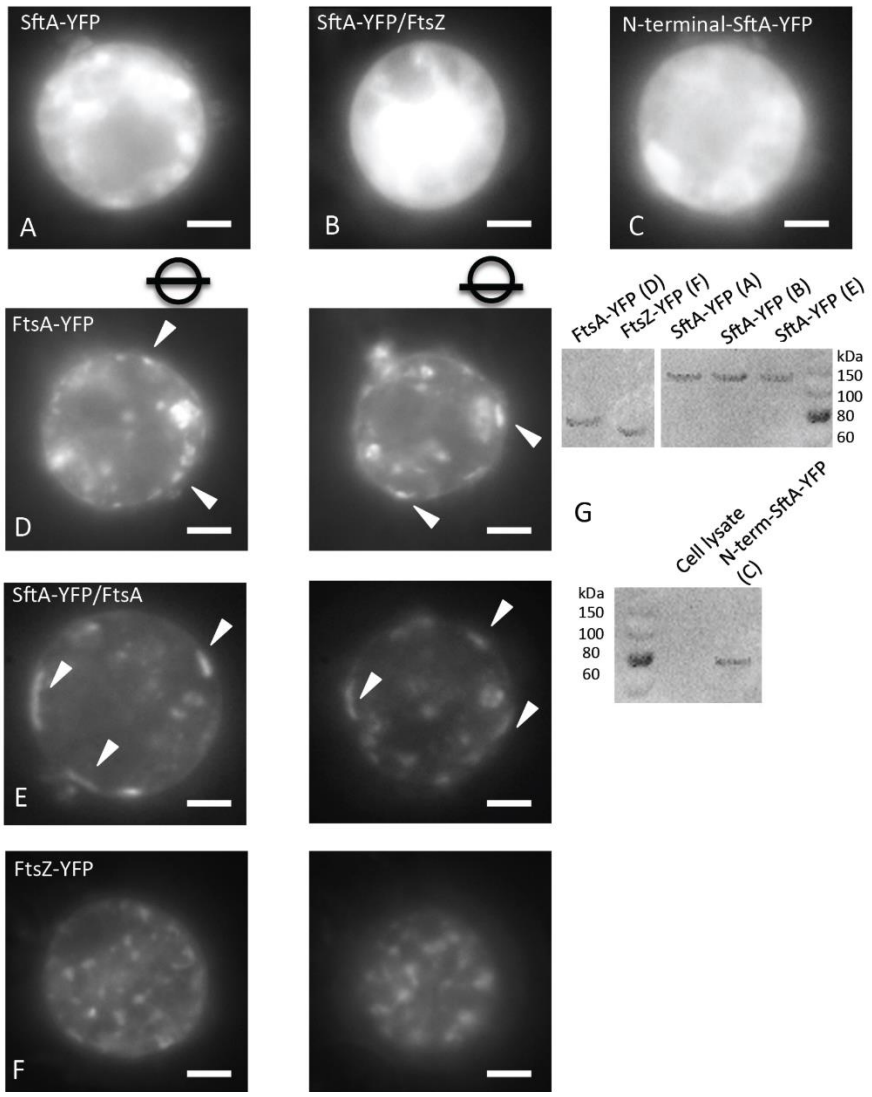

Figure 2. A-F. S2 Schneider cell co-transfection experiments. Cell were transfected with plasmids expressing the corresponding proteins as stated in the panels. White arrows point at membrane assemblies of SftA. Panels A-C were taken through the middle of the cells; circles with bars indicate the focal plane in panels D-F. **G.** Western blot analysis with anti-GFP antibodies of the expressed recombinant proteins in the S2 Schneider cells experiment. The letters between brackets correspond to cells harvested from the respective experiments in images **A-F**. White bars 5 µm.

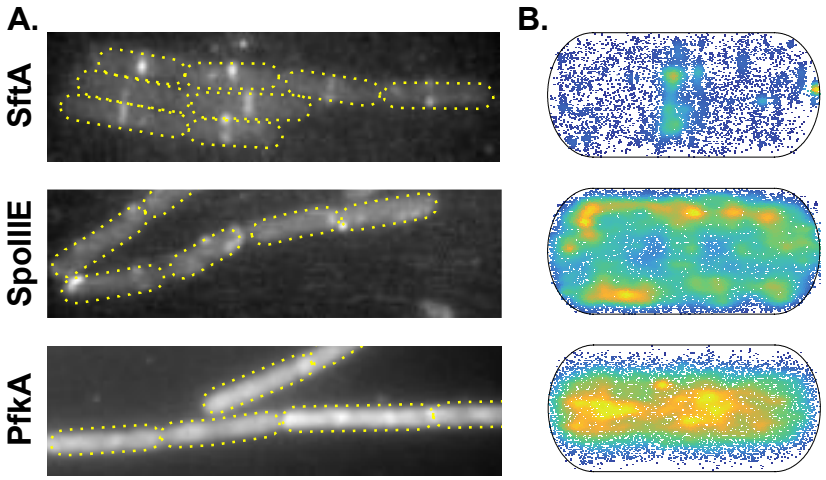

Figure 3. A. Z-Projection of all frames from a selected movie of SftA-YFP, SpoIIIE-YFP and PfkA-YFP. **B.** Heat map of single molecule localizations of SftA-YFP, SpoIIIE-YFP and PfkA-YFP plotted into a standardized cell.

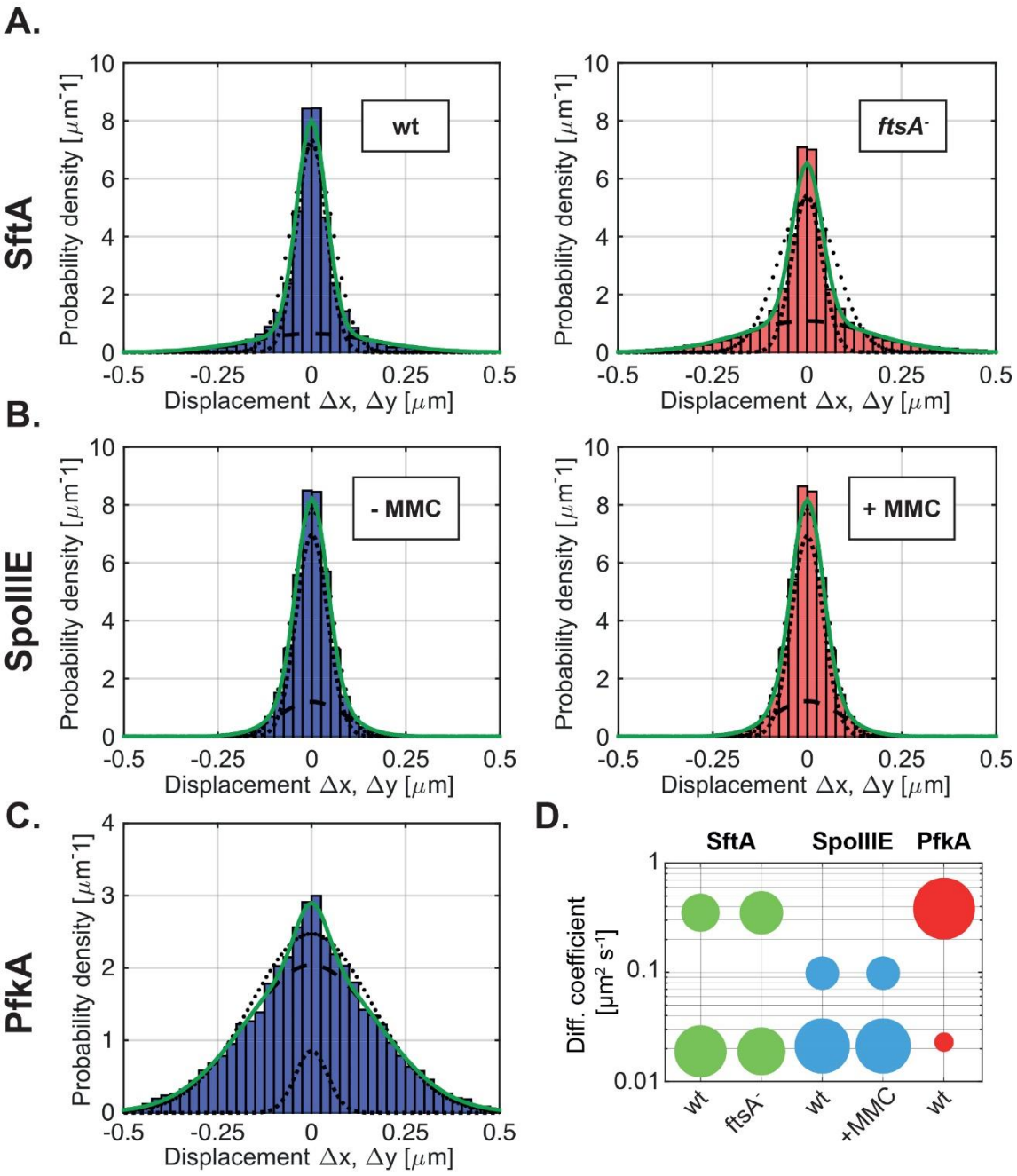

Fig. 4. Single-molecule microscopy of SftA-YFP and SpoIIIE-YFP. **A.** Probability density distribution (PDF) of displacements obtained from SftA-YFP tracked in wild type and *ftsA* depleted cells. Histograms were simultaneously fitted to a Gaussian Mixture Model assuming 2 different types of diffusive behavior (green line). Indeed, the multivariate fit matched the data better than assuming a single Gaussian distribution (dotted line). The intermittent and the implied line correspond to the distributions of the larger and smaller frame-to-frame displacements

representing fast and slowly diffusing molecules. **B.** PDF of SpoIIIE-YFP in undamaged cells and cells treated with 50 ng/ml Mitomycin C (MMC). **C.** PDF of PfkA-YFP. **D.** Bubble plot showing diffusion coefficient of the diffusive subfractions seen for SftA-YFP, SpoIIIE-YFP and PfkA-YFP, respectively.

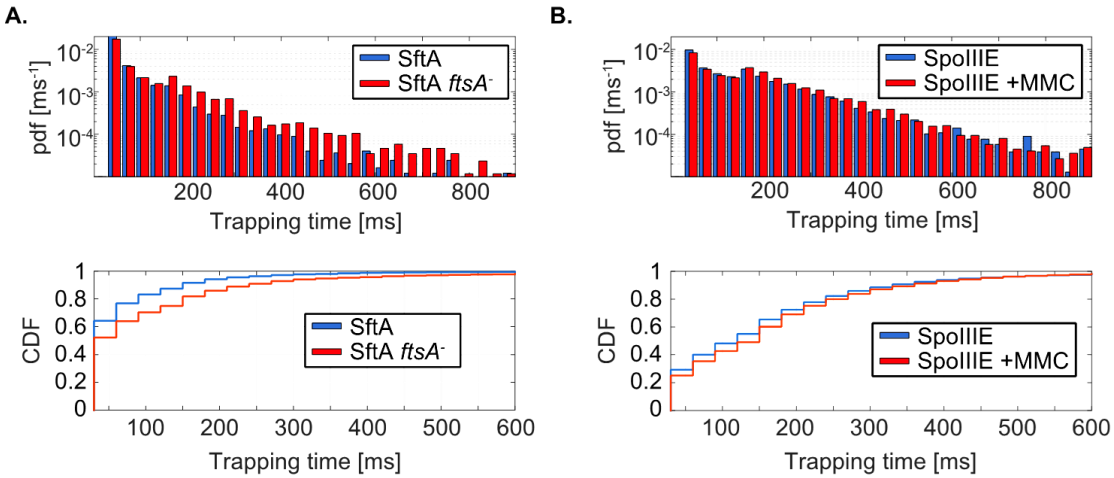

Fig. 5. Dwell time density distributions of SftA-YFP and SpoIIIE-YFP. The dwell time represents the time that a molecule stays within a radius of defined size (here 120 nm). **A.** Probability density distribution function (PDF) and cumulative density distribution function (CDF) of dwell times determined for SftA in wild type and in FtsA depleted cells. **B.** PDF and CDF of dwell times calculated for SpoIIIE-YFP in presence and absence of Mitomycin C (MMC).

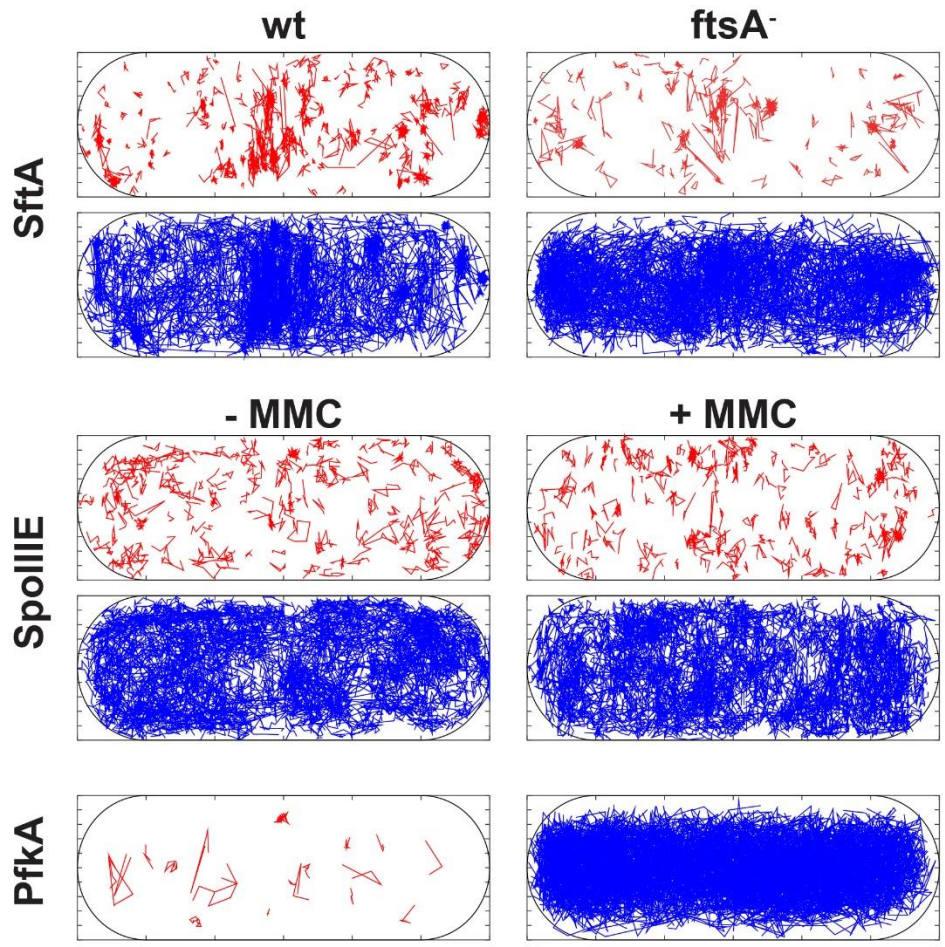

Fig. 6. Determination of the subcellular localization of slow and of fast moving molecules. 1000 tracks of SftA-YFP, SpoIIIE-YFP or PfkA-YFP were projected into a standardized cells of 3 x 1 µm size, and were sorted into slow moving (not leaving an area of 3 x 3 pixels) molecules, indicated by the red tracks, and fast molecules, indicated by blue tracks. FtsA$^-$ indicates depletion of FtsA for 1 hour, + MMC the addition of MMC for 1 hour.

References

1. **Biller SJ, Burkholder WF.** 2009. The *Bacillus subtilis* SftA (YtpS) and SpoIIIE DNA translocases play distinct roles in growing cells to ensure faithful chromosome partitioning. Mol Microbiol **74:**790-809.
2. **Kaimer C, Gonzaler-Pastor E, Graumann PL.** 2009. SpoIIIE and a novel type of DNA translocase, SftA, couple chromosome segregation with cell division in *Bacillus subtilis*. Mol Microbiol **74:**810-825.
3. **Shah JV, Cleveland DW.** 2000. Waiting for anaphase: Mad2 and the spindle assembly checkpoint. Cell **103:**997-1000.
4. **Cleveland DW, Mao Y, Sullivan KF.** 2003. Centromeres and kinetochores: from epigenetics to mitotic checkpoint signaling. Cell **112:**407-421.
5. **Espeli O, Lee C, Marians KJ.** 2003. A physical and functional interaction between Escherichia coli FtsK and topoisomerase IV. Journal of Biological Chemistry **278:**44639-44644.
6. **Yu X-c, Tran AH, Sun Q, Margolin W.** 1998. Localization of cell division protein FtsK to theEscherichia coli septum and identification of a potential N-terminal targeting domain. Journal of bacteriology **180:**1296-1304.
7. **Pichoff S, Lutkenhaus J.** 2002. Unique and overlapping roles for ZipA and FtsA in septal ring assembly in Escherichia coli. The EMBO journal **21:**685-693.
8. **Löwe J, Ellonen A, Allen MD, Atkinson C, Sherratt DJ, Grainge I.** 2008. Molecular mechanism of sequence-directed DNA loading and translocation by FtsK. Molecular cell **31:**498-509.
9. **Bigot S, Saleh OA, Lesterlin C, Pages C, El Karoui M, Dennis C, Grigoriev M, Allemand JF, Barre FX, Cornet F.** 2005. KOPS: DNA motifs that control E. coli chromosome segregation by orienting the FtsK translocase. The EMBO journal **24:**3770-3780.
10. **Blakely G, May G, McCulloch R, Arciszewska LK, Burke M, Lovett ST, Sherratt DJ.** 1993. Two related recombinases are required for site-specific recombination at dif and cer in E. coli K12. Cell **75:**351-361.
11. **Sherratt DJ, Søballe B, Barre FX, Filipe S, Lau I, Massey T, Yates J.** 2004. Recombination and chromosome segregation. Philosophical Transactions of the Royal Society of London B: Biological Sciences **359:**61-69.
12. **Blakely GW, Davidson AO, Sherratt DJ.** 2000. Sequential strand exchange by XerC and XerD during site-specific recombination at dif. Journal of Biological Chemistry **275:**9930-9936.
13. **Barre F-X, Aroyo M, Colloms SD, Helfrich A, Cornet F, Sherratt DJ.** 2000. FtsK functions in the processing of a Holliday junction intermediate during bacterial chromosome segregation. Genes & Development **14:**2976-2988.
14. **Recchia GD, Sherratt DJ.** 1999. Conservation of xer site-specific recombination genes in bacteria. Molecular microbiology **34:**1146-1148.
15. **Sciochetti SA, Piggot PJ, Sherratt DJ, Blakely G.** 1999. The ripX locus of Bacillus subtilis encodes a site-specific recombinase involved in proper chromosome partitioning. J Bacteriol **181:**6053-6062.
16. **Sciochetti SA, Piggot PJ, Blakely GW.** 2001. Identification and Characterization of thedif Site from Bacillus subtilis. J Bacteriol **183:**1058-1068.
17. **Sharpe ME, Errington J.** 1995. Postseptational chromosome partitioning in bacteria.

Proceedings of the National Academy of Sciences **92:**8630-8634.
18. **Wu LJ, Errington J.** 1997. Septal localization of the SpoIIIE chromosome partitioning protein in Bacillus subtilis. The EMBO journal **16:**2161-2169.
19. **Liu NJL, Dutton RJ, Pogliano K.** 2006. Evidence that the SpoIIIE DNA translocase participates in membrane fusion during cytokinesis and engulfment. Molecular microbiology **59:**1097-1113.
20. **Burton BM, Marquis KA, Sullivan NL, Rapoport TA, Rudner DZ.** 2007. The ATPase SpoIIIE transports DNA across fused septal membranes during sporulation in Bacillus subtilis. Cell **131:**1301-1312.
21. **Lemon KP, Kurtser I, Grossman AD.** 2001. Effects of replication termination mutants on chromosome partitioning in Bacillus subtilis. Proceedings of the National Academy of Sciences **98:**212-217.
22. **Kaimer C, Schenk K, Graumann PL.** 2011. Two DNA translocases synergistically affect chromosome dimer resolution in *Bacillus subtilis*. J Bacteriol **193:**1334-1340.
23. **Jaacks K, Healy J, Losick R, Grossman A.** 1989. Identification and characterization of genes controlled by the sporulation-regulatory gene spo0H in Bacillus subtilis. J Bacteriol **171:**4121-4129.
24. **Lewis PJ, Marston AL.** 1999. GFP vectors for controlled expression and dual labelling of protein fusions in Bacillus subtilis. Gene **227:**101-109.
25. **Zellmeier S, Zuber U, Schumann W, Wiegert T.** 2003. The absence of FtsH metalloprotease activity causes overexpression of the σW-controlled pbpE gene, resulting in filamentous growth of Bacillus subtilis. J Bacteriol **185:**973-982.
26. **Dempwolff F, Reimold C, Reth M, Graumann PL.** 2011. *Bacillus subtilis* MreB orthologs self-organize into filamentous structures underneath the cell membrane in a heterologous cell system. PLoS One **6:**e27035.
27. **El Andari J, Altegoer F, Bange G, Graumann PL.** 2015. *Bacillus subtilis* Bactofilins Are Essential for Flagellar Hook- and Filament Assembly and Dynamically Localize into Structures of Less than 100 nm Diameter underneath the Cell Membrane. PLoS One **10:**e0141546.
28. **Defeu Soufo HJ, Reimold C, Linne U, Knust T, Gescher J, Graumann PL.** 2010. Bacterial translation elongation factor EF-Tu interacts and colocalizes with actin-like MreB protein. Proc Natl Acad Sci U S A **107:**3163-3168.
29. **Plank M, Wadhams GH, Leake MC.** 2009. Millisecond timescale slimfield imaging and automated quantification of single fluorescent protein molecules for use in probing complex biological processes. Integrative Biology **1:**602-612.
30. **Reyes-Lamothe R, Sherratt DJ, Leake MC.** 2010. Stoichiometry and architecture of active DNA replication machinery in Escherichia coli. Science **328:**498-501.
31. **Chung K-M, Hsu H-H, Govindan S, Chang B-Y.** 2004. Transcription regulation of ezrA and its effect on cell division of Bacillus subtilis. J Bacteriol **186:**5926-5932.
32. **Low HH, Moncrieffe MC, Löwe J.** 2004. The crystal structure of ZapA and its modulation of FtsZ polymerisation. Journal of molecular biology **341:**839-852.
33. **Singh JK, Makde RD, Kumar V, Panda D.** 2008. SepF increases the assembly and bundling of FtsZ polymers and stabilizes FtsZ protofilaments by binding along its length. Journal of Biological Chemistry **283:**31116-31124.
34. **Arends SR, Kustusch RJ, Weiss DS.** 2009. ATP-binding site lesions in FtsE impair cell division. J Bacteriol **191:**3772-3784.

35. **Salje J, van den Ent F, de Boer P, Lowe J.** 2011. Direct membrane binding by bacterial actin MreB. Mol Cell **43:**478-487.
36. **Pichoff S, Lutkenhaus J.** 2005. Tethering the Z ring to the membrane through a conserved membrane targeting sequence in FtsA. Mol Microbiol **55:**1722-1734.
37. **Crozat E, Rousseau P, Fournes F, Cornet F.** 2014. The FtsK Family of DNA Translocases Finds the Ends of Circles. Journal of molecular microbiology and biotechnology **24:**396-408.
38. **Jaqaman K, Loerke D, Mettlen M, Kuwata H, Grinstein S, Schmid SL, Danuser G.** 2008. Robust single-particle tracking in live-cell time-lapse sequences. Nature methods **5:**695-702.
39. **Garner EC.** 2011. MicrobeTracker: quantitative image analysis designed for the smallest organisms. Molecular microbiology **80:**577-579.
40. **Kumar M, Mommer MS, Sourjik V.** 2010. Mobility of cytoplasmic, membrane, and DNA-binding proteins in *Escherichia coli*. Biophys J **98:**552-559.
41. **Ben-Yehuda S, Rudner DZ, Losick R.** 2003. Assembly of the SpoIIIE DNA translocase depends on chromosome trapping in Bacillus subtilis. Current biology **13:**2196-2200.
42. **Fiche J-B, Cattoni DI, Diekmann N, Langerak JM, Clerte C, Royer CA, Margeat E, Doan T, Nöllmann M.** 2013. Recruitment, assembly, and molecular architecture of the SpoIIIE DNA pump revealed by superresolution microscopy. PLoS Biol **11:**e1001557.
43. **Jensen S, Thompson L, Harry E.** 2005. Cell division in Bacillus subtilis: FtsZ and FtsA association is Z-ring independent, and FtsA is required for efficient midcell Z-ring assembly. J Bacteriol **187:**6536-6544.
44. **Youngman PJ, Perkins JB, Losick R.** 1983. Genetic transposition and insertional mutagenesis in Bacillus subtilis with Streptococcus faecalis transposon Tn917. Proceedings of the National Academy of Sciences **80:**2305-2309.
45. **Gueiros-Filho FJ, Losick R.** 2002. A widely conserved bacterial cell division protein that promotes assembly of the tubulin-like protein FtsZ. Genes & Development **16:**2544-2556.
46. **Hamoen LW, Meile JC, De Jong W, Noirot P, Errington J.** 2006. SepF, a novel FtsZ-interacting protein required for a late step in cell division. Molecular microbiology **59:**989-999.
47. **Tavares JR, de Souza RF, Meira GLS, Gueiros-Filho FJ.** 2008. Cytological characterization of YpsB, a novel component of the Bacillus subtilis divisome. J Bacteriol **190:**7096-7107.

Table 1. Strains and plasmids used in this study.

***E. coli* strains**		**Resistance**	**Source/Reference**
XL 1-Blue	endA1 gyrA96(nal^R) thi-1 recA1 relA1 lac glnV44 F'[::Tn10 proAB$^+$ lacI^q Δ(lacZ)M15] hsdR17(r_K^- m_K^+)	Tet	Stratagene
BL21 Star (DE3)	BF$^-$ ompT gal dcm lon hsdS_B($r_B^-m_B^-$) λ(DE3 [lacI lacUV5-T7 gene 1 ind1 sam7 nin5]) [malB$^+$]$_{K-12}$(λ^S)	none	Invitrogen
Plasmids			
pETDUET-1			Novagen
pPR-IBA 101			IBA lifesciences
pFD1			(26)
***B. subtilis* strains**	**Relevant genotype**	**Resistance**	**Source/Reference**
PY79	Wild type	none	(44)
CK70	*sftA-yfp*	Cm	(2)
CK83	*sftA-yfp*	Tet	This study
WW01	*ftsH::mls*	Mls	(25)
NEJ13	*ftsH::mls sftA-yfp*	Mls/Cm	This study
pFG1	*divIVA::spc*	Spec	(45)
CK100	*sftA-yfp divIVA::spc*	Cm/Spec	This study
FG375	*ezrA*::*spc*	Spec	(45)
CK185	*sftA-yfp ezrA*::*spc*	Cm/Spec	This study
BFA 2863	*sepF::mls*	Mls	(46)
CK187	*sftA-yfp sepF::mls*	Mls/Cm	This study
FG343	*zapA–yshB::tet*	Tet	(45)
CK186	*sftA-yfp zapA–yshB::tet*	Cm/Tet	This study
FG718	Δ*ftsA amyE::*P_{xyl} *ftsA*	Cm	(47)
CK188	Δ*ftsA amyE::*P_{xyl} *ftsA sftA-yfp*	Cm/Tet	This study
NEJ14	*sftA::sftAN-tap*	Cm	This study
PG1006	*amyE::tap*	Spec	Graumann laboratory stock
PG2664	*pfkA-yfp*	Cm	Graumann laboratory stock
CK55	*spoIIIE-yfp*	Cm	This study

Table 2. TAP tag potential interaction candidates

1	ATP dependent Zinc metalloprotease FtsH (strain 168)
2	Protein AroA(G) *Bacillus subtilis* (strain 168)
3	Acetoin:2,6-dichlorophenolindophenol oxidoreductase subunit beta *Bacillus subtilis* (strain 168)
4	Maltodextrin import ATP-binding protein MsmX *Bacillus subtilis* (strain 168)
5	Cell division protein FtsZ *Bacillus subtilis*
6	Succinate dehydrogenase flavoprotein subunit *Bacillus subtilis*
7	Cell division protein FtsA Bacillus subtilis subsp
8	Putative transcriptional regulator yvhJ *Bacillus subtilis* (strain 168)
9	Probable tartrate dehydrogenase/decarboxylase *Bacillus subtilis* (strain 168)
10	Ffh: Signal recognition particle protein *Bacillus subtilis* (strain 168)
11	AcoA: Acetoin:2,6-dichlorophenolindophenol oxidoreductase subunit alpha *Bacillus subtilis* (strain 168)
12	DNA gyrase subunit B *Bacillus subtilis* (strain 168)
13	Cell division ATP-binding protein FtsE *Bacillus subtilis* (strain 168)
14	MurAA: UDP-N-acetylglucosamine 1-carboxyvinyltransferase 1 *Bacillus subtilis* (strain 168)
15	Cell division protein SepF *Bacillus subtilis* (strain 168)

* The pulled down proteins are shown by order of abundance determined by emPAI (exponentially modified protein abundance index) calculated by Mascot. For simplicity reasons, the 15 highest hits are shown. Most of these were completely absent in the control, and a few (FtsE and FtsZ), were present in very low amounts compared to the sample with the bait protein.

Table S1

Oligonucleotide	Sequence	Construct
2622	5’-CATGGGCCCAATCATCATGAAAA-3’	1164-sftAN-tap
2624	5’-CATATCGATCGGAAATACATAGCTGCC-3’	
4406	5’-CATGAATTCATGAACAACAATGAACTTTAC-3’	pPR-IBA 101-FtsA$_{1-425}$
4407	5’-CATGGATCCATGTTCGGCTTGTGTTTTTT-3’	
5509	5’-CATGGTACCATGTTGGAGTTCGAAAC AAAC-3’	pFD1-ftsZ
5510	5’-CATACTAGTGCCGCGTTTATTACGGTT-3'	
5517	5’- CATCTCGAGGCCGCGTTTATTACGGTT-3’	pFD1-ftsZ-yfp
5456	5’-CATGGTACCATGAACAACAATGAACT	pFD1-ftsA
5457	TTAC-3’ 5’-CATACTAGTTTCCCAAAACATGCTTAATAG-3’	
4281	5’-CATGGGCCCATGAACAACAATGAACT TTAC-3’	pFD1-ftsA-yfp
4295	5’-CATCTCGAGTTCCCAAAACATGCTTA ATAG-3’	
2342	5’-CATGGGCCCGACGAACCGAAATCCGCG-3’	pFD1-sftA-yfp
4088	5’-CATGATATCTTCGTTTATTAAATCACTTGC-3’	
2523	5’-CATGGGCCCCGGAAATACATAGCTGCC-3’	pFD1-sftAN-yfp
2624	5’-CATATCGATCGGAAATACATAGCTGCC-3’	

Manuscript 4C

Polyploidy and the processes governing origin segregation of *Bacillus subtilis*

Nina el Najjar[1], Felix Schmidt[1,2], Bruno Eckhardt[1,2], Peter L Graumann[1*]

[1]SYNMIKRO, LOEWE Center for Synthetic Microbiology, and Department of Chemistry, Philipps Universität Marburg.
[2]Department of Physics, Philipps Universität Marburg

[1]SYNMIKRO, LOEWE Center for Synthetic Microbiology, and Department of Chemistry, Philipps Universität Marburg.

*corresponding author, email: peter.graumann@synmikro.uni-marburg.de
49(0)64212822210

Abstract

In recent years, growing evidence has shown that a multitude of species in different phylogenetic groups are polyploid. Such examples can be found among halophilic and methanogenic archaea, proteobacteria, and cyanobacteria. This study aims at investigating the ploidy state in the gram-positive model organism *Bacillus subtilis*. The numbers of origins, termini, and nucleoids of a laboratory strain of *B. subtilis* were quantified both under conditions of fast and slow growth. *B. subtilis* was found to be mero-polyploid in exponential phase with, on average, 4.42 origins and 1.89 termini in rich medium at 37 °C compared to 1.8 and 1.69 respectively in minimal medium at 25 °C. The nucleoid count showed that a majority of the cells are diploid regardless of the growth conditions, with a subset of around 17% being polyploid with 3 or more nucleoids. Induction of DNA double strand breaks using MMC resulted in a higher number of origins under conditions of slow growth (25°C in minimal medium), but not of termini. Hence, a majority of cells were still diploid. Taken together, these results indicate that *B. subtilis* is predominantly diploid during exponential growth with only a subset being polyploid, and an even smaller subset of monoploid cells. Moreover, the dynamics of *B. subtilis* origins were followed through the cell cycle in 10 s intervals, revealing that the main mechanism driving chromosome partitioning may be directed diffusion, and that the process is quite robust against perturbations of the cell cycle, and continues despite the induction of DNA damage.

Introduction

Polyploidy is the heritable condition of possessing more than two complete sets of chromosomes. Most polyploid organisms have an even number of sets of chromosomes, four being the most common (1). Polyploidy is widely distributed in eukaryotes (2).

It is generally assumed that most prokaryotes are monoploid and contain a single copy of a circular chromosome. However, polyploidy can offer fitness advantages to prokaryotes through inferring gene redundancy, which reduces the chance that deleterious mutations become homozygous, and allows for gene diversification and acquisition of new functions (1).

Escherichia coli contains one chromosome under slow growth when its generation time is longer than the time required for chromosome replication and segregation. Under optimal laboratory conditions, the generation time of *E. coli* can become less than the replication time, and a new round of replication is initiated before termination of the previous one. The cells become mero-diploid or mero-oligoploid for the origin-proximal genes (3). Therefore, *E. coli* is not a true monoploid species. Several monoploid prokaryotic species exist with one copy of the chromosome irrespective of growth rate, e.g. *Caulobacter crescentus* or *Wolinella succinogenes* (4).

Other bacteria are known to be polypoid, like the radio-resistant species *Deinococcus radiodurans*, which has about 8 copies of its chromosome (5), or *Azotobacter vinelandii* which contains up to 80 chromosome copies (6). This is only seen in conditions of fast growth, while cultures grown in synthetic medium are not polyploid (7). A few other examples exist, but are thought to be exceptions to the rule that bacteria are essentially monoploid.

Information about ploidy in gram-positive bacteria is limited. Genome copy numbers have been determined for *Lactococcus lactis* as well as for *Bacillus subtilis*. *L. lactis* was found to have two copies of the chromosome under slow growing conditions, which were replicated into four chromosomes during the C period of the cell cycle. Therefore, it can be deduced that this species is diploid without overlapping replication cycles (8).

In *B. subtilis*, tagging the replication origin with YFP showed one to two origins during slow growth in minimal medium at 30 °C, but these numbers increased to two to four origins during faster growth in minimal medium supplemented with amino acids at 30 °C (9). Another study showed that *B. subtilis* has an average of 3 origins per cell in minimal medium at 37 °C through analysis of the DNA content of individual cells by flow cytometry (10). Quantification of

the average genome content by fluorescence microscopy and by a chemical method revealed that slow growing cells with a doubling time of 73 minutes contained around 1.5 genomes, while fast growing cells with a doubling time of 30 minutes contained 3.2 genomes (11).

The mechanisms mediating chromosome segregation in bacteria are poorly understood. The origin attachment model proposed by Jacob, Brenner and Cuzin in 1963 was among the first proposed, postulating that newly replicated origins are tethered to the cell envelope close to mid-cell and separated by growth between them. It is now clear that cell elongation in rod-shaped bacteria is not restricted to zonal growth, but occurs throughout the cell length. Furthermore, movement of origins away from mid-cell is much faster than the rate of cell growth, discrediting the model: in *Bacillus subtilis*, the average movement of chromosome is 0.17 μm/min, while the speed of cell elongation is 0.011–0.025 μm/min^{-1} (9, 12).

Despite evidence of dynamic movement of chromosome regions, mitotic-like mechanisms acting on bacterial chromosomes have only been demonstrated in few cases. Examples of such cases are the The *Vibrio cholerae* ParAI and ParBI system for segregation of the large chromosome. The apparatus pulls the origin region of the large *V. cholerae* chromosome to the cell pole and anchors it there (13) *Caulobacter crescentus* also segregates its chromosome using a partitioning (Par) apparatus that has surprising similarities to eukaryotic spindles (14). The *par* genes of *B. subtilis* are not essential, and no homologous system has yet been discovered in *Escherichia coli*, where a group of nucleoid structural and segregation genes including *mukBEF*, *seqA* and *matP*, appear to have supplanted both the bacterial structural maintenance of chromosomes (SMC) and partitioning (*par*) genes in γ-proteobacteria, suggesting that other mechanisms of segregation may play an important role (15).

The extrusion-capture model for *B. subtilis* proposes that the energy released during replication is harnessed to power, at least in part, partitioning of newly duplicated chromosomal regions (16, 17). In this model, the replisome pulls the DNA template into the cell center, duplicates it, and then releases the products into opposite cell halves. Movement away from the center is kept orderly by proteins involved in chromosome organization, compaction, and supercoiling. A transient association of newly duplicated DNA with the inner face of the membrane, as suggested for *E. coli* (18), might facilitate origin migration. The force generated during transcription by a single stationary RNA polymerase is ~25 picoNewtons (19), more powerful than either a myosin or kinesin motor. Together, DNA polymerase and the replicative

helicase can contribute to template movement. The extrusion-capture model postulates that once released outward from the replisome, the origins are captured and held on opposite sides of the cell via a membrane-associated anchor. The bulk of partitioning can be then achieved by a combination of ongoing replication and chromosome recompaction. Finally, specialized mechanisms exist to ensure that sister terminus regions are not caught in the division septum (17).

Another theory suggests that entropy, by itself, is sufficient to insure successful chromosome partitioning in bacteria. Polymers confined in a box can actively segregate, whereas disconnected, physically identical particles, tend to mix. In polymer physics, overlapping chains have fewer conformational degrees of freedom, or less conformational entropy, than the ones that are completely separated. Thus, entropic forces can actively segregate mixed polymers from one another. When a confinement is added to the chains, they behave like a loaded entropic spring. The bacterial chromosome can also be viewed as a loaded entropic spring of blobs, in which each blob is a structural unit of the chromosome and consists of supercoiled DNA stabilized by DNA-binding proteins, thus storing the free energy produced by the DNA–protein interaction (20).

In this study, we used fluorescence microscopy to quantify the number of origins and termini in both fast and slow growth. These chromosomal positions and others were quantified under normal conditions as well as after induction of chromosomal double strand break with the use of Mitomycin C to assess the role of DNA damage on cell cycle arrest and continuation of replication. Moreover, the dynamics of the tagged origin of replication region of the chromosome, under different growth conditions with agents that affect the cell cycle and consequently chromosome segregation, were assessed in order to describe the mode of chromosomal movement in *B. subtilis*. We performed a quantitative analysis of the motion of *oriC*, one of the first loci to segregate.

Materials and Methods

Bacterial strains

The bacterial strains used in this study are shown in Table 1.

Fluorescence microscopy

To quantify foci under slow growing conditions, *B. subtilis* cells were grown in $S7_{50}$ minimal medium non-supplemented with amino acids at 25°C under shaking conditions until exponential growth. For the quantification under fast growth, cells were grown LB and incubated in a shaking water bath at 37°C. 3 µl of cells were then transferred on an agarose slide - glass slide (Microscope slides standard, Roth) coated with an agarose layer ($S7_{50}$ minimal medium, 10 mg/ml agarose) - and covered with a cover slip (Cover slips, Roth). Conventional light microscopy was performed using a Zeiss Observer Z1 (Carl Zeiss) with an oil immersion objective (100 × magnification, 1.45 numerical aperture, alpha Plan-FLUAR, Carl Zeiss) and a CCD camera (CoolSNAP EZ, Photometrics). Cells were treated with red fluorescent membrane stain FM 4-64 (excitation: 515 nm/emission: 640 nm, final concentration 1 nM) and DNA intercalating blue fluorescent dye DAPI (excitation: 358 nm/emission: 461 nm, final concentration 0.72 nM) and incubated for 2 minutes at room temperature prior to microscopy. Electronic data were processed using ImageJ (Wayne Rasband, National Institutes of Health), which also allows the calibration of fluorescence intensity, and of pixel size to determine cell length.

Time lapse movies were acquired with an interval of 10 seconds at constant laser intensity. For this purpose cells were mounted on a thicker agarose pad enclosed in a small chamber to avoid desiccation as depicted in figure S2. For microscopy of spores, the same setup was used but images were acquired every 90 seconds for a minimum period of two hours.

Prior to analysis, maximal intensity z-projections of 3D image stacks were aligned using the translation function from the ImageJ StackReg plugin (21), and cropped with ImageJ geometric operations. The movies were processed with Fiji (22).

Quantification of foci and nucleoid number

The numbers of foci and nucleoids were counted manually, or, alternatively, the software ChainTracer (Norbert Vischer, University of Amsterdam) was used together with the ImageJ plugin ObjectJ (23) to automatically calculate the amount of DAPI fluorescence in the cell. ChainTracer analyzes multi-channel images of chain forming bacteria while ObjectJ focuses on the organization of image analysis tasks using an integrated approach. The software recognizes different channels and uses them to detect cell chains, resolves individual cells from chains by detecting the cell borders and septa using the membrane stain (red channel), and finally calculates the amount of fluorescence in each cell. The fluorescence was calculated through assigning the DAPI images to the green channel since the software, by default, calculates the fluorescence from the green channel. The length and width of individual cells can also be calculated by the software. The results are displayed by the end of the analysis in the ObjectJ results table.

Purification and germination of *B. subtilis* spores

Spores purification was done according to Graumann, 2000. Briefly, DSM plates with the corresponding strain were first incubated for 24 hours. For spore purification, plates were flooded with 1 M KCl–0.5 M NaCl. Cells were washed twice in distilled water (dH_2O) and incubated in 10 mM Tris buffer (pH 7.5) containing 2 mg of lysozyme per ml for 60 min at 37°C, followed by successive washes in 1 M NaCl, H_2O, 0.05% sodium dodecyl sulfate, and 50 mM Tris–10 mM EDTA (pH 7.5) and three times with distilled water. Purified spores were stored at 4°C or at -80°C in dH_2O–5% glycerol.

For germination of spores, a culture with an optical density (OD) of 0.6 to 0.8 was washed in H_2O and resuspended in 0.5% glucose containing $S7_{50}$ medium supplemented with 10mM L-Alanine, 0.1% glutamate, and 0.025% Casamino Acids. After a heat treatment at 70°C for 30 min, spores were centrifuged, resuspended in the same medium, and incubated at 30°C for 30 min, followed by incubation at 23°C for 30 minutes or 1 hour.

Generation of tracks and tracks analysis

For each condition around 50 pairs of separating origins were tracked and the tracks were analyzed. Tracks were generated with TrackMate, a plugin for Fiji (22) .TrackMate provides a way to semi-automatically segment spots or roughly spherical objects from a 2D or 3D image, and track them over time. It follows the classical scheme, where the segmentation step and the particle-linking steps are separated. To follow the origin region separation, pairs of origins in the acquired movies were followed from the time they were overlapping, which was determined by a fluorescence level twice as high as that for single origins, or when they were in close proximity (less than 0.2 µm separation), till the end of the movie. Movies had a length ranging from 40 minutes to one hour. The obtained tracks were then analyzed using the MATLAB software.

Results

Polyploidy of *Bacillus subtilis*

The numbers of origins and termini were counted under conditions of slow and fast growth at an OD_{600} ranging between 0.5 and 3, and the results are summarized in table 2. Cell samples were collected at 30 minutes intervals, microscoped, and a cumulative of the counts was made. Slow growth refers to cells growing in $S7_{50}$ minimal medium non-supplemented with amino acids at 25°C, while fast growth refers to cells growing at 37°C in LB. The termini counts in table 2 show that *Bacillus subtilis* is most favorably diploid irrespective of the growth conditions, but that it is mero-polyploid in rich medium where it can have multiple origins per cell.

The doubling times of the respective strains were averaged from three different experiments and compared to the wild type in order to assess the effect of the chromosomal tags on the growth rate of the bacterium. Supplementary figure S1 shows a representative growth curve from each strain as well as of the wild type, and the calculated doubling times. The doubling times of the strains AT62 and PG26 were very similar to that of the wild type, proving that the strains can grow and replicate normally. Table 2 shows that *B. subtilis* seems to be diploid most of the time, regardless of the growth medium used or the temperature of growth.

For a more thorough overlook at the polyploidy status of *B. subtilis*, the numbers of origins, termini, as well as chromosomes, were counted every half an hour in in LB, starting from an OD_{600} at 37°C of 0.1. As a control, the state of polyploidy and the chromosomal content was also counted

in cells growing at 25 °C minimal medium at an OD_{600} of 0.7. Results are summarized in table and figure 3. The chromosome exists for the entire cell cycle as a distinct, compact structure termed the 'nucleoid'. Near the end of DNA replication, the nucleoid adopts a bi-lobed, dumb-bell shape that ultimately splits into two independent structures prior to cytokinesis (24). In the AT62 strain, chromosomes forming a dumb-bell shape were counted as two nucleoids when they corresponded with two foci for the terminus tag. However, when only one focus was detected in the GFP channel, a dumb-bell was considered as two nuclei when each lobe measured >0.55μm, or when the lobes were separated by at least 3 dark pixels. The offset of 0.55 was chosen through measuring several small separated lobes and averaging them. For the PG26 strain, the number of origins was not used to assess polyploidy since multi-origination does not correspond to the completion of all replication cycles before cell division. In this strain only the number of nucleoids was used for the classification of cells. Nucleoids with a dumb-bell shape were considered as one chromosome when the lobes were smaller than 0.7 μm and not separated by a minimum of 3 dark pixels. Cells with three or more distinct nucleoids were considered polyploid (Figure 1). Elongated nucleoids occupying >2.5 μm of the cell length were counted as 2 distinct chromosomes, and results were summarized in the tables 3 and 4.

Briefly, the number of termini remained more or less constant while the number of origins increased with time, consistent with the observation that *B. subtilis* is diploid most of the time. However, the number of termini could be underestimated because in many cases it was hard to tell if the focus between 2 nuclei corresponded to one or two termini. Based on the counted number of nuclei according the above criteria, there was always a subset of polyploid cells under fast growth, but this subset never exceeded 22% for the origin tag strain (PG26), and 18% for the terminus tag (AT62) strain. The total polyploidy calculated over all time points under fast growth conditions for both strains was 17.2% and 15.06%, respectively. Figures 1 and are 2 show examples of monoploid, diploid, and polyploid cells in the AT62 and PG26, respectively.

Relation of the cell length to the growth rate

For the PG26 strain, the cell length in minimal medium ranged between 0.894 µm and 4.112 µm (n=207), with an average of 2.347±0.474 µm. The values were comparable for AT62 grown in minimal medium with cell length ranging between 0.684 µm and 3.881 µm and an average of 2.137±0.613 µm (n= 252). At faster growth both strains showed a direct correlation between the chromosomal content and the cell length whereby the polyploid cells were considerably longer than the diploid and the monoploid cells (figure 3).

Estimation of the number of nuclei based on DAPI fluorescence

Though the manual counting provided an idea on the polyploidy state of *B. subtilis*, it was prone to subjectivity and hence needed to be corroborated with an automated count. For this purpose, the ChainTracer software (Norbert Vischer, University of Amsterdam) was used together with the ImageJ plugin ObjectJ (23) to automatically calculate the amount of DAPI fluorescence in the cell.

The software can detect cell chains in a hyperstack, then extract single cells from chains by detecting the septa and cell borders from the membrane stain images assinged to the blue channel. Finally, the fluorescence assigned to the green channel of the hyperstack is calculated, in our case the DAPI. The terminus tag strain (PG62) was chosen to perform the count under slow and fast growth. The cells manually counted previously were re-counted for this purpose: in minimal medium at 25°C and an OD_{600} of 0.7, as well as in LB at 37 °C after 1.5 hours, 2 hours, and 2.5 hours of growth. For this purpose, a threshold was specified for monoploid cells in each condition by averaging through fluorescence intensity of at least 30 cells measuring between 1.1µm and 2 µm in each condition.

The average intensity of a nucleoid in small monoploid cells was comparable in all counted samples. Monoploid cells were those having 1-1.69 genomes calculated from the threshold, diploid cells between 1.7 and 2.69, and polyploid cells had anything ≥2.69 genomes. Results are shown in table 5 and figure 4. The percent polyploidy was underestimated by the manual count when compared to the automated based count. However, from both cases, it can be clearly deduced that *B. subtilis* is preferably diploid under slow and fast growth conditions, and that the number of polyploid cells is very small under slow growth and increases with the growth rate under fast growth. The cell length is also in agreement with our previous measurements where the polyploid

cells are on average longer than 4 µm, the diploid between 3 µm and 4 µm, and the monoploid cells smaller than 2 µm.

Effect of DNA double strand break on the polyploidy state of *B. subtilis*

In order to assess the effect of DNA double strand breaks on the chromosome count as well as the number of origins in *B. subtilis*, Mitomycin C (MMC) was added to a final concentration of 50 ng/ml to cells growing in minimal medium at 25 °C. A concentration of Mitomycin C between 50 and 100 ng/ml causes the formation of base adducts and DNA inter-strand cross-links (in a ~4:1 ratio), which can lead to single strand gaps and to double strand breaks (DSBs) (32, 33). The repair of inter-strand cross-links can be achieved via two pathways, one including nucleotide excision repair, and the other through DNA polymerase II, or proteins mediating homologous recombination (HR) (34). DSBs can be either repaired through direct non homologous-end joining, which could result in connecting the wrong ends, or through RecA mediated DNA repair via HR, in which the intact sister chromosome is used to fix a DSB (35).

The DNA damage also triggers an SOS response. There are two regulatory components to this response: RecA and LexA. Once DNA damage occurs, the amount of ssDNA increases in the cell (26). RecA binds to ssDNA exposed during DNA damage and catalyzes a recombination processes inside the cell. When RecA is bound to ssDNA, it also stimulates the autocleavage of LexA (also called DinR in *B. subtilis*) (27). LexA is a transcriptional repressor that binds within the promoter region of target genes as a dimer and prevents transcription from these promoters. Autocleavage of LexA relieves repression, allowing transcription of LexA-repressed genes (28). In *E. coli,* treatment with MMC causes a large transcriptional effect on approximately 1,000 genes, of which only around 50 are likely to be regulated directly by LexA (29).

In *B. subtilis*, In addition to the *recA*-dependent transcriptional response, replication arrest also induces a *recA*-independent response, which is mediated in part by DnaA (30). MMC was shown to cause a relative increase of the dosage of the origin of replication proximal genes. It was concluded that this increase in gene dosage was most likely caused by a reduced rate of elongation of replication, rather than by over-initiation. In other terms, the use of MMC slows down replication elongation, causing an increase in origin-proximal DNA and a relative increase in transcripts from origin-proximal genes (30).

The addition of MMC resulted in the stopping of growth for three hours to follow. Cells microscoped 30 minutes after MMC addition showed nucleoids with a condensed morphology where the vast majority of cells (~ 70% of 250 cells counted) contained one nucleoid instead of two, and 2.5 origins on average. The rest of the cells had two nucleoids that looked fused (figures 5 and 6).

90 minutes after MMC addition, around 15% of the cells were dead in each imaging field, and these were excluded from the count. The number of origins increased from around 2 per cell prior to the induction of damage to 3.5±1.47 (n=200 cells), which in accordance to previously published data (30). The cells were also elongated and the average cell length increased from 2.17±0.52 before addition of MMC (n=150 cells) to 3.7±1.413µm after MMC addition. The cell length fell in a range between 1.6 and 7.7µm, with 20% of the cells being above 5 µm. 16% of the 200 cells counted had 5 origins or more, with a few having up to 8 origins. The nucleoids were decondensed in the majority of cells. A subset of the cells was anucleated (around 3%), and cells longer than 5µm contained an elongated unsegregated nucleoid. 0.5% of the cells had nucleoids bisected by a septum. The terminus tag strain showed a comparable phenotype where the cells were elongated and the nucleoids were decondensed 90 minutes after MMC addition. However, excluding the dead cells, the average number of termini was 1.7±0.613 (n=224 cells), with 7.14% of the cells having 3 termini or even 4 in very rare cases.

This shows that despite the replication arrest and the atypical nucleoid morphology, many cells were either still able to complete a replication cycle and have a double set of chromosomes after induction of double strand breaks, or that the cells simply retained the number of nucleoid and termini it had before damage induction. The latter is in accordance with the idea that MMC slows down the cell cycle considerably but does not stop it completely. Goranov et al. showed that double strand breaks induced by MMC inhibit the replication elongation beyond the origin proximal region. This can be confirmed since our experiments show an increase in number of origins but not of termini.

B. subtilis showed a growth defect when subjected to blue light

Microscoping the PG26 strain which carries a LacO/LacI-CFP array in a 10 seconds interval with a 445 nm laser resulted in an obvious hindering of growth. The cells imaged for an average of an hour stopped growing completely, with some dying towards the end of the acquisition time.

However, the PG26 grew normally under the microscope when subjected to white light or to the 516 nm laser, indicating that the growth defect was indeed an outcome of light toxicity rather than a defect in the strain itself.

Despite the light toxicity, around 4.5% of the imaged cells (n=300) had a separation event of sister origins, as can be seen in panel A of figure 7. The panel only shows the frames in a movie from the moment the two indicated origins started separating (around 200 seconds), till they assumed their final positions in the cell quarters (movie S1).

Through looking at the spores of PG26, it was obvious that the initial division process seems to be an early event, since 48% of them (n=400) had already two visible origins of replication before emerging out of the spore coat, one hour after spore activation and incubation at 23 °C.

We also noticed that the spores of the PG26 strain did not germinate under the blue laser light, but germinated normally when subjected to the 516 nm laser.

Exit from dormancy starts with the synthesis of RNA and proteins while synthesis of DNA and chromosome replication do not occur until at least 30 minutes into the germination process (31). When acquisition was made at an early stage of germination, around half an hour only after incubation at 23 °C, the spores were still very small, most of them ranging between 0.4 and 0.8 µm. Fluorescence of the single origin inside was masked by that of the coat (Fig. 7C).

However, when germination was followed after around 60 minutes of incubation, most spores were around 1µm in length or slightly longer, and the origins(22) were already viewable (Fig. 7B).

The halting of the germination and growth process did not affect the separation of a small subset of origins (around 5% in 200 counted spores) (Fig. 7B, movie S2). All supplementary movies are shown with an interval time of 10 seconds except for movie S2, where 90 seconds were used.

The spores of the PG 26 strain germinated normally when subjected to green light (Fig. 7D). For comparison, the original culture of spores was left incubating at 23 °C during the time of acquisition of the movie in figure 1D. A few images were then taken both with the YFP and the CFP laser to compare the germination level in the test tube to that under the laser (Fig. 7E).

The KS188 strain, however, which bears a TetO/TetR-YFP array, seemed to grow normally under the laser intensity of 516 nm for the above mentioned imaging times, and its growth was comparable to that of the wild type under normal white light or under the 516 nm laser. This has lead us to switch to using the KS188 strain, even though its doubling time was slower than that of

the PG26 (35 min. vs 27.99, respectively). Therefore, the CK188 strain was used in all further experiments aiming at characterizing the mode of origin separation in *B. subtilis*.

In most cells observed, the initial locus dynamics was characterized by the locus remaining localized to mid-cell, until replication was started. Replication is initiated at the chromosomal origin of replication (*oriC*), and proceeds bi-directionally down the two arms of the circular chromosome. The newly replicated sister loci then split and undergo rapid translocation towards the quarter cell positions. After reaching the quarter cell positions, *oriC* dynamics is again slower and the replicated *oriC* regions stay at the acquired positions without considerable movement (movies S3A and S3B).

Under the used microscopy conditions, 19.7% of the cells had an origin separation event. For the mathematical analysis of the movement, all the separating origins in an imaging field were tracked from different movies. Fig. 8 shows an exemplary separation over time. According to our observation from the acquired movies, the process seems to be quite stochastic and several modes of movements were observed: In some cases the origins separate and then move back together, in others they separate completely but with differing rates, in some fast, in others more slowly. Further experiments were made to assess the role of cell cycle arrest and the blocking of the topoisomerase IV on the origin separation. Fig. 10 shows the step displacement over time of the origins under all experimental conditions. Fig. 10A shows exemplary tracks of two origins in one cell; part 1 shows all the time points in the tracks with their actual position in the cell, and part 2 shows the distance between the two origins over time, with darker dots reflecting later time points. The subsequent analysis uses the relative distance between the separating origins rather than the actual positions of the spots to circumvent interferences created by the processes of cell growth and elongation during the imaging time. Part 3 is a projection of the distances over a horizontally laid cell. This is important for further analysis in order to have all the tracks on the same x and y coordinate axis. In part 4, the movement is separated on the x and y directions, and the trend line shows in this case a linear pattern typical for a Brownian motion, but also a directionality of the movement.

Fig. 10B1 is similar to the one in 10A3, except that it includes tracks form all analyzed cells, under different conditions. 10B2 shows the displacement in μm against a lag time τ for all tracks, where $\tau = n\Delta t$. Δt is the time delay between the consecutive frames, and n is the interval of frames over which the distance is measured and averaged. For simplicity, the x axis shows 'frames'

instead of Ƭ (s), so a lag time of 20 frames corresponds to a Ƭ of 200 seconds. The step displacement shown in this graph is better descriptive of the movement and the average for all tracks for the wild type (solid dark blue line) shows what can be best described as simple diffusion as can be seen by the linearly growing line for movement along the long cell axis. The movement on the y axis, however, is much more restricted as would be expected because of the space limitation in that direction.

Effect of Mitomycin C on origin separation

In response to MMC treatment, the cells were clearly elongated and cell division was inhibited. This is due to SOS induction, which is activated by the presence of ssDNA through activation of RecA (36). The cells also stopped growing, which could be seen throughout the process of acquisition. In every field of imaging, around 15% of cells were dead or dying, in which either no *oris* or a single *oriC* was seen in the middle. An *ori* separation event was seen in 18% of 364 counted cells, which is comparable to the wild type (Fig. 9A) (movies S4A and S4B). However, figure 10B shows that the addition of MMC to exponentially growing cells resulted in the slowing of the separation process compared to the wild type. Though the origins eventually separated, they moved smaller distances in the same time window along the x axis. Again, the movement was restricted for the y axis.

Effect of ciprofloxacin on origin separation

Another thing we wanted to investigate was the effect of blocking the topoisomerase IV (TopoIV) on *ori* segregation in *B. subtilis.* In *E. coli*, in the absence of functional TopoIV, MukBEF (the *E. coli* SMC) formed multiple foci that were distributed uniformly throughout the nucleoid, whereas multiple catenated *ori*s clustered at midcell. Once functional TopoIV was restored, the decatenated *ori*s segregated to positions that are largely coincident with the MukBEF foci, thereby proving a role for topoisomerase IV in origin segregation (37).

The gyrase and Topoisomerase IV (TopoIV) belong to the family of class II topoisomerases. The gyrase controls DNA supercoiling and relieves topological stress arising from the translocation of transcription and replication complexes, while topoIV resolves interlinked chromosomes following replication (38). TopoIV and the gyrase are targets of the 4-quinolones like ciprofloxacin. Quinolones cause reversible trapping of these enzymes on the DNA. At higher drug

concentrations, cell death occurs as double-strand DNA breaks are released from trapped gyrase and/or topoIV complexes. Repair of quinolone-induced DNA damage occurs largely via recombination pathways (39).

Although gyrase is the main target for quinolones in Gram negative bacteria, topoIV is the preferred target in some Gram-positive organisms such as *B. subtilis*, and trapping of the gyrase happens at much higher drug concentrations (40-43).

In *B. anthracis* for instance, three high levels of ciprofloxacin resistance were detected, the irst and last of which were characterized by mutations in *gyrA* or *gyrB* quinolone resistance-determining region (QRDR) (44).

For our experimental purposes, we aimed to block the topoIV only, so we used 0.125 µg/ml of ciprofloxacin, the lower recognized MIC for *B. subtilis* (45, 46). Around one hour after the addition of ciprofloxacin to the growing culture we noticed that the cells started to have multiple origins (an average of 5 per cell (n=200) versus 2 under the wild type conditions). Therefore, it was hard to single out and track two *oris* out of the several in very close proximity, and we chose *oris* that were relatively easier to tell apart. Many of the cells had a clear segregation defect, whereby around 10% of the cells were either anucleated or had unsegregated nucleoids. Moreover, the rate of separation was by 20.6% (n=218 cells), almost like the wild type level, which shows that despite the damage, the cells were still able to separate their origins (Fig. 9B) (movies S5A and S5B). Figure 10B shows that the separation is affected by the addition of Ciprofloxacin, and this is mostly apparent when the displacement was plotted for 20 seconds intervals. The distance moved by the separating origins along the long cell axis was smaller than that for the wild type, but higher than for Mitomycin C for the time window of 30 minutes.

Conclusion

The number of origins, termini, and nucleoids were counted under slow and fast growing conditions to assess the ploidy state of *B. subtilis.* The number of termini was constant under both conditions, falling slightly below the border of two termini per cell, and consequently two chromosomes. The nucleoid count was performed both manually and using an ImageJ plugin. In both cases, *B. subtilis* seemed to be diploid in minimal medium at 25°C, and under fast growth in rich medium at 37°C, more than 60% of the cells growing exponentially were diploid. The number

of polyploid cells never exceeded 25%, while a small subset of monoploid cells existed at all times.

There was a direct correlation between the polyploidy state and the cell length, whereby the longest cells contained the highest amount of nucleoids. The number of origins was higher under fast growth than under slow growth, and some cells, mostly the long ones, contained more than 6 origins. Very often, cells with 2 nucleoids contained more than 2 origins, proving that *B. subtilis*, like *E. coli*, is meropolyploid, and can start several rounds of replication that are not completed before the next division.

Upon induction of DNA damage by adding MMC to an exponentially growing culture, the cells became elongated, some nucleoids fused, and most of them were decondensed. The majority of cells had more than three origins, with some extremely long cells having up to 8 origins. The number of termini was however comparable to the wild type grown in the same medium and at the same temperature. This either means that the cells managed to complete a round of replication, which is highly unlikely, or that they retained the same number of termini and hence nucleoids before the induction of damage. The higher number of origins could be due to an over-initiation as a direct response of the cells to DNA damage. The idea that the cells continue originating but that the replication initiation is compromised is in good accordance with previously published data. Using ObjectJ and ChainTracer revealed similar outcomes: the addition of MMC resulted in similar outcomes: out of 200 cells counted, 23% were monolploid, 53% diploid, 21% polyploid, and 3% anucleated. Moreover, the induction of double strand breaks resulted in a slight delay in origin separation compared to the wild type in the same time window. Ciprofloxacin, which results in the blockage of topoisomerase IV, also resulted to a delay in separation, but to a lesser extent than MMC. Remarkably, *B. subtilis* seems to respond to damages that affect the cell cycle by becoming meropoliploid, and restarting replication. This is probably a response to stalled forks: starting a new round of replication could be an attempt to ensure and intact copy of the genome prior to cell division. Multi-origination could also possibly help process of separation through DNA crowding and strand repulsion.

References

1. **Comai L.** 2005. The advantages and disadvantages of being polyploid. Nature reviews genetics **6:**836-846.
2. **Breuert S, Allers T, Spohn G, Soppa J.** 2006. Regulated polyploidy in halophilic archaea. PloS one **1:**e92.
3. **Bremer H, Dennis PP.** 2008. Modulation of chemical composition and other parameters of the cell at different exponential growth rates. EcoSal Plus **3**.
4. **Pecoraro V, Zerulla K, Lange C, Soppa J.** 2011. Quantification of ploidy in proteobacteria revealed the existence of monoploid,(mero-) oligoploid and polyploid species. PloS one **6:**e16392.
5. **Hansen MT.** 1978. Multiplicity of genome equivalents in the radiation-resistant bacterium Micrococcus radiodurans. Journal of bacteriology **134:**71-75.
6. **Nagpal P, Jafri S, Reddy M, Das H.** 1989. Multiple chromosomes of Azotobacter vinelandii. Journal of bacteriology **171:**3133-3138.
7. **Maldonado R, Jimenez J, Casadesús J.** 1994. Changes of ploidy during the Azotobacter vinelandii growth cycle. Journal of bacteriology **176:**3911-3919.
8. **Michelsen O, Hansen FG, Albrechtsen B, Jensen PR.** 2010. The MG1363 and IL1403 laboratory strains of Lactococcus lactis and several dairy strains are diploid. Journal of bacteriology **192:**1058-1065.
9. **Webb CD, Graumann PL, Kahana JA, Teleman AA, Silver PA, Losick R.** 1998. Use of time-lapse microscopy to visualize rapid movement of the replication origin region of the chromosome during the cell cycle in Bacillus subtilis. Molecular microbiology **28:**883-892.
10. **Kadoya R, Hassan AK, Kasahara Y, Ogasawara N, Moriya S.** 2002. Two separate DNA sequences within oriC participate in accurate chromosome segregation in Bacillus subtilis. Molecular microbiology **45:**73-87.
11. **Sharpe ME, Hauser PM, Sharpe RG, Errington J.** 1998. Bacillus subtilis cell cycle as studied by fluorescence microscopy: constancy of cell length at initiation of DNA replication and evidence for active nucleoid partitioning. Journal of bacteriology **180:**547-555.
12. **Teleman AA, Graumann PL, Lin DC-H, Grossman AD, Losick R.** 1998. Chromosome arrangement within a bacterium. Current biology **8:**1102-1109.
13. **Fogel MA, Waldor MK.** 2006. A dynamic, mitotic-like mechanism for bacterial chromosome segregation. Genes & development **20:**3269-3282.
14. **Ptacin JL, Lee SF, Garner EC, Toro E, Eckart M, Comolli LR, Moerner W, Shapiro L.** 2010. A spindle-like apparatus guides bacterial chromosome segregation. Nature cell biology **12:**791-798.
15. **Livny J, Yamaichi Y, Waldor MK.** 2007. Distribution of centromere-like parS sites in bacteria: insights from comparative genomics. Journal of bacteriology **189:**8693-8703.
16. **Lemon KP, Grossman AD.** 1998. Localization of bacterial DNA polymerase: evidence for a factory model of replication. Science **282:**1516-1519.
17. **Lemon KP, Grossman AD.** 2000. Movement of replicating DNA through a stationary replisome. Molecular cell **6:**1321-1330.
18. **Brendler T, Sawitzke J, Sergueev K, Austin S.** 2000. A case for sliding SeqA tracts at anchored replication forks during Escherichia coli chromosome replication and segregation. The EMBO Journal **19:**6249-6258.
19. **Gelles J, Landick R.** 1998. RNA polymerase as a molecular motor. Cell **93:**13-16.
20. **Jun S, Wright A.** 2010. Entropy as the driver of chromosome segregation. Nature Reviews Microbiology **8:**600-607.

21. **Thevenaz P, Ruttimann UE, Unser M.** 1998. A pyramid approach to subpixel registration based on intensity. IEEE transactions on image processing **7:**27-41.
22. **Schindelin J, Arganda-Carreras I, Frise E, Kaynig V, Longair M, Pietzsch T, Preibisch S, Rueden C, Saalfeld S, Schmid B.** 2012. Fiji: an open-source platform for biological-image analysis. Nature methods **9:**676-682.
23. **Pandey R, Ter Beek A, Vischer NO, Smelt JP, Brul S, Manders EM.** 2013. Live cell imaging of germination and outgrowth of individual Bacillus subtilis spores; the effect of heat stress quantitatively analyzed with SporeTracker. PloS one **8:**e58972.
24. **Woldringh CL, Nanninga N.** 2006. Structural and physical aspects of bacterial chromosome segregation. Journal of structural biology **156:**273-283.
25. **Dronkert ML, Kanaar R.** 2001. Repair of DNA interstrand cross-links. Mutation Research/DNA Repair **486:**217-247.
26. **Friedberg EC, Walker GC, Siede W, Wood RD.** 2005. DNA repair and mutagenesis. American Society for Microbiology Press.
27. **Winterling KW, Chafin D, Hayes JJ, Sun J, Levine AS, Yasbin RE, Woodgate R.** 1998. The Bacillus subtilis DinR binding site: redefinition of the consensus sequence. Journal of bacteriology **180:**2201-2211.
28. **Groban ES, Johnson MB, Banky P, Burnett P-GG, Calderon GL, Dwyer EC, Fuller SN, Gebre B, King LM, Sheren IN.** 2005. Binding of the Bacillus subtilis LexA protein to the SOS operator. Nucleic acids research **33:**6287-6295.
29. **Khil PP, Camerini-Otero RD.** 2002. Over 1000 genes are involved in the DNA damage response of Escherichia coli. Molecular microbiology **44:**89-105.
30. **Goranov AI, Kuester-Schoeck E, Wang JD, Grossman AD.** 2006. Characterization of the global transcriptional responses to different types of DNA damage and disruption of replication in Bacillus subtilis. Journal of bacteriology **188:**5595-5605.
31. **Horsburgh MJ, Thackray PD, Moir A.** 2001. Transcriptional responses during outgrowth of Bacillus subtilis endospores. Microbiology **147:**2933-2941.
32. **Palom Y, Suresh Kumar G, Tang L-Q, Paz MM, Musser SM, Rockwell S, Tomasz M.** 2002. Relative toxicities of DNA cross-links and monoadducts: new insights from studies of decarbamoyl mitomycin C and mitomycin C. Chemical research in toxicology **15:**1398-1406.
33. **Jonnalagadda VS, Matsuguchi T, Engelward BP.** 2005. Interstrand crosslink-induced homologous recombination carries an increased risk of deletions and insertions. DNA repair **4:**594-605.
34. **Berardini M, Foster PL, Loechler EL.** 1999. DNA polymerase II (polB) is involved in a new DNA repair pathway for DNA interstrand cross-links inEscherichia coli. Journal of bacteriology **181:**2878-2882.
35. **Blaisdell JO, Wallace SS.** 2001. Abortive base-excision repair of radiation-induced clustered DNA lesions in Escherichia coli. Proceedings of the National Academy of Sciences **98:**7426-7430.
36. **Baharoglu Z, Mazel D.** 2014. SOS, the formidable strategy of bacteria against aggressions. FEMS microbiology reviews **38:**1126-1145.
37. **Nicolas E, Upton AL, Uphoff S, Henry O, Badrinarayanan A, Sherratt D.** 2014. The SMC complex MukBEF recruits topoisomerase IV to the origin of replication region in live Escherichia coli. MBio **5:**e01001-01013.
38. **Watt PM, Hickson ID.** 1994. Structure and function of type II DNA topoisomerases. Biochemical Journal **303:**681.
39. **Drlica K, Zhao X.** 1997. DNA gyrase, topoisomerase IV, and the 4-quinolones. Microbiology and molecular biology reviews **61:**377-392.

40. **Barnes MH, LaMarr WA, Foster KA.** 2003. DNA gyrase and DNA topoisomerase of Bacillus subtilis: expression and characterization of recombinant enzymes encoded by the gyrA, gyrB and parC, parE genes. Protein expression and purification **29:**259-264.
41. **Hooper DC.** 1999. Mechanisms of fluoroquinolone resistance. Drug resistance updates **2:**38-55.
42. **Cunha B, Qadri S, Ueno Y, Walters E, Domenico P.** 1997. Antibacterial activity of trovafloxacin against nosocomial Gram-positive and Gram-negative isolates. Journal of Antimicrobial Chemotherapy **39:**29-34.
43. **Morrissey I, George JT.** 2000. Bactericidal activity of gemifloxacin and other quinolones against Streptococcus pneumoniae. Journal of Antimicrobial Chemotherapy **45:**107-107.
44. **Price LB, Vogler A, Pearson T, Busch JD, Schupp JM, Keim P.** 2003. In vitro selection and characterization of Bacillus anthracis mutants with high-level resistance to ciprofloxacin. Antimicrobial agents and chemotherapy **47:**2362-2365.
45. **Citron DM, Appleman MD.** 2006. In vitro activities of daptomycin, ciprofloxacin, and other antimicrobial agents against the cells and spores of clinical isolates of Bacillus species. Journal of clinical microbiology **44:**3814-3818.
46. **Mariner KR, Ooi N, Roebuck D, O'Neill AJ, Chopra I.** 2011. Further characterization of Bacillus subtilis antibiotic biosensors and their use for antibacterial mode-of-action studies. Antimicrobial agents and chemotherapy **55:**1784-1786.

Table 1. Strains used in this study

Strains	Genotypes	References
PG26	*spo0J(359°)::lacO cassette (cm^R, 359°) thrC::lacI-cfp (mls^R)*	Lemon and Grossman, 2000
AT62	*thrC::lacI-gfp (mls^R) cgeD::lacO cassette (cm^R, 181°)*	Teleman *et al*., 1998
KS188	*Spo0J tetO array (kan^R) cgeD::P_{pen} tetR-yfp (tet^R)*	Graumann, unpublished

Table 2. Origins and termini count under slow and fast growth

	Slow growth (25 °C)		Fast growth (37 °C)	
	Foci/cell	**n_t**	**Foci/cell**	**n_t**
PG26 (origin tag)	1.8±0.51	620	4.42±1.49	848
AT62 (terminus tag)	1.69±0.6	700	1.89±0.66	848

*n_t refers to the total number of cells counted in each experiment

Table 3. Percent polyploidy and average number of origins over time

	25°C	37°C				
PG26	**Control**	**1h**	**1.5h**	**2h**	**2.5h**	**3h**
OD	0.75	0.11	0.3	0.7	1.8	2.5
% monoploid	37.1	19	14	11.42	12	10
% diploid	59.2	70	71	69.71	64	71
% polyploid	3.7	12	15	18.8	23	19
Origins per cell	1.8±0.51	4.8±1.6	4.5±2	3.9±1.1	3.7±0.55	3.1±0.89
n_t	620	300	300	350	400	400

% polyploidy calculated over all time points= 17.56%

Table 4. Percent polyploidy and average number of termini over time

	25°C	37°C				
AT62	**Control**	**1h**	**1.5h**	**2h**	**2.5h**	**3h**
OD	0.82	0.13	0.4	1	1.9	3
% monoploid	35	17	13	12	15	12
% diploid	61	74	72	71	69	75
% polyploid	4	9	15	17	16	13
Termini per cell	1.69±0.6	1.71±0.5	1.93±0.6	1.8±1.1	1.72±0.73	1.95±0.8
n_t	700	200	300	300	400	400

% polyploidy calculated over all time points at 37°C = 16.2%

*n_t refers to the total number of cells counted in each time interval.

Table 5. Percent polyploidy estimated from automatically calculated average DAPI fluorescence

	25°C	37°C		
AT62	**Control**	**1.5h**	**2h**	**2.5h**
OD	0.84	0.4	1	1.9
% monoploid	27.8	11.7	15	11.5
% diploid	67.5	68.3	63.3	59.25
% polyploid	4.6	20	21.7	29.25
n_t	540	300	300	400

% polyploidy calculated over all time points at 37°C = 23.65%.

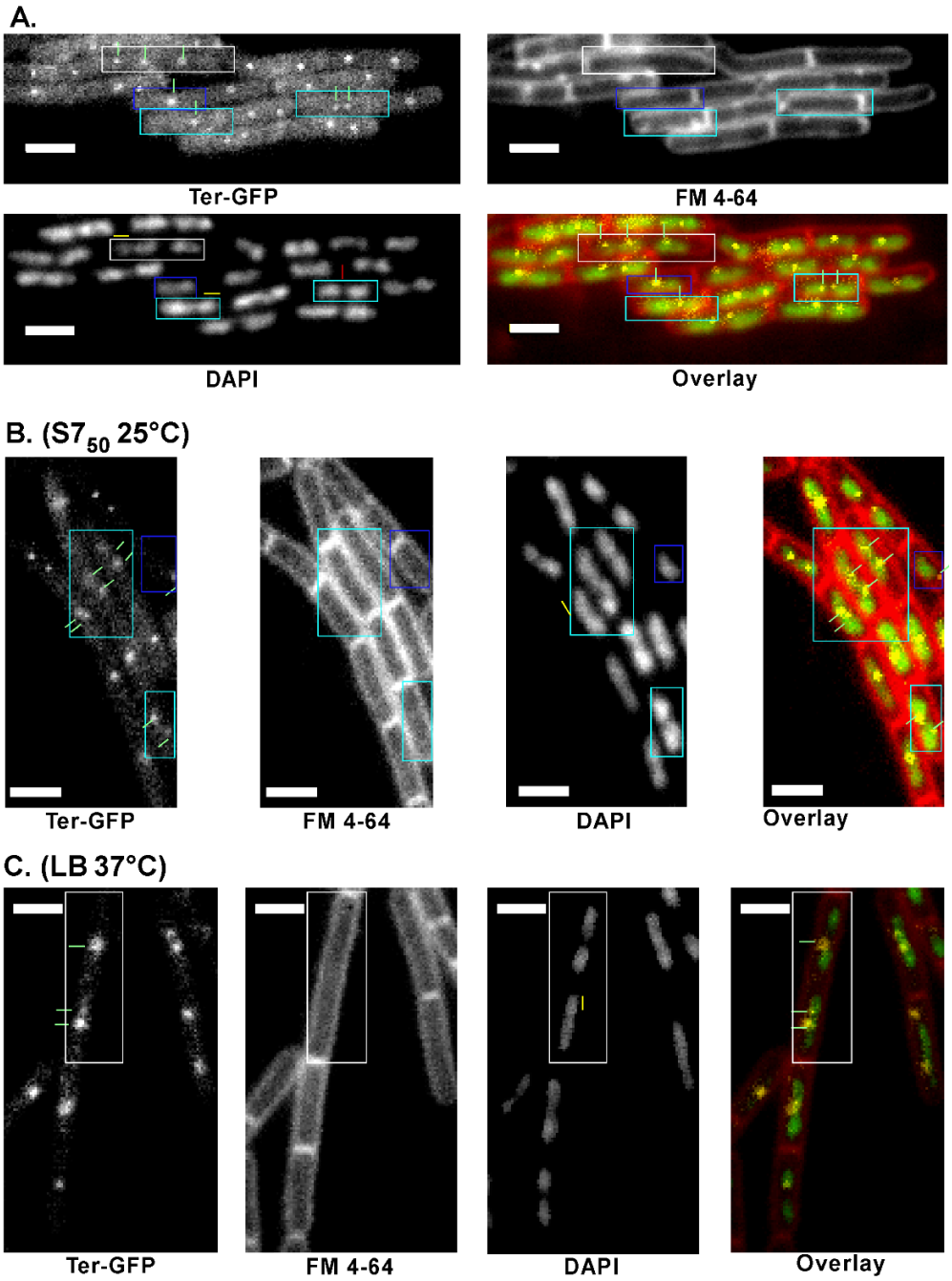

Figure 1. AT62 (Terminus tag). **A**. Example of monoploid (dark blue rectangle), diploid (light blue rectangle), and polyploid cells (White rectangle). Green dashes point at the termini, the yellow dash represents 0.55µm (the minimal length of a single nucleoid), and the red dash represents a distance of at least 3 pixels between 2 nuclei. **B.** Cells grown in minimal medium at 25 °C: Cells are either diploid or monoploid. **C.** Cells grown in LB at 37°C. An elongated cell with 4 nucleoids is shown. White bars represent 2 µm.

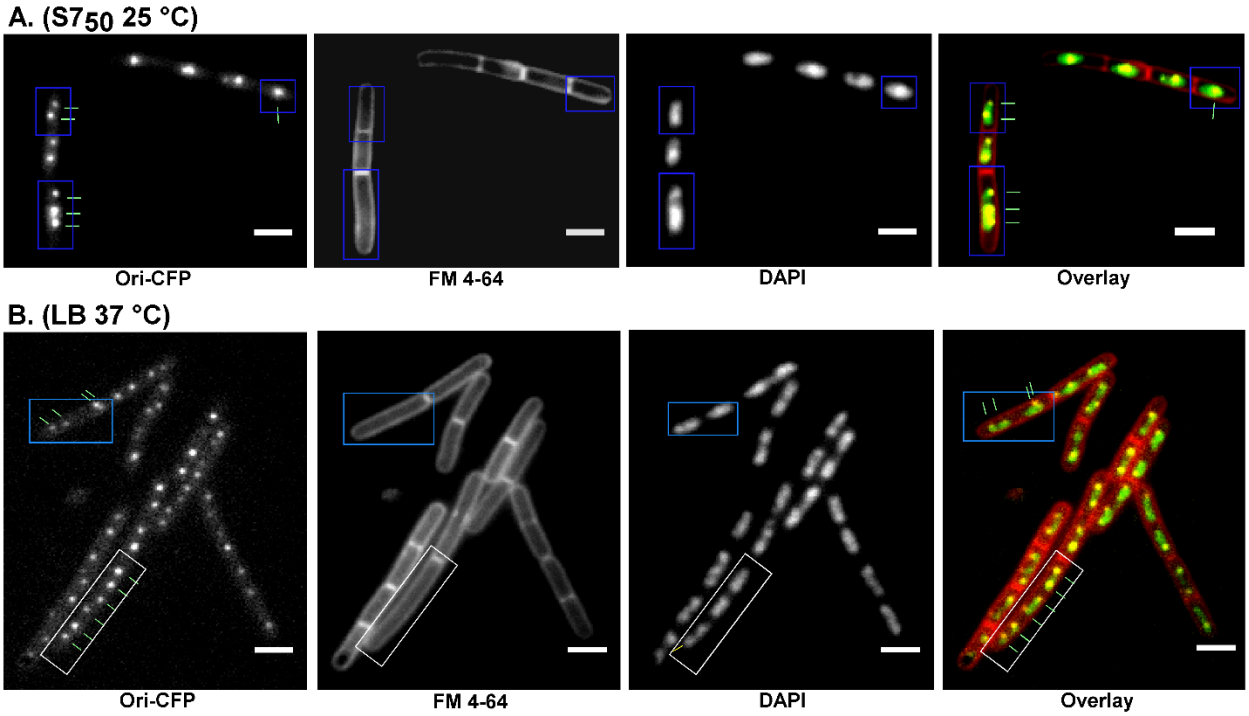

Figure 2. AT26 (Origin tag). **A**. Cells grown in $S7_{50}$ minimal medium at 25 °C. Cells usually had 2 origins on average and were either monoploid or diploid. Only monoploid cells are shown (dark blue rectangle). **B.** Cells grown in LB at 37 °C had on average 4.5 origins per cell after 1.5 hours of growth. Shown is a diploid cell with 4 origins (light blue rectangle), and an elongated polyploid cell with 4 nucleoids and 6 origins (white rectangle).Green dashed lines point at the origins, and the yellow dashed line represents 0.55 µm (the minimal nucleoid length). White bars represent 2 µm.

A.

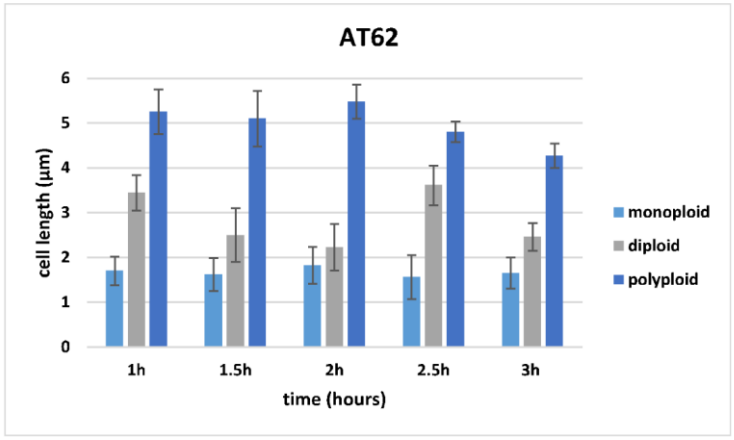

B.

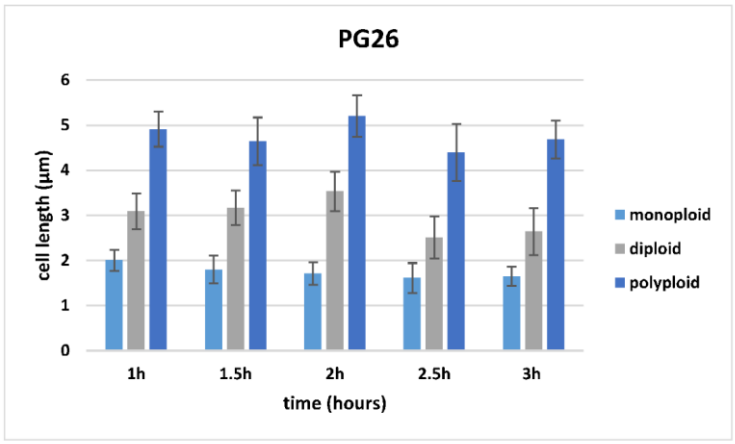

Figure 3. Cell length measured at different time points of fast growth for the origin tag (AT62) and terminus tag (PG26) strains. A direct relation can be seen between the chromosomal content and the cell length in both cases.

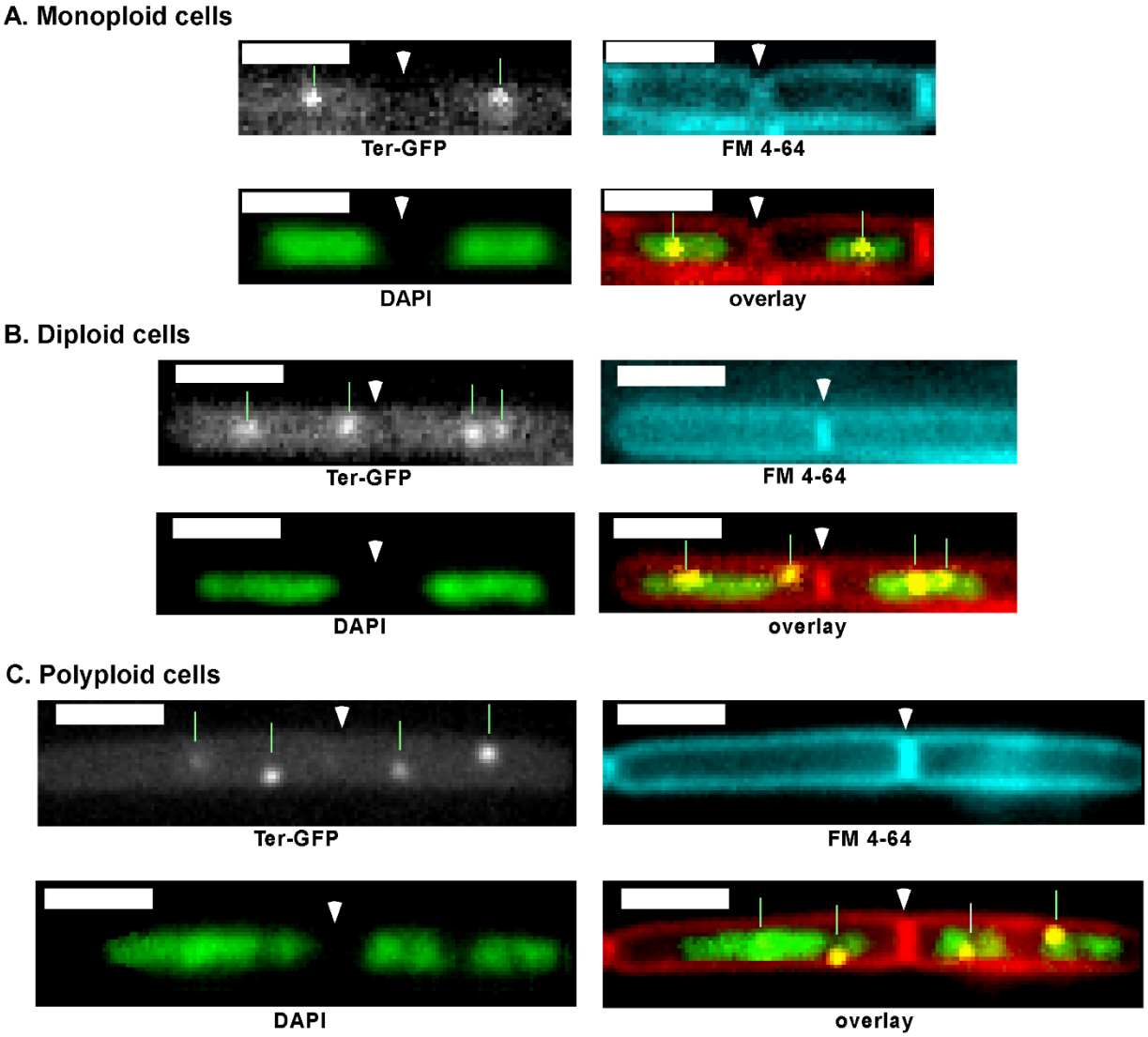

Figure 4. Example of **A.** monoploid, **B.** diploid, and **C.** polyploid cells based on ChainTracer and ObjectJ calculations. White arrows show automatically detected septa, and green lines point at the termini. Bars indicate 2 µm.

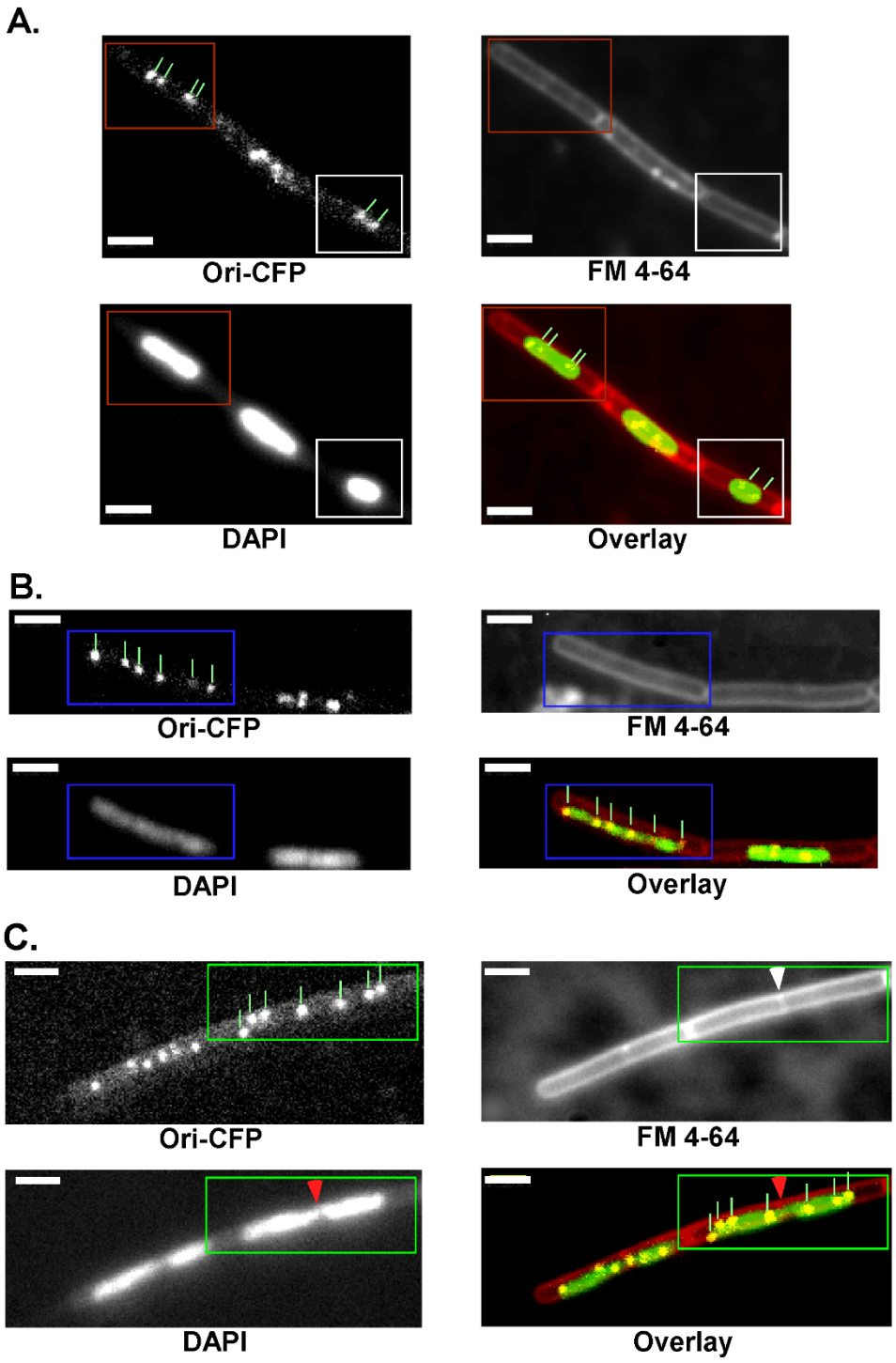

Figure 5. AT26 (Origin tag) **A**. 30 minutes after induction of DNA damage by MMC, **B.** and **C.** 90 minutes after MMC addition. In **A.** an example of one condensed nucleoid (white box) and fused nucleoids (red box) are shown. **B.** shows an example of decondensed DNA in an elongated cell (green box), and **C.** shows DNA bisected by a septum (green box). The red arrow points to

the bisected nucleoid, while the white arrow shows the septum in question. Green lines point at the origins, of which up to seven can be seen in one cell in panel **B.** White bars indicate 2 µm.

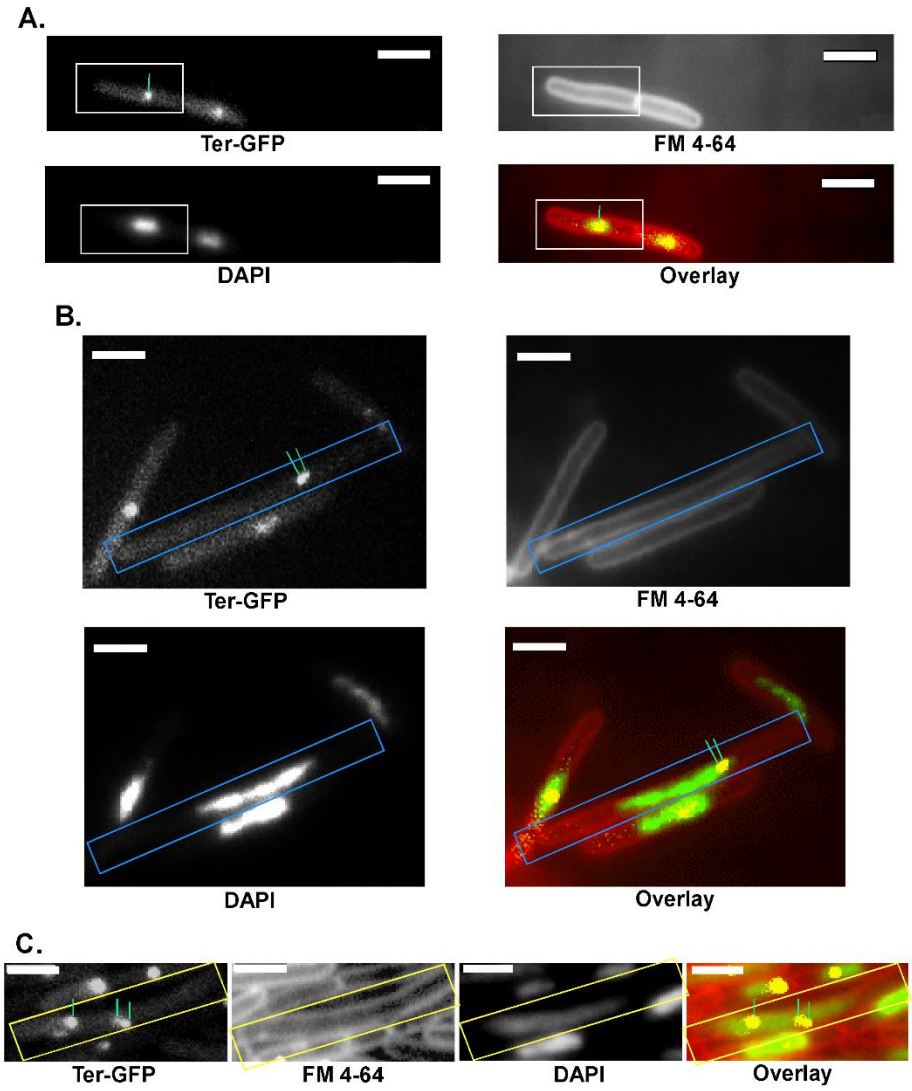

Figure 6. AT62 (Terminus tag). **A.** 30 minutes after MMC addition. The cell in the white box is an example of a cell with one condensed nucleoid only. **B.** 90 minutes after MMC addition: an elongated cell is shown in the blue box with has multiple nucleoids and two termini. **C.** Elongated cell with decondensed nuclei and 3 termini is indicated by the yellow box. Green dashes point at the termini, white bars represent 2µm.

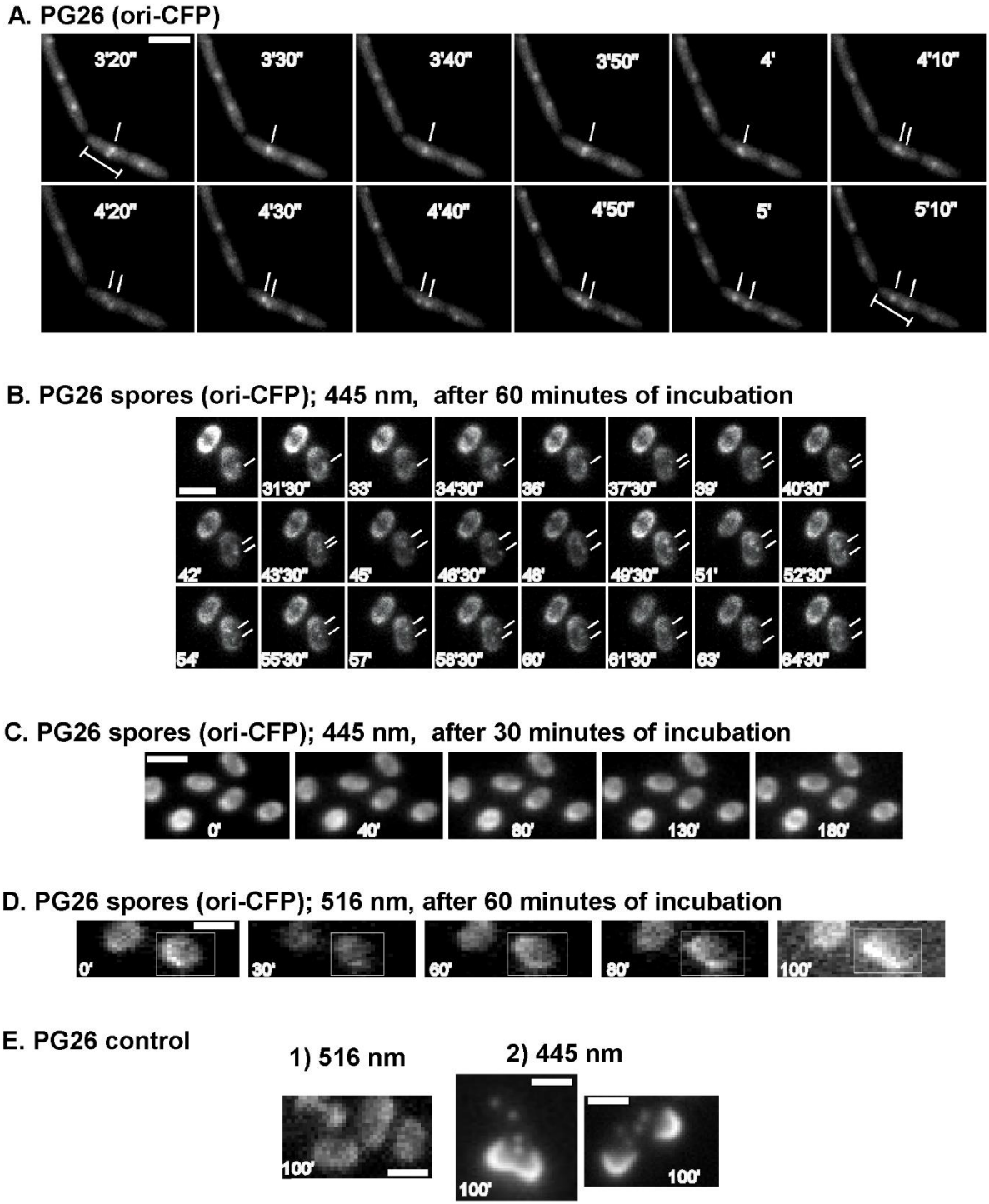

Figure 7. A. PG26 imaged with the 445 nm laser in intervals of 10 seconds. Cell growth was completely stopped but one separation can be seen (white dashes). **B.** PG26 spores imaged after 60 minutes of incubation. In one of them two separating origins can be seen (white dashes), though

the CFP laser stopped the germination process. **C.** Also PG26 spores, imaged after 30 minutes of incubation at 23 degrees. Germination failed to proceed, origins cannot be seen because the CFP signal was masked by the brightness of the coat. **D.** PG 26, imaged with the 516 nm (YFP laser). Germination proceeds in rates comparable to panel **E.** in which spores were left to germinate under test tubes conditions in the time during which microscopy was ongoing.

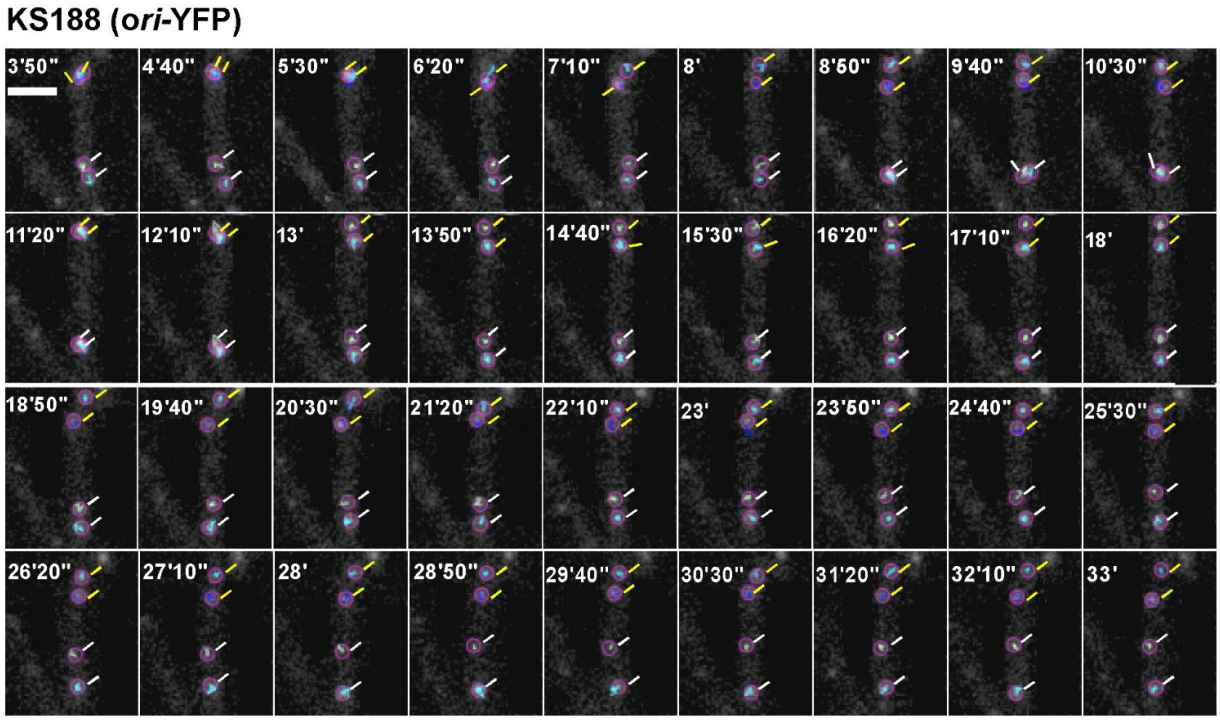

Figure 8. KS188 imaged with the 516 nm laser with 10 seconds interval. The montage was done based on TrackMate movie. The tracked origins are encircled, and local tracks, not entire tracks, are shown within the circles in order to avoid crowding in the image. Green, yellow, and white lines point at separating couples of origins. White bar represents 2 µm.

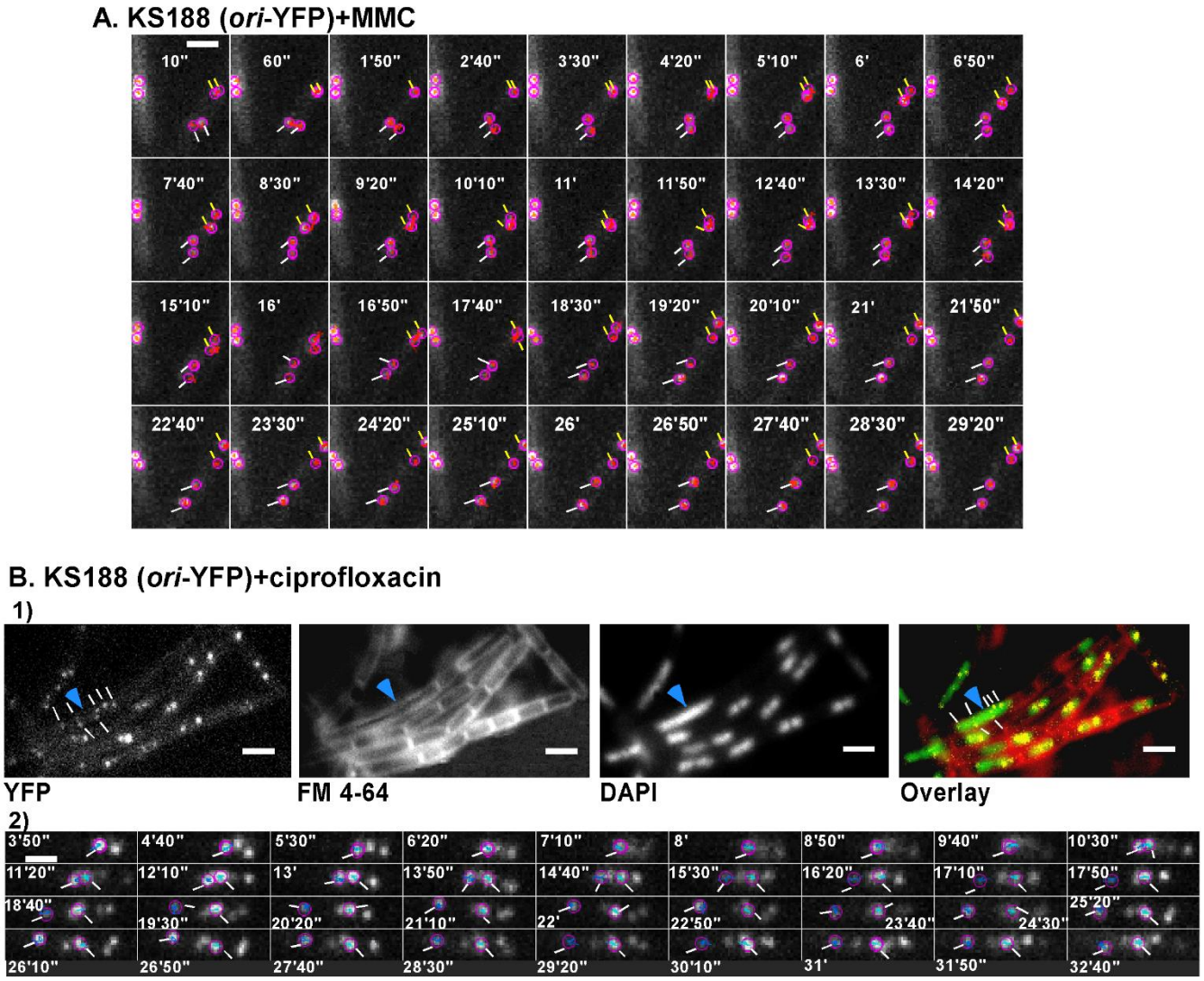

Figure 9. KS188 imaged with the 516 nm laser with 10 seconds interval under two different types of stress: MMC in **A** and Ciprofloxacin in **B**. The montages in panels **A** and **B 2** was done based on trackmate movie. Again, the tracked origins are encircled, and local tracks, not entire tracks, are shown within the circles in order to avoid crowding in the image. Lines of the same color show a couple of separating origins. Panel **B 1** shows cells after Ciprofloxacin treatment. Most cells show several origins (white lines), and an elongated cell with an unsegregated nucleoid is shown with a blue arrow. White bar represents 2 µm.

A.

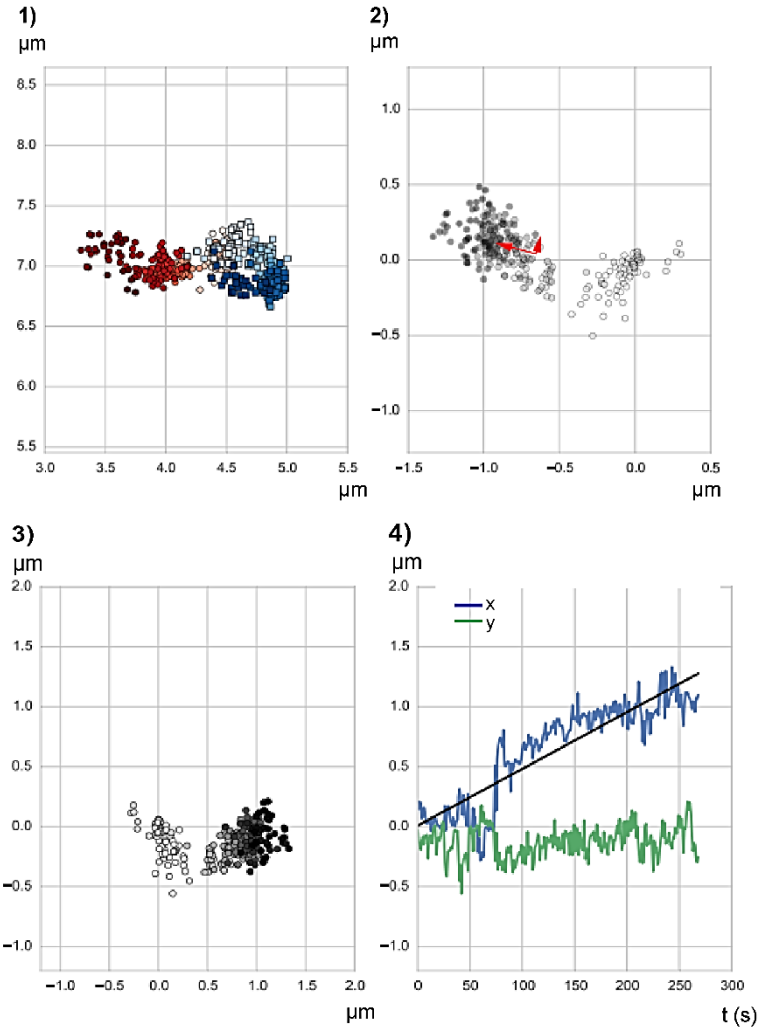
1)
µm
8.5
8.0
7.5
7.0
6.5
6.0
5.5
3.0
3.5
4.0
4.5
5.0
5.5
µm
2)
µm
1.0
0.5
0.0
−0.5
−1.0
−1.5
−1.0
−0.5
0.0
0.5
µm
3)
µm
2.0
1.5
1.0
0.5
0.0
−0.5
−1.0
−1.0
−0.5
0.0
0.5
1.0
1.5
2.0
µm
4)
µm
x
y
2.0
1.5
1.0
0.5
0.0
−0.5
−1.0
0
50
100
150
200
250
300
t (s)

B.

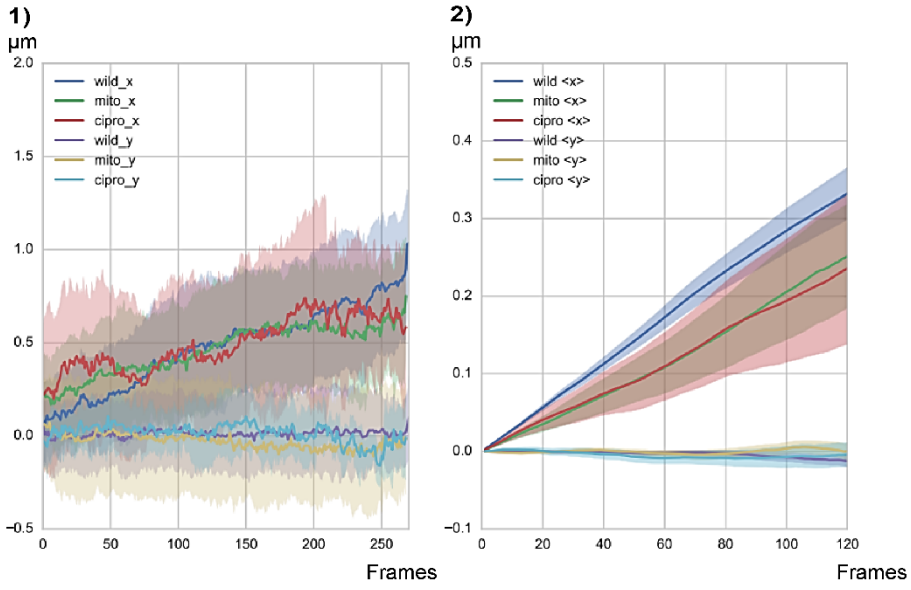
1)
µm
wild_x
mito_x
cipro_x
wild_y
mito_y
cipro_y
2.0
1.5
1.0
0.5
0.0
−0.5
0
50
100
150
200
250
Frames
2)
µm
wild <x>
mito <x>
cipro <x>
wild <y>
mito <y>
cipro <y>
0.5
0.4
0.3
0.2
0.1
0.0
−0.1
0
20
40
60
80
100
120
Frames

Figure 10. A. Graphs describing the separation of two origins. **A 1** position in the cell of all the points in the tracks. The first origin is shown in red, the second in blue. Colors goes gradually from bright to dark along time. **A 2** the increasing distance between the two origins; darker dots reflect the distances in later time points. **A 3** projection of the distances in **A 2** on a horizontal cell of 2µm in length. **A 4** distance between the origins along the x and y axis versus time. Black line is the trend line for movement in the x direction. **B.** Movement over time for all tracks generated in all three different conditions. **B 1** distance between the origins along the x and y axis versus time. **B 2** distance moved in all tracks along the x and y axis at every time lag ζ shown in frames. In panel **B**, solid lines reflect averages of all graphs for every condition. Color code is provided in the figure.

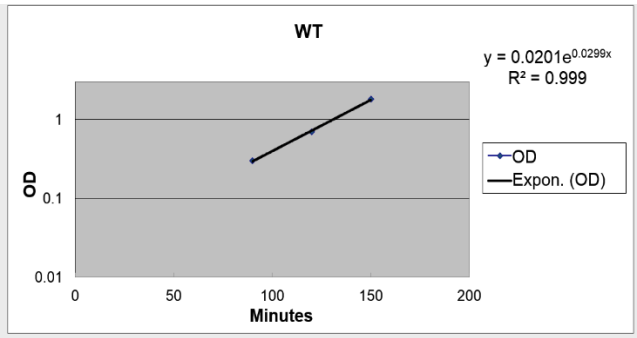

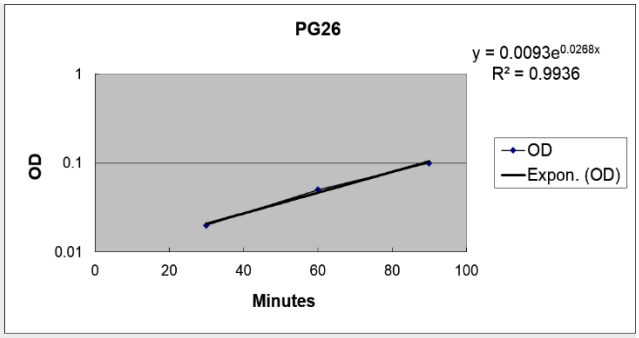

	WT	PG26	AT62
Experiment 1	23.18218	24.93335182	26.25557502
Experiment 2	25.18224	27.18224237	28.40119213
Experiment 3	25.23456	25.8670077	23.9
Average	**24.53299±1.17**	**25.99420063±1.13**	**26.18558905±2.25**

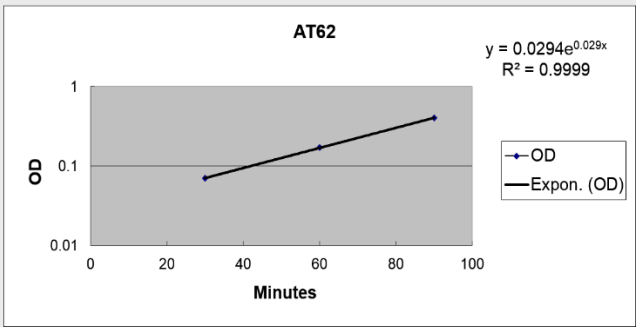

Figure S 1. Exemplary growth curves of the *Bacillus subtilis* PY79 wild type (WT), PG26, and AT62 strains. An exponential trend line was added that best fits the values, and from it the corresponding equation and R^2 value were deduced from each curve. The doubling time was calculated according to the formula $dt = \ln(2)/\mu$. For each strain, the experiment was repeated three times and an average of the doubling time was calculated and shown in the accompanying table.

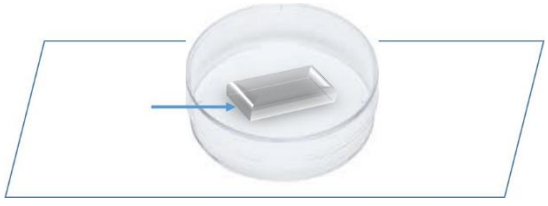

Figure S2. Microscopy slides setup used for the live imaging of the *B. subtilis* KS 188 strain.

5. GENERAL DISCUSSION

DNA translocases, like the *E. coli* protein FtsK, actively move DNA out of the division plane in order to complete chromosome partitioning and to avoid damage by the invaginating division septum. Combined genetic, cytological, biochemical approaches, as well as single molecule tracking were used to gain further information on the solubility of SftA, its localization/movement within the cell. Interaction partner(s) that help target it to the septum were investigated, and its dynamics in vivo were compared to SpoIIIE, a membrane associated translocase. SftA and SpoIIIE have different but complementary functions during the cell cycle. Hence, the coordination of cell division and chromosome segregation in *B. subtilis* is accomplished by a particular strategy, different from the *E. coli* system, which uses a single DNA translocase.

It was previously shown that SftA acts a functional hexamer in vitro. Phenotypic effects in a Δ*sftA* mutant are very similar to those reported for Δ*spoIIIE* in *B. subtilis*, and the double mutant resulted in exacerbated effects, indicating that in *B. subtilis* two pathways exist for the coordination of chromosome segregation and cell division (72).

This current work has further shown that incorporating a truncated copy of the protein expressed from an ectopic locus into a functional hexamer obliterates the function and results in a deletion phenotype. An expression level of the truncations 4 times lower than the wild type protein resulted in a defect in segregation to the same extent to that of a deletion strain. Even with no induction, the leaky level of expression of the truncation resulted in a segregation defect in a subset of cells, further stressing the importance of all or most peptides within a hexamer in insuring functionality.

SftA seems to be predominantly a soluble protein as revealed by cell fractionation experiments, while SpoIIIE, as expected, was detected exclusively in the membrane fraction, and PfkA, a phosphofructokinase, in the cytosolic fraction.

We were also able to narrow down the region responsible for membrane targeting to 47 residues. A truncation from residue 20 to 105 localized normally in both the wild type and SftA deletion strains. A truncation 67 residues long localized normally in a SftA deletion background, while a truncation 20-67 residues still localized, but not in all cells. This could highlight the importance of the stretch 67-105 residues for efficient binding of an interaction partner, as well as

the importance of the 20-67 residues stretch in hexamerization and efficient septal targeting. Deleting the first 60 amino acids obliterated septal recruitment, and the truncations shorter than 67 residues did not localize.

After having narrowed down the stretch in the N-terminus responsible for septal targeting and hexamerization, it became important to pin down the proteins which play a role in guiding SftA to the septum. While a Tap-tag pull down experiment offered some hints, the focus was mainly set on FtsZ, FtsA, and FtsH since other division proteins that were pulled down were ruled out in previous work (SepF, FtsL) (72). SftA localized normally in a FtsH deletion background, and pull down assays against FtsA and FtsZ where SftA was used a bait were inconclusive.

In order to test possible interactions between SftA and FtsZ/FtsA, a heterologous expression system was used. A Schneider S2 cell line was transfected with vectors containing the following constructs: SftA-YFP, SftA-YFP + FtsA, FtsA-YFP; SftA-YFP + FtsZ, and FtsZ-YFP. SftA-YFP showed a diffused localization pattern when transfected alone, but a co-transfection with untagged FtsA resulted in a membrane localization similar to that of FtsA-YFP, proving an interaction between the two proteins. Such an interaction, however, was not confirmed for SftA with FtsZ, where co-transfection did not alter the diffuse localization of SftA. While this experiment is not enough to rule out an interaction with FtsZ, it provided a very strong hint for an interaction with FtsA.

A further confirmation of an interaction of SftA with FtsA was obtained through single molecule tracking (SMT) experiments. SMT has proven to be a potent tool in the recent years to gain insights into the dynamics and behavior of proteins in vivo. We used SMT and step size distribution to extract information about the subset of dynamic and static fractions of the protein, and calculated the respective diffusion coefficients for each fraction. While SftA seems to be a very static protein in epifluorescence imaging, a dynamic fraction of the protein was detected in vivo when tracking with 30 ms interval. The dynamic fraction was shown to move freely in the cytosol. However, this fraction was small, had a diffusion coefficient of 0.35 $\mu m^2/s$ compared to the static fraction which constituted 73% of the molecules and had a diffusion coefficient of 0.019 $\mu m^2/s$. Depletion of FtsA resulted in an increase of the dynamic fraction from 27% to 46%, though the diffusion coefficients remained the same for both fractions. This further confirmed the effect of FtsA on the septal targeting of SftA, and proved that though it may not be the only player in the process, it is definitely an important one.

SMT experiments were also performed on SpoIIIE with the same experimental setup used for SftA, and the effect of double strand break and cell cycle arrest through the addition of MMC was tested. SpoIIIE seemed to be quite static at the single molecule level, comprising 73% static molecules with a diffusion constant of 0.021 $\mu m^2/s$, and a more dynamic fraction which had a diffusion coefficient of 0.1 $\mu m^2/s$. Surprisingly, the induction of double strand break with MMC had no detectable effect on the behavior of the protein on the single molecule level under the experimental conditions used. This could be explained through the fact that the subset of SpoIIIE molecules that localize to the septum upon damage induction is too small to result in a detectable change on the totality of the proteins at the single molecule level. Additionally, tracking at 30ms could have resulted in missing out on a faster, soluble fraction, and that only the more static molecules were observed and tracked.

PfkA was used as a control for a freely diffusing cytosolic proteins. As expected, most of the molecules (91%) were dynamic, with a diffusion constant of 0.38 $\mu m^2/s$. However, tracking with 30 ms may have resulted in missing the fast moving molecules, or may have captured a slower apparent movement of these proteins. This indicates that SftA, which has a diffusion coefficient for the soluble dynamic fraction similar to PfkA, might be in reality faster than observed.

Despite the possibilities of optimization of the experimental setup, especially when it comes to decreasing the exposure time used, SMT was still a powerful comparative tool which provided us with valuable insights concerning the behavior of different proteins under the same conditions, as well as of the same proteins under different conditions. The obtained numbers confirmed our theories of an interaction between SftA and FtsA, and the effect of the depletion was clear, though SftA might still bind to remnants of FtsA on the membrane resulting in a lower representation of the soluble non-bound fraction.

The second part of this work focused on the processes of chromosome replication, specifically the origin region, as well as the ploidy state of *B. subtilis* under different conditions of temperature and growth media.

It was generally assumed that most prokaryotes are monoploid and contain a single copy of a circular chromosome. However, recent studies conducted in several organisms have proven that bacteria can be polyploid, and that polyploidy offers fitness and redundancy to the organism. For instance, *E. coli* contains one chromosome under slow growth when its generation time is longer than the time required for replication and segregation. Under optimal laboratory conditions,

the generation time of *E. coli* can become lower than the replication time, and a new round of replication is initiated before termination of the previous one. This results in the cells becoming mero-diploid or mero-oligoploid for the origin-proximal genes (105).

In *B. subtilis*, tagging the replication origin with YFP showed one to two origins during slow growth in minimal medium at 30 °C, but these numbers increased from two to four origins during faster growth in minimal medium supplemented with amino acids at 30 °C (106).

We determined the numbers of origins, termini, and nucleoids of *B. subtilis* under fast growth (LB, 37ºC), and slow growth ($S7_{50}$, 25 ºC). The number of termini remained more or less constant (around two per cell in both conditions), while the number of origins increased. Under fast growth, the cells had on average ~ 4 origins versus ~ 2 under slow growth in the exponential phase. This means that *B. subtilis* is diploid most of the time. However, the number of termini could be underestimated because in many cases it was hard to tell if the focus between two nuclei corresponded to one or two termini. Based on the counted number of nuclei, there was always a subset of polyploid cells under fast growth, but this subset never exceeded 22% for the origin tag strain (PG26), and 18% for the terminus tag (AT62) strain. The total polyploidy calculated over all time points under fast growth conditions for both strains was 17.2% and 15.06%, respectively. A subset of cells was monoploid at all times, and this subset was higher under conditions of slow growth than in those of fast growth (~35% and ~15% respectively).

For the origin tag strain, the cell length in minimal medium ranged between 0.894 µm and 4.112 µm, with an average of 2.347±0.474 µm. The values were comparable to the terminus tag strain grown in minimal medium where the cell length ranged between 0.684 µm and 3.881 µm with an average of 2.137±0.613 µm. At faster growth both strains showed a direct correlation between the chromosomal content and the cell length whereby the polyploid cells were considerably longer than the diploid and the monoploid cells.

MMC was shown to cause a relative increase of the dosage of the origin of replication proximal genes. The increase in gene dosage was most likely caused by a reduced rate of elongation of replication, rather than by over-initiation. In other terms, the use of MMC slows down replication elongation, causing an increase in origin-proximal DNA and a relative increase in transcripts from origin-proximal genes (107).

Upon addition of MMC, we have observed that the nucleoids became condensed or fused, with up to 3 origins per cell, which is in accordance with the increase of transcription in the origin

proximal regions. 90 minutes after MMC addition, the number of origins increased from around 2 per cell prior to the induction of damage to 3.5±1.47, which is in accordance with previously published data (107). The cells were also elongated and the average cell length increased from 2.17±0.52 µm before addition of MMC to 3.7±1.413 µm after MMC addition. The cell length fell in a range between 1.6 µm and 7.7 µm, with 20% of the cells being above 5 µm. 16% of the cells counted had 5 origins or more, with a few having up to 8 origins. The nucleoids were decondensed in the majority of cells, and a subset of cells was anucleated (around 3%). Cells longer than 5 µm contained an elongated unsegregated nucleoid.

Despite the replication arrest and the atypical nucleoid morphology, many cells were either still able to complete a replication cycle and have a double set of chromosomes after induction of double strand breaks, or simply retained the number of nucleoid and termini they had before damage induction. The latter is in accordance with the idea that MMC slows down the cell cycle considerably but does not stop it completely.

An *ori* separation event was seen in 18% of 364 counted cells, which is comparable to the wild type. However, a plot of step sizes over time has shown that the addition of MMC to exponentially growing cells resulted in the slowing of the separation process compared to the wild type. Though the origins eventually separate, they move smaller distances in the same time window.

Another aspect we wanted to investigate was the effect of blocking the topoisomerase IV (TopoIV) on *ori* segregation in *B. subtilis.* The gyrase and Topoisomerase IV (TopoIV) belong to the family of class II topoisomerases. The gyrase controls DNA supercoiling and relieves topological stress arising from the translocation of transcription and replication complexes, while topoIV resolves interlinked chromosomes following replication (108).

TopoIV and the gyrase are targets of the 4-quinolones like ciprofloxacin. Quinolones cause reversible trapping of these enzymes on the DNA. At higher drug concentrations, cell death occurs as double-strand DNA breaks are released from trapped gyrase and/or topoIV complexes (109).

For our experimental purposes, we blocked the topoIV with 0.125 µg/ml ciprofloxacin.

Around one hour after the addition of ciprofloxacin to the growing culture, the cells started to have multiple origins (5 per cell versus 2 under wild type conditions). Many of the cells showed a clear segregation defect. The rate of separation was very similar to the wild type level, which shows that despite the damage, the cells were still able to separate their origins.

Origin separation was affected by the addition of Ciprofloxacin, and the distance moved by the separating origins was smaller than that for the wild type, but higher than for Mitomycin C for the same time window.

The aforementioned outcomes prove the robust nature of the origin separation and chromosome segregation processes in *B. subtilis*, and highlights the ability of the cells to overcome stress and preserve a complete copy of the genome.

6. REFERENCES

1. **Fall R, Kinsinger RF, Wheeler KA.** 2004. A simple method to isolate biofilm-forming Bacillus subtilis and related species from plant roots. Systematic and applied microbiology **27:**372.
2. **Earl AM, Losick R, Kolter R.** 2008. Ecology and genomics of Bacillus subtilis. Trends in microbiology **16:**269-275.
3. **La Ragione RM, Casula G, Cutting SM, Woodward MJ.** 2001. Bacillus subtilis spores competitively exclude Escherichia coli O78: K80 in poultry. Veterinary microbiology **79:**133-142.
4. **Kunst F, Ogasawara N, Moszer I, Albertini A, Alloni G, Azevedo V, Bertero M, Bessieres P, Bolotin A, Borchert S.** 1997. The complete genome sequence of the gram-positive bacterium Bacillus subtilis. Nature **390:**249-256.
5. **Srivatsan A, Han Y, Peng J, Tehranchi AK, Gibbs R, Wang JD, Chen R.** 2008. High-precision, whole-genome sequencing of laboratory strains facilitates genetic studies. PLoS Genet **4:**e1000139.
6. **Levin PA, Grossman AD.** 1998. Cell cycle and sporulation in Bacillus subtilis. Current opinion in microbiology **1:**630-635.
7. **Barák I, Wilkinson AJ.** 2007. Division site recognition in Escherichia coli and Bacillus subtilis. FEMS microbiology reviews **31:**311-326.
8. **Susanna KA, Fusetti F, Thunnissen A-MW, Hamoen LW, Kuipers OP.** 2006. Functional analysis of the competence transcription factor ComK of Bacillus subtilis by characterization of truncation variants. Microbiology **152:**473-483.
9. **Katayama T, Ozaki S, Keyamura K, Fujimitsu K.** 2010. Regulation of the replication cycle: conserved and diverse regulatory systems for DnaA and oriC. Nature Reviews Microbiology **8:**163-170.
10. **Messer W.** 2002. The bacterial replication initiator DnaA. DnaA and oriC, the bacterial mode to initiate DNA replication. FEMS microbiology reviews **26:**355-374.
11. **Kornberg A, Baker TA.** 1980. DNA replication. Wh Freeman San Francisco.
12. **Kurokawa M, Nukina M, Nakanishi H, Tomita S, Tamura T, Shimoyama T.** 1999. [Resuscitation from the viable but nonculturable state of Helicobacter pylori]. Kansenshogaku zasshi The Journal of the Japanese Association for Infectious Diseases **73:**15-19.
13. **Keyamura K, Fujikawa N, Ishida T, Ozaki S, Su'etsugu M, Fujimitsu K, Kagawa W, Yokoyama S, Kurumizaka H, Katayama T.** 2007. The interaction of DiaA and DnaA regulates the replication cycle in E. coli by directly promoting ATP–DnaA-specific initiation complexes. Genes & development **21:**2083-2099.
14. **Fukuoka T, Moriya S, Yoshikawa H, Ogasawara N.** 1990. Purification and characterization of an initiation protein for chromosomal replication, DnaA, in Bacillus subtilis. Journal of Biochemistry **107:**732-739.
15. **Bruand C, Ehrlich SD, Janniere L.** 1995. Primosome assembly site in Bacillus subtilis. The EMBO journal **14:**2642.
16. **Bruand C, Sorokin A, Serror P, Ehrlich SD.** 1995. Nucleotide sequence of the Bacillus subtilis dnaD gene. Microbiology **141:**321-322.
17. **Bell SP, Dutta A.** 2002. DNA replication in eukaryotic cells. Annual review of biochemistry **71:**333-374.
18. **Katayama T.** 2001. Feedback controls restrain the initiation of Escherichia coli chromosomal replication. Molecular microbiology **41:**9-17.

19. **Nishitani H, Lygerou Z.** 2002. Control of DNA replication licensing in a cell cycle. Genes to Cells **7:**523-534.
20. **Barnes MH, Hammond RA, Kennedy CC, Mack SL, Brown NC.** 1992. Localization of the exonuclease and polymerase domains of Bacillus subtilis DNA polymerase III. Gene **111:**43-49.
21. **Sanjanwala B, Ganesan A.** 1989. DNA polymerase III gene of Bacillus subtilis. Proceedings of the National Academy of Sciences **86:**4421-4424.
22. **Sonenshein AL, Hoch JA, Losick R.** 2002. Bacillus subtilis and its closest relatives: from genes to cells. Asm Press.
23. **Graumann P.** 2012. Bacillus: cellular and molecular biology. Horizon Scientific Press.
24. **Le Chatelier E, Bécherel OJ, d'Alençon E, Canceill D, Ehrlich SD, Fuchs RP, Jannière L.** 2004. Involvement of DnaE, the second replicative DNA polymerase from Bacillus subtilis, in DNA mutagenesis. Journal of Biological Chemistry **279:**1757-1767.
25. **McHenry CS.** 2011. DNA replicases from a bacterial perspective. Annual review of biochemistry **80:**403-436.
26. **Pellegrini L.** 2012. The Pol α-primase complex, p 157-169, The eukaryotic replisome: a guide to protein structure and function. Springer.
27. **Gorbalenya AE, Koonin EV.** 1993. Helicases: amino acid sequence comparisons and structure-function relationships. Current opinion in structural biology **3:**419-429.
28. **Grainger WH, Machón C, Scott DJ, Soultanas P.** 2010. DnaB proteolysis in vivo regulates oligomerization and its localization at oriC in Bacillus subtilis. Nucleic acids research **38:**2851-2864.
29. **Zhang W, Machón C, Orta A, Phillips N, Roberts CJ, Allen S, Soultanas P.** 2008. Single-molecule atomic force spectroscopy reveals that DnaD forms scaffolds and enhances duplex melting. Journal of molecular biology **377:**706-714.
30. **Velten M, McGovern S, Marsin S, Ehrlich SD, Noirot P, Polard P.** 2003. A two-protein strategy for the functional loading of a cellular replicative DNA helicase. Molecular cell **11:**1009-1020.
31. **Thirlway J, Soultanas P.** 2006. In the Bacillus stearothermophilus DnaB-DnaG complex, the activities of the two proteins are modulated by distinct but overlapping networks of residues. Journal of bacteriology **188:**1534-1539.
32. **Chintakayala K, Machón C, Haroniti A, Larson MA, Hinrichs SH, Griep MA, Soultanas P.** 2009. Allosteric regulation of the primase (DnaG) activity by the clamp-loader (τ) in vitro. Molecular microbiology **72:**537-549.
33. **Kobayashi K, Ehrlich SD, Albertini A, Amati G, Andersen K, Arnaud M, Asai K, Ashikaga S, Aymerich S, Bessieres P.** 2003. Essential Bacillus subtilis genes. Proceedings of the National Academy of Sciences **100:**4678-4683.
34. **Lecointe F, Sérèna C, Velten M, Costes A, McGovern S, Meile JC, Errington J, Ehrlich SD, Noirot P, Polard P.** 2007. Anticipating chromosomal replication fork arrest: SSB targets repair DNA helicases to active forks. The EMBO journal **26:**4239-4251.
35. **Polard P, Marsin S, McGovern S, Velten M, Wigley DB, Ehrlich SD, Bruand C.** 2002. Restart of DNA replication in Gram-positive bacteria: functional characterisation of the Bacillus subtilis PriA initiator. Nucleic acids research **30:**1593-1605.
36. **Costes A, Lecointe F, McGovern S, Quevillon-Cheruel S, Polard P.** 2010. The C-terminal domain of the bacterial SSB protein acts as a DNA maintenance hub at active chromosome replication forks. PLoS Genet **6:**e1001238.
37. **Okazaki R, Okazaki T, Sakabe K, Sugimoto K, Sugino A.** 1968. Mechanism of DNA chain growth. I. Possible discontinuity and unusual secondary structure of newly synthesized chains. Proceedings of the National Academy of Sciences **59:**598-605.

38. **Tamanoi F, Okazaki T, Okazaki R.** 1977. Persistence of RNA attached to nascent short DNA pieces in Bacillus subtilis cells defective in DNA polymerase I. Biochemical and biophysical research communications **77:**290-297.
39. **Weller GR, Kysela B, Roy R, Tonkin LM, Scanlan E, Della M, Devine SK, Day JP, Wilkinson A, di Fagagna FdA.** 2002. Identification of a DNA nonhomologous end-joining complex in bacteria. Science **297:**1686-1689.
40. **Köhler P, Marahiel MA.** 1997. Association of the histone-like protein HBsu with the nucleoid of Bacillus subtilis. Journal of bacteriology **179:**2060-2064.
41. **Lindow JC, Kuwano M, Moriya S, Grossman AD.** 2002. Subcellular localization of the Bacillus subtilis structural maintenance of chromosomes (SMC) protein. Molecular microbiology **46:**997-1009.
42. **Mascarenhas J, Soppa J, Strunnikov AV, Graumann PL.** 2002. Cell cycle-dependent localization of two novel prokaryotic chromosome segregation and condensation proteins in Bacillus subtilis that interact with SMC protein. The EMBO journal **21:**3108-3118.
43. **Lemon KP, Grossman AD.** 2000. Movement of replicating DNA through a stationary replisome. Molecular cell **6:**1321-1330.
44. **Migocki MD, Lewis PJ, Wake RG, Harry EJ.** 2004. The midcell replication factory in Bacillus subtilis is highly mobile: implications for coordinating chromosome replication with other cell cycle events. Molecular microbiology **54:**452-463.
45. **Bravo A, Serrano-Heras G, Salas M.** 2005. Compartmentalization of prokaryotic DNA replication. FEMS microbiology reviews **29:**25-47.
46. **Duggin IG, Wake RG, Bell SD, Hill TM.** 2008. The replication fork trap and termination of chromosome replication. Molecular microbiology **70:**1323-1333.
47. **Lemon KP, Grossman AD.** 2001. The extrusion-capture model for chromosome partitioning in bacteria. Genes & development **15:**2031-2041.
48. **Mirkin EV, Mirkin SM.** 2007. Replication fork stalling at natural impediments. Microbiology and Molecular Biology Reviews **71:**13-35.
49. **Michel B, Grompone G, Florès M-J, Bidnenko V.** 2004. Multiple pathways process stalled replication forks. Proceedings of the National Academy of Sciences of the United States of America **101:**12783-12788.
50. **Bruand C, Velten M, McGovern S, Marsin S, Sérèna C, Ehrlich SD, Polard P.** 2005. Functional interplay between the Bacillus subtilis DnaD and DnaB proteins essential for initiation and re-initiation of DNA replication. Molecular microbiology **55:**1138-1150.
51. **Bruand C, Farache M, McGovern S, Ehrlich SD, Polard P.** 2001. DnaB, DnaD and DnaI proteins are components of the Bacillus subtilis replication restart primosome. Molecular microbiology **42:**245-256.
52. **Merrikh H, Zhang Y, Grossman AD, Wang JD.** 2012. Replication–transcription conflicts in bacteria. Nature Reviews Microbiology **10:**449-458.
53. **Sanders GM, Dallmann HG, McHenry CS.** 2010. Reconstitution of the B. subtilis replisome with 13 proteins including two distinct replicases. Molecular cell **37:**273-281.
54. **Lestini R, Michel B.** 2007. UvrD controls the access of recombination proteins to blocked replication forks. The EMBO journal **26:**3804-3814.
55. **Duigou S, Ehrlich SD, Noirot P, Noirot-Gros MF.** 2004. Distinctive genetic features exhibited by the Y-family DNA polymerases in Bacillus subtilis. Molecular microbiology **54:**439-451.
56. **Friedberg EC, Walker GC, Siede W, Wood RD.** 2005. DNA repair and mutagenesis. American Society for Microbiology Press.

57. **Kokoska RJ, Bebenek K, Boudsocq F, Woodgate R, Kunkel TA.** 2002. Low fidelity DNA synthesis by a Y family DNA polymerase due to misalignment in the active site. Journal of Biological Chemistry **277:**19633-19638.
58. **Rivas-Castillo AM, Yasbin RE, Robleto E, Nicholson WL, Pedraza-Reyes M.** 2010. Role of the Y-family DNA polymerases YqjH and YqjW in protecting sporulating Bacillus subtilis cells from DNA damage. Current microbiology **60:**263-267.
59. **Lu M, Campbell JL, Boye E, Kleckner N.** 1994. SeqA: a negative modulator of replication initiation in E. coli. Cell **77:**413-426.
60. **Million-Weaver S, Samadpour AN, Moreno-Habel DA, Nugent P, Brittnacher MJ, Weiss E, Hayden HS, Miller SI, Liachko I, Merrikh H.** 2015. An underlying mechanism for the increased mutagenesis of lagging-strand genes in Bacillus subtilis. Proceedings of the National Academy of Sciences **112:**E1096-E1105.
61. **Shah JV, Cleveland DW.** 2000. Waiting for anaphase: Mad2 and the spindle assembly checkpoint. Cell **103:**997-1000.
62. **Niki H, Jaffé A, Imamura R, Ogura T, Hiraga S.** 1991. The new gene mukB codes for a 177 kd protein with coiled-coil domains involved in chromosome partitioning of E. coli. The EMBO journal **10:**183.
63. **Britton RA, Lin DC-H, Grossman AD.** 1998. Characterization of a prokaryotic SMC protein involved in chromosome partitioning. Genes & development **12:**1254-1259.
64. **Graumann PL.** 2000. Bacillus subtilis SMC is required for proper arrangement of the chromosome and for efficient segregation of replication termini but not for bipolar movement of newly duplicated origin regions. Journal of bacteriology **182:**6463-6471.
65. **Wang LH-C, Schwarzbraun T, Speicher MR, Nigg EA.** 2008. Persistence of DNA threads in human anaphase cells suggests late completion of sister chromatid decatenation. Chromosoma **117:**123-135.
66. **Draper GC, McLennan N, Begg K, Masters M, Donachie WD.** 1998. Only the N-terminal domain of FtsK functions in cell division. Journal of bacteriology **180:**4621-4627.
67. **Yu X-c, Tran AH, Sun Q, Margolin W.** 1998. Localization of cell division protein FtsK to theEscherichia coli septum and identification of a potential N-terminal targeting domain. Journal of bacteriology **180:**1296-1304.
68. **Löwe J, Ellonen A, Allen MD, Atkinson C, Sherratt DJ, Grainge I.** 2008. Molecular mechanism of sequence-directed DNA loading and translocation by FtsK. Molecular cell **31:**498-509.
69. **Bigot S, Saleh OA, Lesterlin C, Pages C, El Karoui M, Dennis C, Grigoriev M, Allemand JF, Barre FX, Cornet F.** 2005. KOPS: DNA motifs that control E. coli chromosome segregation by orienting the FtsK translocase. The EMBO journal **24:**3770-3780.
70. **Recchia GD, Aroyo M, Wolf D, Blakely G, Sherratt DJ.** 1999. FtsK-dependent and-independent pathways of Xer site-specific recombination. The EMBO journal **18:**5724-5734.
71. **Sciochetti SA, Piggot PJ, Blakely GW.** 2001. Identification and Characterization of thedif Site from Bacillus subtilis. Journal of bacteriology **183:**1058-1068.
72. **Kaimer C, González-Pastor JE, Graumann PL.** 2009. SpoIIIE and a novel type of DNA translocase, SftA, couple chromosome segregation with cell division in Bacillus subtilis. Molecular microbiology **74:**810-825.
73. **Kaimer C, Schenk K, Graumann PL.** 2011. Two DNA translocases synergistically affect chromosome dimer resolution in Bacillus subtilis. Journal of bacteriology **193:**1334-1340.
74. **Fiche J-B, Cattoni DI, Diekmann N, Langerak JM, Clerte C, Royer CA, Margeat E, Doan T, Nöllmann M.** 2013. Recruitment, assembly, and molecular architecture of the SpoIIIE DNA pump revealed by superresolution microscopy. PLoS Biol **11:**e1001557.

75. **Biller SJ, Burkholder WF.** 2009. The Bacillus subtilis SftA (YtpS) and SpoIIIE DNA translocases play distinct roles in growing cells to ensure faithful chromosome partitioning. Molecular microbiology **74:**790-809.
76. **Kaimer C, Graumann PL.** 2011. Players between the worlds: multifunctional DNA translocases. Current opinion in microbiology **14:**719-725.
77. **Gamba P, Veening J-W, Saunders NJ, Hamoen LW, Daniel RA.** 2009. Two-step assembly dynamics of the Bacillus subtilis divisome. Journal of bacteriology **191:**4186-4194.
78. **Anderson DE, Gueiros-Filho FJ, Erickson HP.** 2004. Assembly dynamics of FtsZ rings in Bacillus subtilis and Escherichia coli and effects of FtsZ-regulating proteins. Journal of bacteriology **186:**5775-5781.
79. **Jensen S, Thompson L, Harry E.** 2005. Cell division in Bacillus subtilis: FtsZ and FtsA association is Z-ring independent, and FtsA is required for efficient midcell Z-Ring assembly. Journal of bacteriology **187:**6536-6544.
80. **Gueiros-Filho FJ, Losick R.** 2002. A widely conserved bacterial cell division protein that promotes assembly of the tubulin-like protein FtsZ. Genes & development **16:**2544-2556.
81. **Kawai Y, Ogasawara N.** 2006. Bacillus subtilis EzrA and FtsL synergistically regulate FtsZ ring dynamics during cell division. Microbiology **152:**1129-1141.
82. **Claessen D, Emmins R, Hamoen LW, Daniel RA, Errington J, Edwards DH.** 2008. Control of the cell elongation–division cycle by shuttling of PBP1 protein in Bacillus subtilis. Molecular microbiology **68:**1029-1046.
83. **Errington J, Daniel RA, Scheffers D-J.** 2003. Cytokinesis in bacteria. Microbiology and Molecular Biology Reviews **67:**52-65.
84. **Daniel RA, Errington J.** 2000. Intrinsic instability of the essential cell division protein FtsL of Bacillus subtilis and a role for DivIB protein in FtsL turnover. Molecular microbiology **36:**278-289.
85. **Real G, Autret S, Harry EJ, Errington J, Henriques AO.** 2005. Cell division protein DivIB influences the Spo0J/Soj system of chromosome segregation in Bacillus subtilis. Molecular microbiology **55:**349-367.
86. **Thompson L, Beech P, Real G, Henriques A, Harry E.** 2006. Requirement for the cell division protein DivIB in polar cell division and engulfment during sporulation in Bacillus subtilis. Journal of bacteriology **188:**7677-7685.
87. **Lu Z, Takeuchi M, Sato T.** 2007. The LysR-type transcriptional regulator YofA controls cell division through the regulation of expression of ftsW in Bacillus subtilis. Journal of bacteriology **189:**5642-5651.
88. **Daniel RA, Harry EJ, Errington J.** 2000. Role of penicillin-binding protein PBP 2B in assembly and functioning of the division machinery of Bacillus subtilis. Molecular microbiology **35:**299-311.
89. **Edwards DH, Errington J.** 1997. The Bacillus subtilis DivIVA protein targets to the division septum and controls the site specificity of cell division. Molecular microbiology **24:**905-915.
90. **Hamoen LW, Meile JC, De Jong W, Noirot P, Errington J.** 2006. SepF, a novel FtsZ-interacting protein required for a late step in cell division. Molecular microbiology **59:**989-999.
91. **Webb CD, Graumann PL, Kahana JA, Teleman AA, Silver PA, Losick R.** 1998. Use of time-lapse microscopy to visualize rapid movement of the replication origin region of the chromosome during the cell cycle in Bacillus subtilis. Molecular microbiology **28:**883-892.
92. **Wang X, Llopis PM, Rudner DZ.** 2013. Organization and segregation of bacterial chromosomes. Nature Reviews Genetics **14:**191-203.
93. **Wu LJ, Errington J.** 1998. Use of asymmetric cell division and spoIIIE mutants to probe chromosome orientation and organization in Bacillus subtilis. Molecular microbiology **27:**777-786.
94. **Viollier PH, Thanbichler M, McGrath PT, West L, Meewan M, McAdams HH, Shapiro L.** 2004. Rapid and sequential movement of individual chromosomal loci to specific subcellular locations

during bacterial DNA replication. Proceedings of the National Academy of Sciences of the United States of America **101:**9257-9262.

95. **Umbarger MA, Toro E, Wright MA, Porreca GJ, Bau D, Hong S-H, Fero MJ, Zhu LJ, Marti-Renom MA, McAdams HH.** 2011. The three-dimensional architecture of a bacterial genome and its alteration by genetic perturbation. Molecular cell **44:**252-264.
96. **Fogel MA, Waldor MK.** 2006. A dynamic, mitotic-like mechanism for bacterial chromosome segregation. Genes & development **20:**3269-3282.
97. **Ptacin JL, Shapiro L.** 2010. Initiating bacterial mitosis: understanding the mechanism of ParA-mediated chromosome segregation. Cell Cycle **9:**4033-4034.
98. **Brendler T, Sawitzke J, Sergueev K, Austin S.** 2000. A case for sliding SeqA tracts at anchored replication forks during Escherichia coli chromosome replication and segregation. The EMBO journal **19:**6249-6258.
99. **Gelles J, Landick R.** 1998. RNA polymerase as a molecular motor. Cell **93:**13-16.
100. **Jun S, Wright A.** 2010. Entropy as the driver of chromosome segregation. Nature Reviews Microbiology **8:**600-607.
101. **Jaacks K, Healy J, Losick R, Grossman A.** 1989. Identification and characterization of genes controlled by the sporulation-regulatory gene spo0H in Bacillus subtilis. Journal of bacteriology **171:**4121-4129.
102. **Dubnau D, Davidoff-Abelson R.** 1971. Fate of transforming DNA following uptake by competent Bacillus subtilis: I. Formation and properties of the donor-recipient complex. Journal of molecular biology **56:**209-221.
103. **Dubnau D.** 1991. The regulation of genetic competence in Bacillus subtilis. Molecular microbiology **5:**11-18.
104. **Laemmli UK.** 1970. Cleavage of structural proteins during the assembly of the head of bacteriophage T4. Nature **227:**680-685.
105. **Bremer H, Dennis PP.** 2008. Modulation of chemical composition and other parameters of the cell at different exponential growth rates. EcoSal Plus **3**.
106. **Webb CD, Graumann PL, Kahana JA, Teleman AA, Silver PA, Losick R.** 1998. Use of time-lapse microscopy to visualize rapid movement of the replication origin region of the chromosome during the cell cycle in Bacillus subtilis. Molecular microbiology **28:**883-892.
107. **Goranov AI, Kuester-Schoeck E, Wang JD, Grossman AD.** 2006. Characterization of the global transcriptional responses to different types of DNA damage and disruption of replication in Bacillus subtilis. Journal of bacteriology **188:**5595-5605.
108. **Watt PM, Hickson ID.** 1994. Structure and function of type II DNA topoisomerases. Biochemical Journal **303:**681.
109. **Drlica K, Zhao X.** 1997. DNA gyrase, topoisomerase IV, and the 4-quinolones. Microbiology and molecular biology reviews **61:**377-392.

7. CURRICULUM VITAE

Nina El Najjar
Date of birth: July 23rd, 1984
Place of birth: Dar Chmezzin, Lebanon

January 2011- September 2016	Department of Chemistry, Philipps Universität Marburg PhD thesis in Biology/Microbiology under the supervision of Prof. Peter L. Graumann Title: *"DNA translocases and origin region segregation in B. subtilis"*
September 2006- July 2009	Lebanese American University (LAU), School of Arts and Sciences, Byblos, Lebanon Master in Molecular biology. Thesis under the supervision of Dr. Sima Tokajian Title: *"Antibiotic resistance patterns and sequencing of class I integron from uropathogenic Escherichia coli in Lebanon"*
September 2002- August 2005	University of Balamand**,** school of arts and sciences, Koura, Lebanon Bachelor of Science in Biology
August 2002	College des Soeurs des Saints Coeurs**,** Tripoli, Lebanon Baccalaureate in life sciences

8. ACKNOWLEDGMENTS

This work was carried out from January 2011 to September 2016 in the laboratory of Prof. Dr. Peter L. Graumann at the University of Marburg, Germany.

First of all, I would like to thank Prof. Peter Graumann for his supervision and constant support. Throughout the time I have spent in the lab I appreciated our discussions, his encouragement, and his valuable advice and suggestions.

My gratitude also goes to my scholarship, the "Katholische Akademische Ausländer Dienst" (KAAD) for having funded me for 3 and a half years, and for their moral and social guidance in the first years I spent in Germany.

For his input in the single molecule tracking analysis I would like to thank Dr. Thomas Rösch, and Felix Schmidt for the analysis of the separation of the origin region movies.

Many thanks to all members of the Graumann Lab, especially to the "big lab members": Dr. Jihad El Andari, Dr. Ana Hervás Veguillas, Dr. Danialla Cavalcanti de Lucena, Dr. Mingle Cao, Dr. Christian Reimold, Simon Dersch, and Dr. Thomas Rösch, as well as to all the rest, both old and new members: Patricia Bedrunka, Dr. Stephan Altenburger, Hector Romero, Dr. Joel Defeu Soufo, Dr. Felix Dempwolff, Sonja Schibany, Daniel Rotter, Dr. Mara Specht, Dr. Katrin Schenk, Mathilda Diehl, and Marie Burghard.

I am also indebted to our amiable technicians: Astrid Steindorf, Frauke Koerner, Anja Spies-Naumann, to Sabrina Steidl, and to our wonderful secretary Julia Witsch.

For being there in the good and the bad times, I would like to thank my friends in Lebanon, Germany, and elsewhere, especially Alex, Jihad, Elma, Natalie, Mathieu, Nadine, Evi, Rahada, and to my late friend and brother Nazih who left us too early. None of this would have been possible without you.

I'm thankful to my flat mates, for making home a pleasing and comfortable space.

Finally, my uttermost gratitude goes to my family for their endless love, my mother Nasra and my brothers Joseph, Nizar and Andrei who have always been my inspiration in life, and the drive behind every step I take. My mother has taught me patience and perseverance, and this thesis is dedicated to her.